REPORT DOCUMENTATION PAGE

Form Approved
OMB No. 0704-0188

1. AGENCY USE ONLY (Leave Blank)	2. REPORT DATE	3. REPORT TYPE AND DATES COVERED

4. TITLE AND SUBTITLE
Post stall Control of Swept Wings

5. FUNDING NUMBERS
F49620-92-J-0088
AFOSR-TR-95 0646

6. AUTHOR(S)
Demetri Telionis

7. PERFORMING ORGANIZATION NAME(S) AND ADDRESS(ES)
Virginia Polytechnic Institute & State University
Blacksburg VA 24061-0219

8. PERFORMING ORGANIZATION REPORT NUMBER

9. SPONSORING/MONITORING AGENCY NAME(S) AND ADDRESS(ES)
Air Force Office Of Scientific Research
Aerospace & Materials Sciences Directorate
110 Duncan Avenue, Suite B-115
Bolling AFB DC 20332-0001
NA

10. SPONSORING/MONITORING AGENCY REPORT NUMBER
F49620-92-J-0088

11. SUPPLEMENTARY NOTES

12a. DISTRIBUTION/AVAILABILITY STATEMENT
APPROVED FOR PUBLIC RELEASE
DISTRIBUTION IS UNLIMITED

12b. DISTRIBUTION CODE

13. ABSTRACT (Maximum 200 words)

The work conducted on this effort is described in detail in six papers which were presented at various meetings. Copies of the papers are attached to this report. A brief description of this material is provided below.

At the beginning of this effort, the fundamental character of the flow was investigated. In the first publication generated[1], we discuss the transient flow field over a delta wing during pitch-up motions to very large angles of attack. Emphasis was directed at the growth and the eventual breakdown of leading edge vortices. Delta wing models were tested in a

14. SUBJECT TERMS	15. NUMBER OF PAGES
stall control, swept wings	60
	16. PRICE CODE

17. SECURITY CLASSIFICATION OF REPORT	18. SECURITY CLASSIFICATION OF THIS PAGE	19. SECURITY CLASSIFICATION OF ABSTRACT	20. LIMITATION OF ABSTRACT

A detailed investigation of the velocity and vorticity fields over a 75°-sweep delta wing undergoing a ramp-like pitch-up motion was then carried out[2], through three-component LDV measurements. The evolution of the flow field in four planes normal to the free-stream was captured at 100 time instants through the wing motion. The delta wing was pitched through angles of attack ranging from 28° to 60°. The corresponding vorticity field was calculated from the velocity data at each incidence. Hysteresis effects on vortex development and breakdown with respect to the steady case were studied through axial velocity and vorticity contours. The topology of streamlines and vortex lines was compared with the corresponding topologies of the steady case. It was found that vortex breakdown can be detected first by a drastic reduction of the axial velocity. In fact, it was discovered that this effect is developing asymmetrically, beginning in the inboard side of the vortex. This is followed by a reduction of the axial vorticity component and finally by a complete reversal of the circumferential vorticity component. Some effects of parameters like Reynolds number, model thickness, non-dimensional pitch-up rate, free-stream turbulence on the developing flow field are addressed in this paper[2].

The possibility of delaying vortex breakdown further at higher angles of attack by employing control surfaces was then studied experimentally[3]. The effect of control surfaces was tested for fixed and dynamically pitching delta wings. Flow visualization, surface pressure measurements and laser-Doppler velocimetry were employed to map out pressure, velocity and vorticity fields. It was found that a drooping apex flap can delay vortex breakdown by an angle of 8° beyond the steady flow breakdown angle of attack. The apex flap effect was equally pronounced in dynamic maneuvers.

The ability of vortex cavity flaps to delay vortex breakdown over the planform of a delta wing at high angles of attack was then considered as described in Ref. 4. Surface pressure measurements were made over a range of angles of attack to determine when vortex breakdown occurs over the planform with the flap deployed. Laser-Doppler velocimetry was used to map out the flow field over the delta wing at an angle of attack of 35°. The effect of

vortex cavity flaps on the structure of leading edge vortices was documented. It was found that for a 70° swept delta wing, cavity flaps can delay the appearance of vortex breakdown over the wing to higher angles of attack than could be otherwise realized.

Some of these tests were repeated at higher Reynolds numbers[5], employing again the dynamic strut to drive a delta wing into dynamic pitch up motions. Flow visualizations and surface pressure measurements were obtained. The effect of deploying cavity flaps was found to be significant in steady flows for angles as high as 42°. In unsteady flows it appears that the benefits of cavity flaps are more pronounced at even higher angles of attack.

Finally, the internal structure of vortex breakdown was examined again more carefully[6]. Periodic and quasi-periodic phenomena associated with the post-breakdown flowfield over slender delta wings were investigated. In particular, the structure of the helical mode instability as the source of these phenomena was investigated through flow visualization, digital particle image velocimetry and hot-wire anemometry. Evidence was provided to further support the conjecture that the rotation of the helical structure originating at breakdown with a spiraling sense opposite to that of the vortex rotation is responsible for the quasi-periodic oscillations that appear in the form of distinct peaks in the velocity and surface pressure spectra. Two regions of the helix with different growth rates and non-dimensional frequencies were identified and the coherence and path of the disturbance were quantified.

Personnel

Dr. Rediniotis worked on this project as a post-doctoral fellow until December 1994. Dr. Rediniotis has been offered a faculty position at Texas A&M University and since January 1995, he serves as an assistant professor at this institution.

Mr. Schaeffler returned to VPI to work on this project. In the past three years, Mr. Schaeffler has devoted his time exclusively to this effort. He has now completed all the required courses for his Ph.D. and intends to defend his thesis is the Fall of 1995. His dissertation will be a detailed account of most of the work carried out on this project and

will be submitted to AFOSR as soon as it becomes available.

References

The following is a list of the papers generated from the present project. Copies of these papers are attached and should be considered as the main body of this report.

1. "Pitch-up Motion of Delta Wings," presented at the AIAA Aerospace Sciences Meeting, Jan. 1992, Paper No. 92-0278, by Rediniotis, O. K., Klute, S. M., Hoang, N. G., and Telionis, D. P., also *AIAA Journal*, Vol. 32, pp. 716-725, 1994.
2. "Three-Dimensional LDV Measurements Over a Delta Wing in Pitch-Up Motions," AIAA 31st Aerospace Sciences Meeting, Paper No. AIAA-93-0185, by Hoang, N. T., Rediniotis, O. K., and Telionis, D. P., also the same material under a new title: "The Temporal Evolution of a Pair of Streamwise Vortices," *Experiments in Fluids*, in press.
3. "Flow Control Over Delta Wings at High Angles of Attack," AIAA Applied Aerodynamics Conference, August 1993, Paper No. AIAA 93-3494, by Klute, S. M., Rediniotis, O. K., and Telionis, D. P., also AIAA Journal, in press.
4. "Controlling of Delta Wing Leading-Edge Vortex with Vortex Cavity Flaps," presented at the Symposium Flow Acoustics Interaction and Fluid Flow Control of the 1993 Winter Annual Meeting, November, !993, Paper No. 93-WA/NCA-27, by Schaeffler, N. W., Hoang, N. T., and Telionis, D. P.
5. "Control of Transient Development of Leading Edge Vortices by Vortex Cavity Flaps," 12th AIAA Applied Aerodynamics Conference, Paper No. AIAA-94-1857, by Schaeffler, N. W., Rediniotis, O. K., and Telionis, D. P.
6. "Instabilities of Vortex Breakdown: Their Structure and Growth," AIAA Applied Aerodynamics Conference, Paper No. AIAA-95-2308, by Traub, L. W., Rediniotis, O. K., Klute, S. M., Moore, C. T., and Telionis, D. P.

AIAA

also AIAA J.

Vol 32, pp 716-720, 1994

AIAA 92-0278

Pitching-Up Motions of Delta Wings

O. K. Rediniotis, S. M. Klute, N. T. Hoang and D. P. Telionis
Virginia Polytechnic Institute and State University
Blacksburg, VA 24061-0219

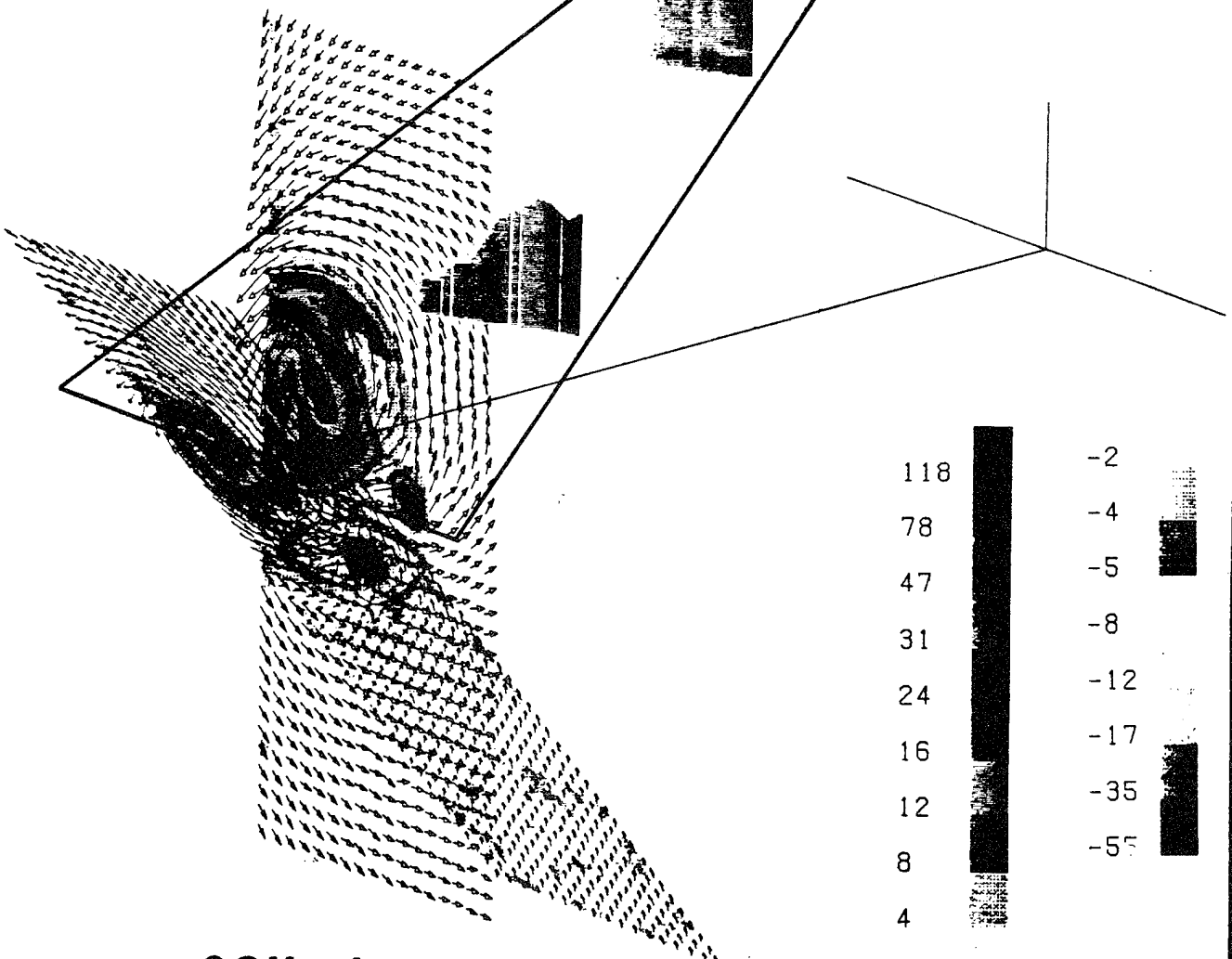

30th Aerospace Sciences Meeting & Exhibit

January 6-9, 1992 / Reno, NV

PITCH-UP MOTIONS OF DELTA WINGS

O. K. Rediniotis[1], S. M. Klute[1], N. T. Hoang[1] and D. P. Telionis[2]
Department of Engineering Science and Mechanics
Virginia Polytechnic Institute and State University
Blacksburg, VA 24061–0219

Abstract

The transient flow field over a delta wing during pitch–up motions to very large angles of attack was investigated. Emphasis was directed at the growth and the eventual breakdown of leading edge vortices. Delta wing models were tested in a wind tunnel at Reynolds number of order 10^5. Instantaneous pressure measurements were obtained, while the flow field was mapped out via a seven–hole probe designed, constructed and calibrated to generate time–varying information. Earlier qualitative evidence of hysteresis in the development of the flow was confirmed. Moreover, the present data indicate significant differences of vorticity content between the steady and the unsteady motions.

Introduction

Modern technologies in propulsion, materials, and on–board computers will allow combat aircraft to operate over a much expanded maneuvering envelope. These technologies have outpaced our understanding of unsteady aerodynamics. Some of the desirable maneuvers will require a swift pitch up motion and/or a roll about the velocity vector at high angles of attack. A good model for the study of unsteady aerodynamics at high angles of attack is the delta wing. The dynamics of a pitching delta wing were considered as early as 1969[1]. However, the bulk of the contributions on this topic appeared only in the past few years[2-12]. With very few exceptions, these investigations were confined to moderate angles of attack. The practical aspects of possible aircraft maneuvers are discussed in Refs. 13–15. Nguyen and Gilbert[16] provide a more recent discussion on the impact of emerging technologies on the potential of the next generation of combat aircraft. In the present paper we confine out attention to the aerodynamics of delta wings in sharp ramp–like pitch up motions.

The flow over a delta wing at a fixed angle of attack is dominated by two leading–edge vortices. The circumferential velocity component along a plane normal to such a vortex is reminiscent of a potential vortex with a viscous core, while the axial component resembles a jet. The structure is symmetric about the symmetry plane of the wing. Lift stall is greatly delayed to angles of attack as large as 30°. A large number of investigators have studied this steady flow problem and many reviews have appeared (Tobak and Peak[17], Peak and Tobak[18], Hunt[19], Lee & Ho[20]). Recent investigations report on the use of powerful experimentl techniques, like laser–Doppler velocimetry, double cross wires and others to document quantitatively the complex vortical fields over delta wings[21-26].

A phenomenon that cannot be avoided in all three–dimensional flows over bodies at large angles of attack is vortex breakdown. The imprint of a vortex, namely the pressure distribution on the solid surface clearly displays the main characteristics of this phenomenon. The suction peak for a well organized vortex may even invert itself downstream of breakdown[26]. If the pressure is observed along a ray and the increasing parameter is the angle of attack, then again bursting can be identified as a sudden drop of suction peak pressure[27,28].

In the steady flow case, the predominant direction of convection is the direction of the mean flow. The vortex is fed with vorticity all along the length of the leading edge. It appears then physically reasonable and in fact, it has been demonstrated analytically[29] and experimentally[30] that in some cases, the flow is very nearly conical. The physics of the problem change drastically if the angle of attack is increased dynamically. For rapid pitch–up motions leading to large angles of attack, events are influenced mostly by local phenomena. The dominant direction of convection changes. This aspect of the flow is bound to influence both the development of the vortex as well as its breakdown characteristics.

The past three years have seen a lot of activity in the area of unsteady aerodynamics of delta wings. We have constructed a list with the basic parameters of most of the experimental efforts in this area which is displayed in Table 1. With the exception of the work of Rockwell and his associates[10], these research programs aim mostly at global characteristics like lift or drag hysteresis diagrams. Very little effort is directed in documenting carefully the detailed structure of the flow. Moreover, no such information on velocity and pressure fields is available for angles of attack higher than 40°.

In this paper we present for the first time measured data on the developing velocity and vorticity fields, for very large angles of attack. These data are complemented with instantaneous pressure distributions on the suction surface of the model. Such data can be obtained only by point measurements. Constructing fields of evolving information becomes possible by displacing the measuring instruments, repeating the motions thousands of times and ensemble–averaging the results.

2. Facilities, Models & Instrumentation

Tests were conducted in a 20" × 20" wind tunnel at a Reynolds number equal to 10^4. Two models with a 75° sweep angle were employed. The first was a solid model while the second was instrumented with pressure transducers as shown in Fig. 1. The second model was a scaled–down version of the model employed in an earlier investigation of the present group[28].

---

[1]Graduate Research Assistant

[2]Professor, Associate Fellow AIAA

Table 1

Paper No. No.	Test Section Size	Model Size	Reynolds Number (Re/1K+3)	Free Stream Velocity (U in m/sec)	Max Angle Of Attack (in deg)	Range of Angles of Attack (in deg)	Type of Motion	Topics of Investigation
1	Water Tunnel 0.33×0.25 (all in m)	(a).255×.09× 0.005 (in m) (b).178×.13× 0.005 (in m) (c).141×16.4× 0.005 (in m)	5.8–5.9 20		20,45	20,20	Oscillatory Pitching	Flow visualization to study the behavior of the leading–edge vortices over a delta wing, at a sudden change of incidence.
2	Towing Tank	(a)RC=0.25 AR = 2.3 (b)RC = 0.25, AR = 4	6.25–350	0.05–1.4	30	30	Oscillatory Pitching	Flow visualization to study the three–dimensional effects on a pitching delta wing.
3	0.23×0.23 ×2 (all in m)	0.1×0.1× 0.001(all in m)	13–30	0.13–0.30	45	20	Oscillatory Pitching	Steady and unsteady lift coefficient. Vortex breakdown locations.
4	7'×10' (actually used 27"×83")	(a)16×8×.3 (b)12×6×.25 (k)12×9×.25 (in inches)	420–820	20–40	40,60,90	40,60,90	Oscillatory Pitching, Ramp Motion	Steady and unsteady force measurements (six components). Vortex flow visualization.
5	The 12' tunnel at Langley	(a)AR = 1.46 SA = 70 deg (b) SA = 45 deg	400	18	60	60	Oscillatory Pitching	Six–component force and moment data in oscillating motion. Flow visualization.
6	Wind Tunnel 5'×3'×8'	20.61"×15"× 0.25"	1540	46.2	55	55	Oscillatory Pitching, Ramp Motion	Six–component force and moment data in oscillatory and ramp motions.
7	Wind Tunnel 2'×2'×6'	16.48"×12"× 0.5"	90–350	3.25–12.67	39,45	10,45	Oscillatory Pitching	Flow visualization to study the dynamic behavior of the leading edge vortices, in sinusoidal pitching.
8	Wind Tunnel 3'×5'	20"×15"	1–1.97× 10^6		15–30	20	Oscillatory Pitching	Flow visualization to study the leading–edge vortices on a pitching delta wing.
9	7'×10' used 27"×83"	(a)16"×8"×3 (b)12"×6"×.05" (c)12"×9"×.25"	420–820		55°	55	Oscillatory Pitching	Force & moment measurements; effects of sideslip, frequency & Reynolds number.
10	Water Channel .254×/457×.4676,.102 (all in m)	SA=52 deg RC = 0.51	2.9–13.4		40,60,90	40,60,90°	Oscillatory Pitch	Force and moment measurements.
11	Water Tunnel 0.254×0.457m	SA = 52° 0.76×1.02m	2.9–13.4		40°	40°	Pitch ups and downs Oscillations	Velocity & Vorticity contours obtained via particle trackin and image processing.

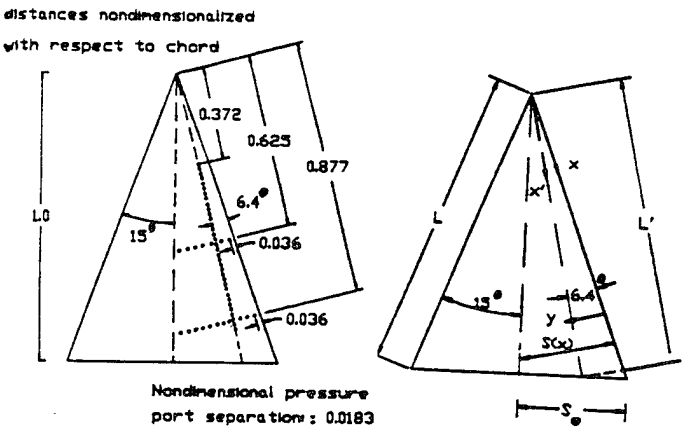

Fig. 1. The model.

The models were mounted on a dynamic strut allowing oscillations in pitch about an arbitrary axis normal to their axis of symmetry. In the experiments discussed here the models were pitched about their apex. A four–bar linkage and a pushing rod connected to a variable speed motor provided pitch–up schedules controlled by a laboratory computer. The schedule employed here involved a rapid increase of the angle of attack as shown in Fig. 2. The motion was always initiated from the position of $\alpha = 28°$. Two cases were tested corresponding to final angles of attack of $\alpha = 68°$ and 90°, respectively.

Surface pressures were measured by Endevco transducers mounted on the model. Pressure taps were provided along a ray aligned with the axis of the vortex as well as along two normals to it as shown in Fig. 1. The full scale reading of these transducers was 100 Torr which corresponded to 220 mV. However, our readings were confined to values lower than 6 mV. After a few hours of operation, a drift of about 0.05 mV was observed. To improve upon the accuracy of the measurements we calibrated these instruments before testing. It was thus confirmed that the calibration error was not more than 0.01 mV at any time during the data taking process. Data were ensemble averaged over 20 to 30 realizations of the

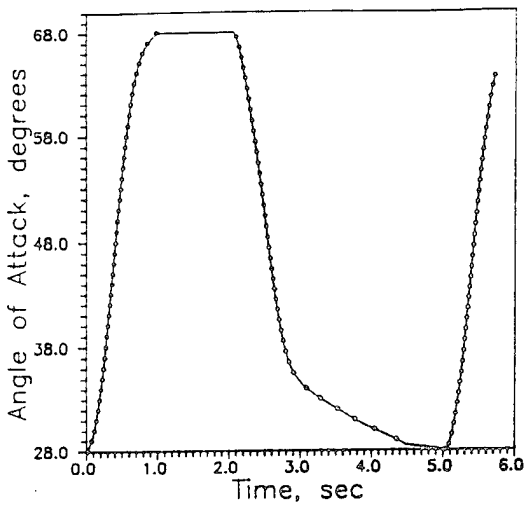

Fig. 2. The dynamic motion of the model presented as a temporal function of the angle of attack. Data were obtained only during pitch up.

motion. Velocity data were obtained along two planes as shown in Fig. 3. Plane A was normal to the oncoming stream positioned immediately downstream of the trailing edge when the wing was at its initial position, namely at $\alpha = 28°$. Plane B was rotated with respect to plane A (Fig. 3) to capture the velocity field closer to the trailing edge during its motion. Both sets of data provide a cross–section of the vorticity field shed by the wing and therefore contain the accumulated history of events that occurred over the wing surface during its dynamic motion.

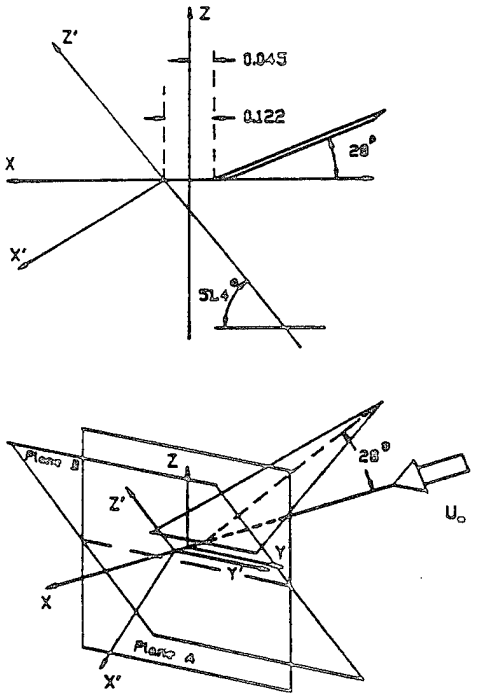

Fig. 3. Definition of coordinate systems. The axis x' mounted on the model along the direction of the vortex axis. Velocity data were obtained along the fixed planes A and B.

The velocity field was measured by a seven–hole probe. This probe was designed, constructed and calibrated especially for this project and is described in detail in Refs. 28 and 31. To obtain time–resolved data, seven Endevco transducers were mounted on a manifold which was in turn connected by short hoses to the seven–hole probe. These hoses were 10" long and had an internal diameter of 1/32. The frequency response of this instrument was studied by direct comparison of hot–wire measurements. These calibration studies were performed in the wake of a circular cylinder. In Fig. 4 we present the cross–spectrum and phase difference of the two signals. It

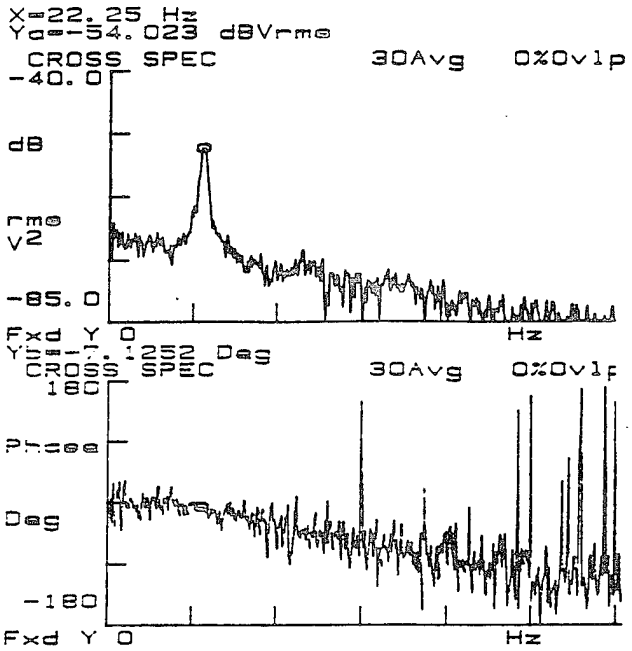

Fig. 4. Cross–spectrum and phase difference of a hot–wire and a seven–hole probe positioned in the wake of a vortex shedding circular cylinder.

appears that for a frequency of 34 Hz, there is a phase lag of the seven–hole probe of about 7°. The error involved in steady flow measurements was estimated to be less than 1%. No calibration of the magnitude readings in unsteady flow was attempted.

3. Results & Discussion

Results are presented first for the pressure distributions on the suction side of the model. These are pressures along the axis x' as shown in Fig. 1. For steady flow, all earlier studies indicate that the pressure trough beneath the axis of the vortex has its lowest value near the apex and increases towards the trailing edge. This trend is evident in the data presented in Fig. 5.

The pressure distribution over the suction side of the wing decreases as the angle of attack increases, thus generating higher values of lift. This trend, however, is reversed when breakdown sets in. In Fig. 5. we observe that indeed, for steady flow, the suction levels are reduced as the angle of attack increases. These trends are in agreement with data obtained earlier by the present investigators[29]. However, for the same angles of attack, the unsteady distributions continue to drop.

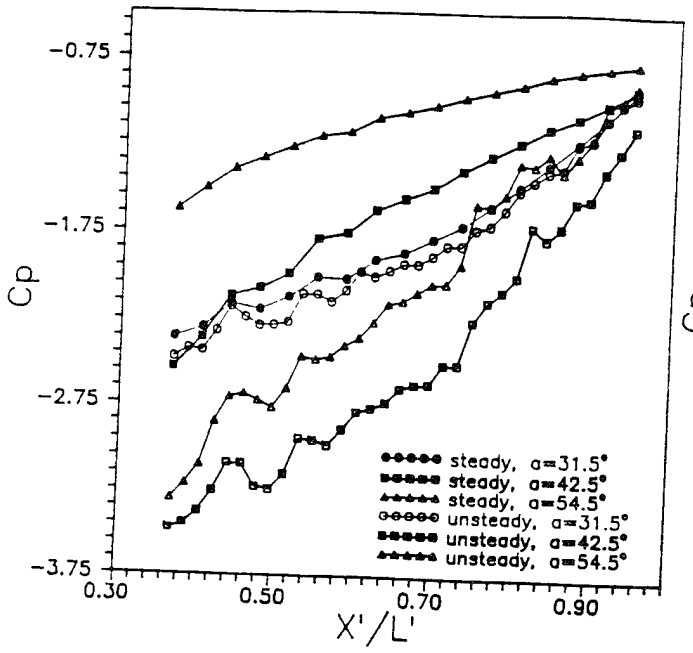

Fig. 5. Pressure coefficients for steady and unsteady flow along the axis x′ (Fig. 3).

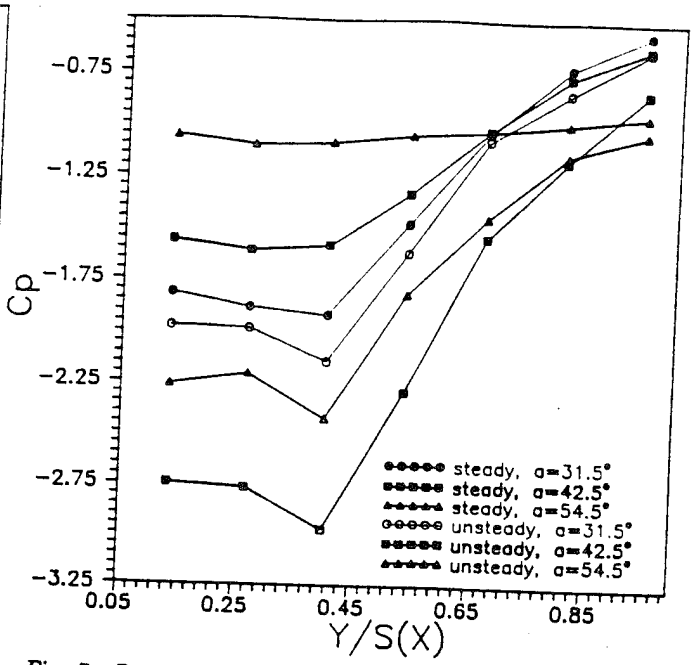

Fig. 7. Pressure coefficients across the vortex at x′/L′ = 0.61 for steady and unsteady flow.

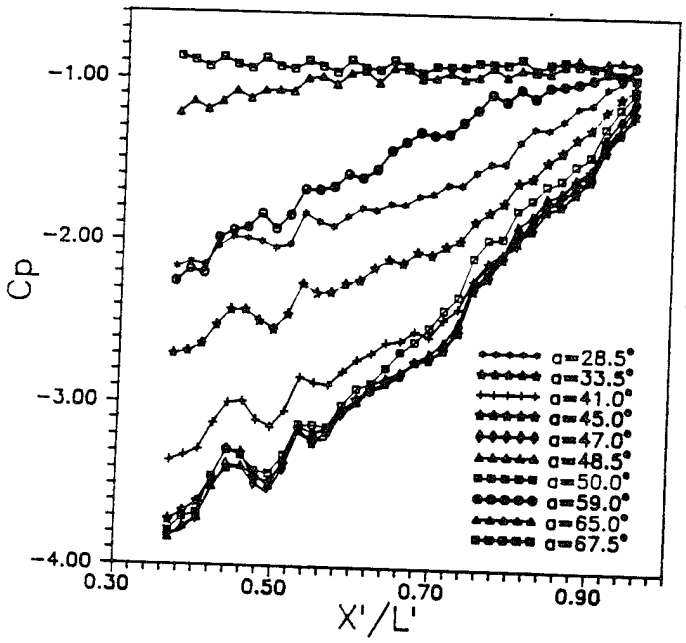

Fig. 6. Pressure coefficients during pitch–up along the axis x′ (Fig. 3).

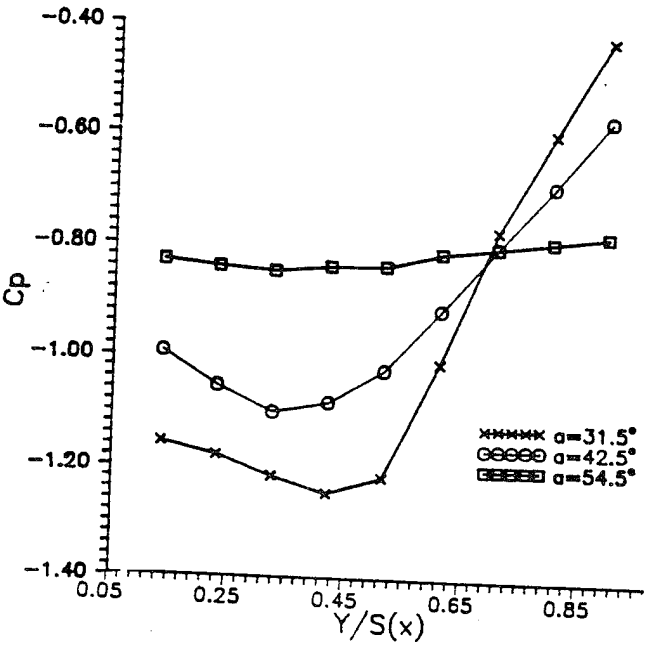

Fig. 8. Pressure coefficients across the vortex at x′/L′ = 0.81 for steady flow.

Pressure distributions for dynamic motions of the model are shown in Fig. 6. Once again, the pressure levels drop for angles of attack far larger than the steady state case. Moreover, a very interesting phenomenon can be observed. Pressures rise simultaneously at all points. This indicates that if breakdown occurs, it does not creep up from the trailing edge as it does in the steady–state case.

Pressure distributions were also plotted along a normal to the vortex axis. Figures 7 and 8 present data along x′/L′ = 0.62 and 0.81, respectively. The trends discussed earlier are again evident for the cross–section of the vortex. The trends for steady and unsteady flow beyond $\alpha = 31.5°$ are opposite. For steady flow, the suction troughs become more shallow as we increase the angle of attack beyond $\alpha = 3.15°$. However, a strong hysteresis is observed again in data obtained during pitch

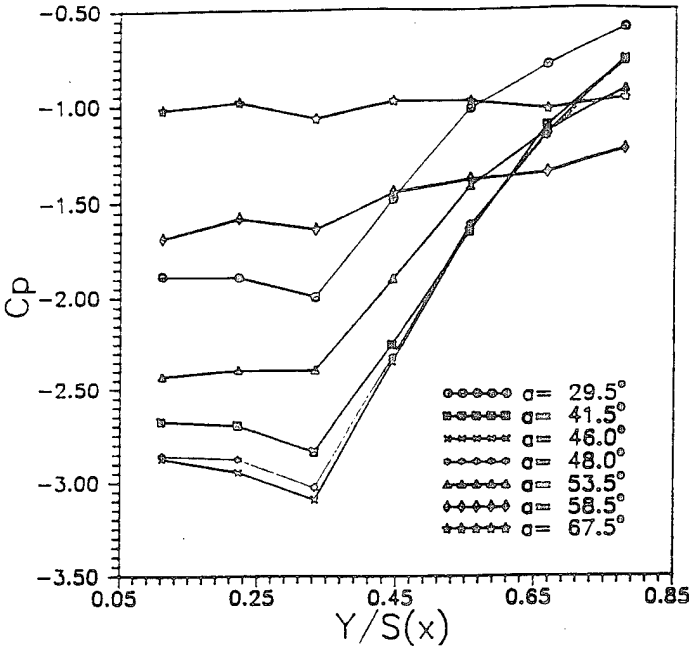

Fig. 9. Pressure coefficeints across the vortex at $x'/L' = 0.6$ during pitch–up.

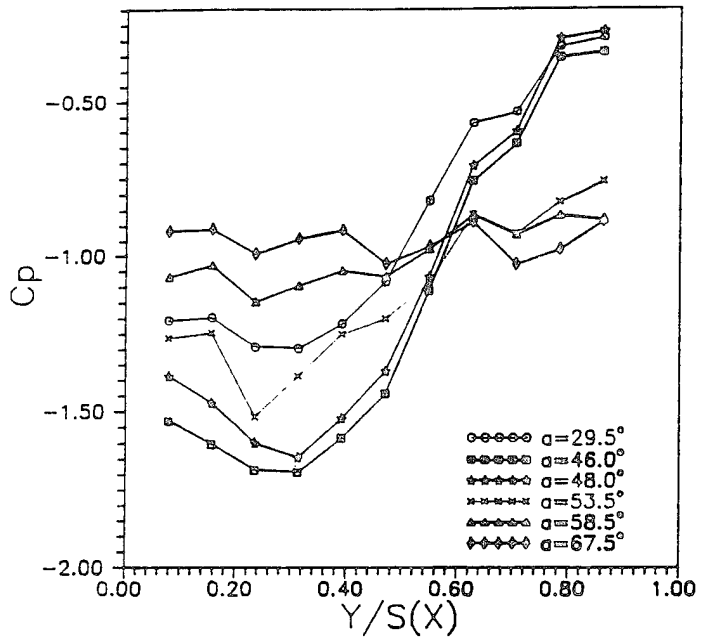

Fig. 10. Pressure coefficients across the vortex at $x'/L' = 0.81$ during pitch–up.

up, as shown in Figs. 7 and for larger angles of attack in Figs. 9 and 10. The trough appears to deepen continuously until $\alpha = 46°$ and a pressure coefficient value of –3.0 is achieved, which should be contrasted to the steady–state value of –2.2 of Fig. 7. Again, we observe that the curves at both stations reverse their trend at the same angle of attack, namely between $\alpha = 46°$ and $\alpha = 48°$ which confirms the fact that breakdown occurs simultaneously along the entire chord of the wing. Moreover, the onset of this phenomenon does not signal a sharp flattening of the pressure profile. Instead the trough gradually becomes more shallow, indicating that perhaps the core of the vortex breaks down first, and this event spreads smoothly radially outward all along the length of the vortex.

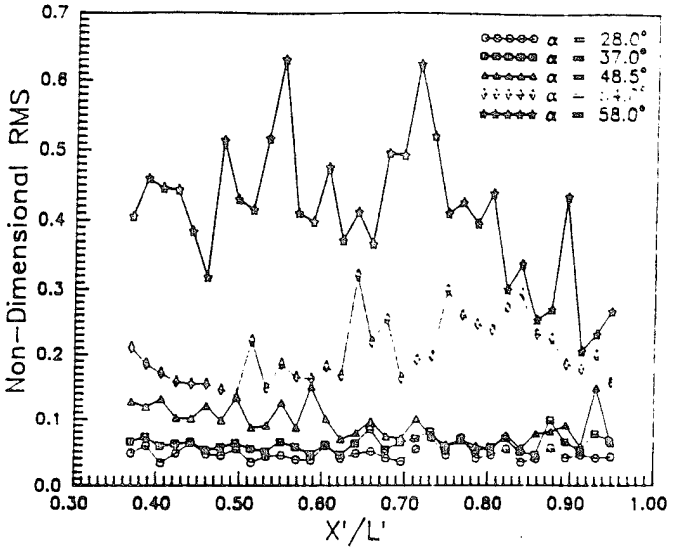

Fig. 11. RMS pressure distributions along the x′ axis for $\alpha = 28°$ to 58°.

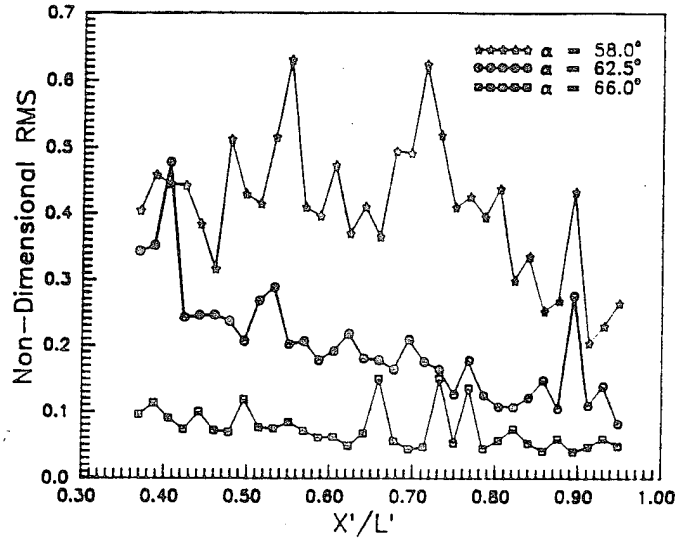

Fig. 12. RMS pressure distributions along the x′ axis for $\alpha = 58°$ to 66°.

Evidence for the phenomenon of breakdown we can seek in terms of the RMS of the pressure fluctuations. Once a vortex breaks down, the motion becomes very unstable and the overall level of fluctuation increases. All earlier studies indicate that the RMS of the pressure increases sharply beyond the location of breakdown. The RMS of the pressure along the axial distance is plotted in Figs. 11 and 12. For angles of attack less than 48°, the levels of RMS are uniformly low. At 48° though, the level indicates a moderate increase. For higher angles of attack, the RMS increases further, but uniformly, along the entire chord of the wing. This confirms our earlier observation that breakdown emerges at about 46° and 48°.

A sequence of frames representing cross–sections of the flow along the plane B during pitch–up are displayed in Fig. 13. In these frames we plot the velocity vectors representing the projection of the local velocity along the plane B. We also superimpose the component of vorticity normal to this plane, calculated by finite differences in terms of the velocity components. The vertical scale is measured along the axis Z′ in terms of half–spans S_o. The

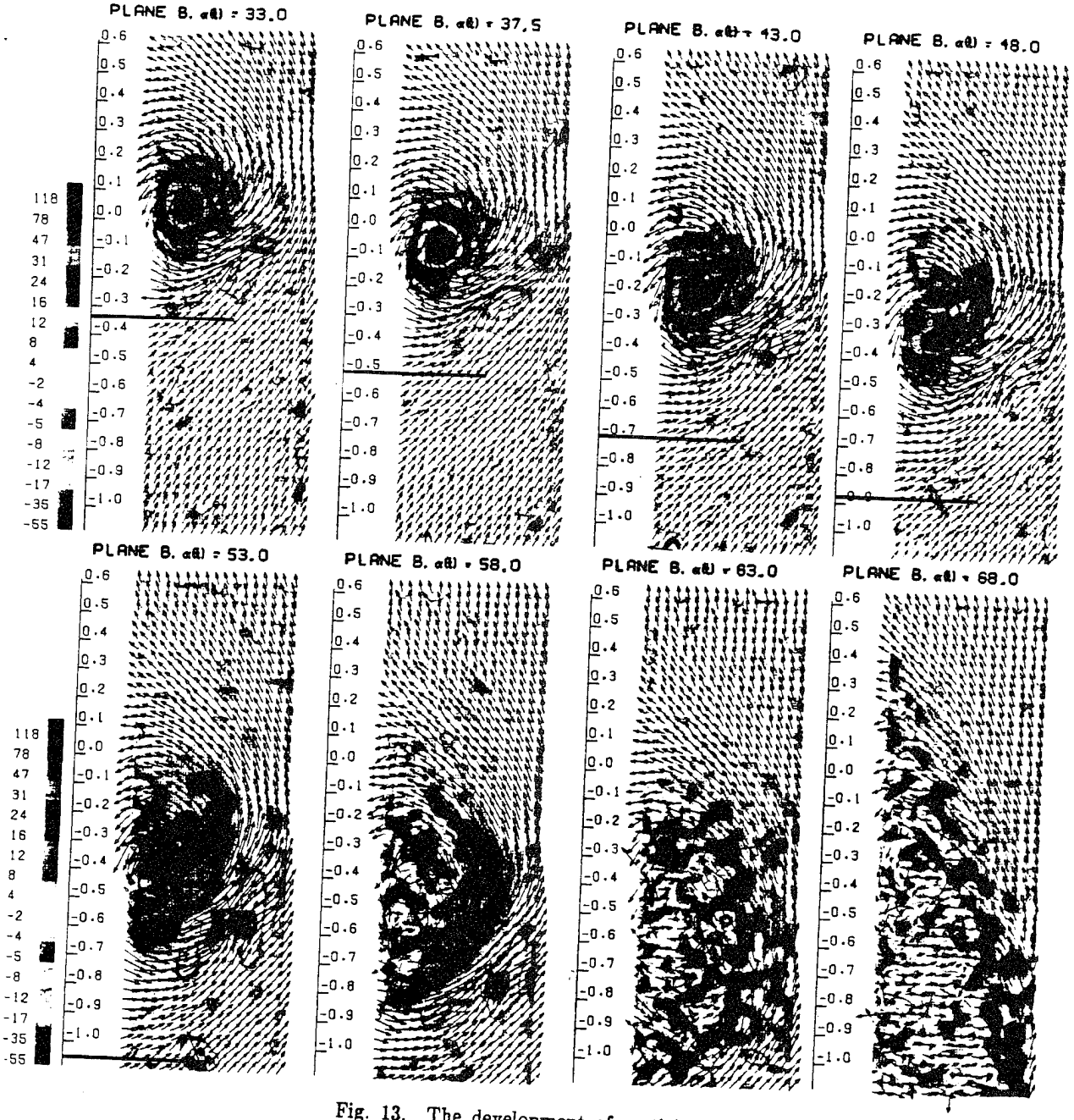

Fig. 13. The development of vorticity and velocity field during pitch–up along plane B.

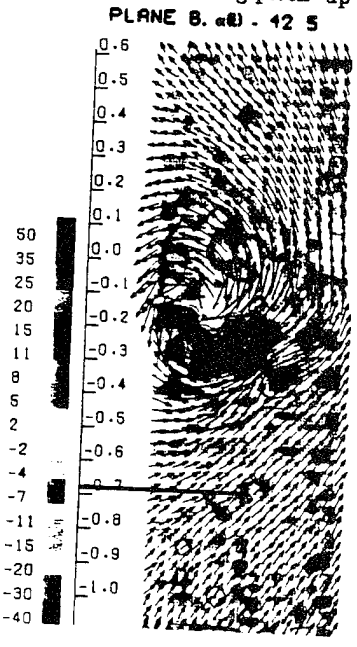

Fig. 14. The Y–component of vorticity superimposed on the velocity field in plane B.

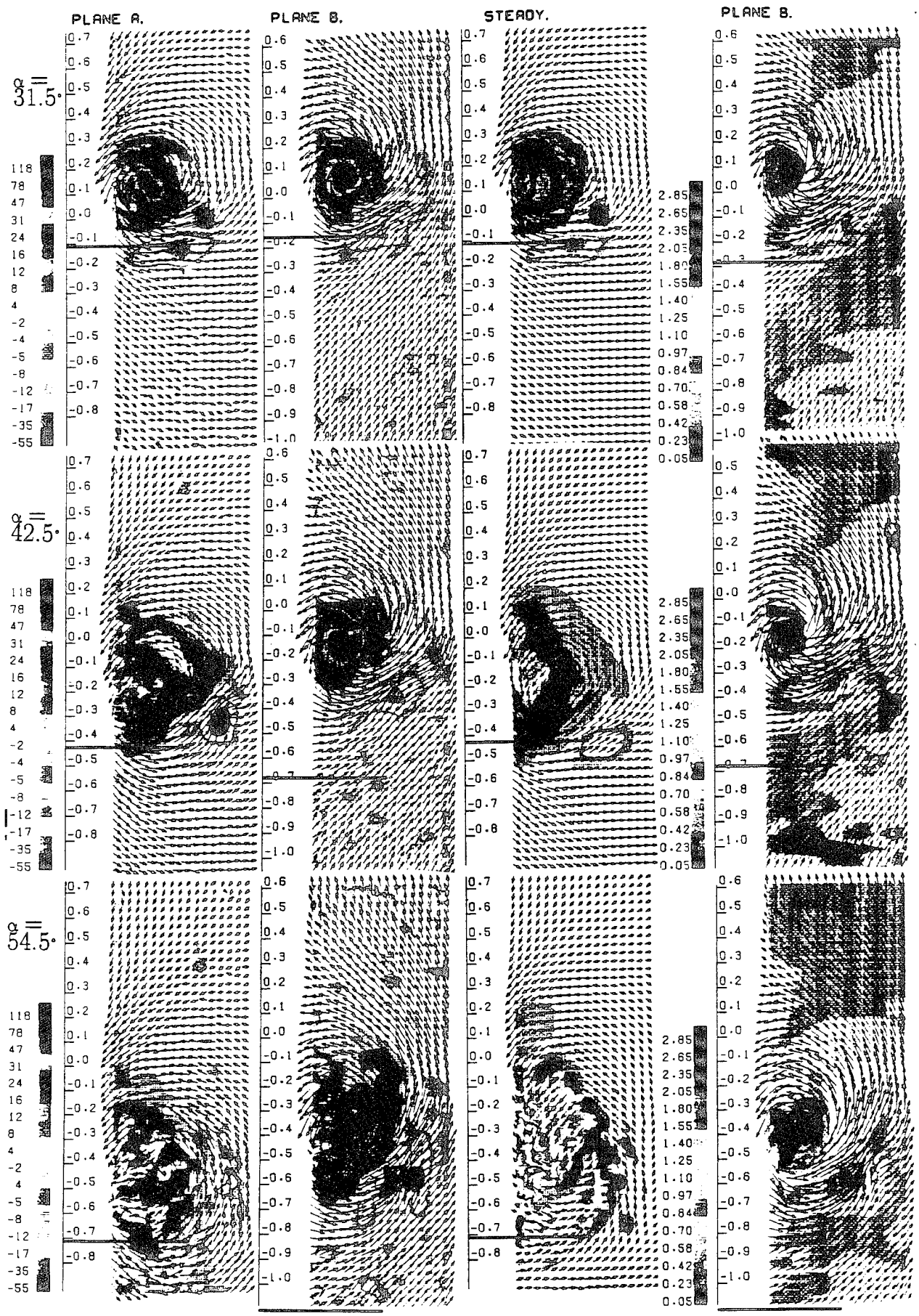

Fig. 15. Flow fields in the wake of the model Column 1:Vorticity and velocity in plane A during pitch–up. Column 2: Vorticity and velocity in plane B during pitch–up. Column 3: Vorticity and velocity for steady flow. Column 4: Axial component of velocity during pitch–up.

thick horizontal line shown in these frames represents the projection of the trailing edge on plane B. This provides an indication of the location of the wing.

Earlier studies[29] indicate that a seven–hole probe may interfere with the flow and actually induce vortex breakdown. Therefore this instrument can not be trusted to indicate when vortex breakdown occurs. On the other hand, seven–hole probe readings are reliable, if they indicate a coherent vortex.

We observe that the magnitude of the vorticity in the core remains essentially constant until $\alpha = 48°$. Once again this is in agreement with our earlier observation on breakdown. The vortex is pulled downward, following the motion of the wing. It starts at an elevation of about 0.2 at $\alpha = 28°$ and displaces to –0.3 for $\alpha = 48°$, but appears to be trailing the trailing edge with some delay. At higher angles of attack the vortex breaks down. Vorticity spreads out and reduces in magnitude. If we observe the velocity vectors for $\alpha = 68°$ we notice that the core lacks any organization, but not far from the center of the vortex, the velocity distributions are coherent and the flow pattern is consistent with the vortical motion.

In Fig. 14 we present the Y–component of the vorticity. In this Figure, we have captured the trailing edge vortex which is shed because of the dynamic motion of the wing which forces the sharp trailing edge downward.

In Figure 15 we present comparisons of velocity and vorticity fields along planes A and B for steady and unsteady cases. We also present the axial component of the velocity in terms of contours superimposed on the velocity vectors contained in the plane of measurement. A comparison between the steady and the unsteady case clearly indicates significant differences in the core of the vortex. Even at $\alpha = 54.5°$, the vorticity distribution in unsteady flow retains considerable levels and coherence. Another indication that the vortex has not broken down is the axial component of the velocity. We observe that at $\alpha = 42.5°$ the axial component is almost three times as high as the velocity of the free stream, whereas at $\alpha = 54.5°$, the core contains very low axial flow velocities.

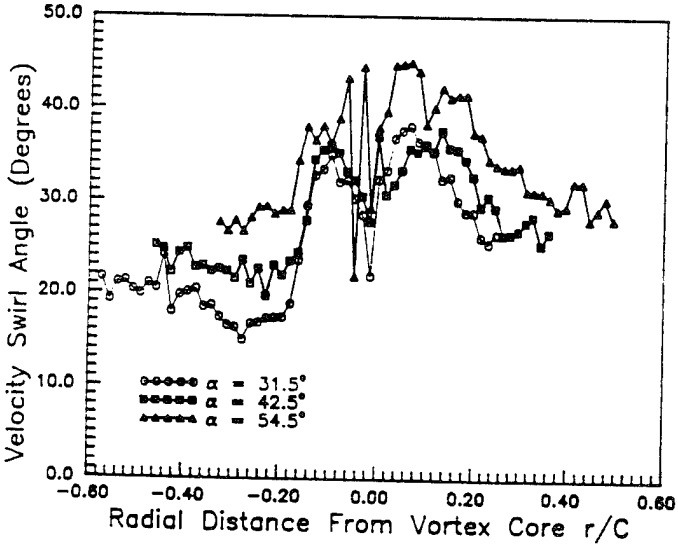

Fig. 16. Helical angle of the velocity vector across the vortex.

Finally, we present the helical angle of the streamlines. We define this quantity as the angle between the velocity vector and the axis of the vortex. In Fig. 16, we plot this quantity for three different values of the angle of attack, obtained during pitch up. It appears that higher helical angles are found in the core. Moreover, these angles increase as we move into breakdown. This fact implies that while the axial component of the velocity decreases as we enter breakdown, the swirling motion is sustained and thus larger helical angles are observed.

4. Conclusions

Evidence is presented here that during dynamic pitch–up motions, breakdown doe not creep up from downstream, but instead, its onset appears simultaneously along the entire chord of the wing. It then spreads radially outward. Mean and RMS pressure distributions as well as velocity field data were presented to confirm this finding. However, this phenomenon has not been observed before and more evidence is required to corroborate it.

It should be mentioned that the elevation of the vortex axis increases beyond $\alpha = 48°$ and loss of pressure suction could be attributed to this fact as well. However, it is believed that the dominant phenomenon is vortex breakdown.

The pressure distributions generated by such flow developments display a smooth behavior. In other words, unsteady stall should be smooth but perhaps harder to control.

Detailed information is presented for the first time on the structure of the flow during the hysteresis phase. Our data indicate that the tip vortices retain a core with concentrated large values of vorticity and a strong axial velocity component for angles of attack as large as 48°. Breakdown follows and eventually a bluff body wake pattern sets in.

5. Acknowledgement

This work was supported by the Air Force Office of Scientific Research, Project No. AFOSR–91–0310 and was monitored by Major Daniel Fant.

References

1. Lambourne, N. C., et al., "The Behavior of the Leading–Edge Vortices Over a Delta Wing Following a Sudden Change of Incidence." NPL Aero Report 1294–ARC 81 056, 1969.

2. Gad–el–Hak, M. and Ho,C.–M., "Three–Dimensional Effects on a Pitching Lifting Surface," AIAA Paper No. 85–0041, 1985.

3. Lee, Mario, Shih, C., and Ho, C.–M., "Response of a Delta Wing in Steady and Unsteady Flows," ASME 1987 Fluids Engineering Conference, Vol. 52, pp. 19–24, 1987.

4. Naumowicz, T., Jarrah, M. A., Margason, R. J., "Aerodynamic Investigation of Delta Wings with Large Pitch Amplitudes," AIAA Paper No. 88–4332, 1988.

5. Brandon, J. M., and Shah, G. H., "Effect of Large Amplitude Motions on the Unsteady Aerodynamic Characteristics of Flat–Plate Wings," AIAA Paper No. 88–4331, 1988.

6. Bragg, M. B. and Soltani, M. R., "An Experimental Study of the Effect of Asymmetrical Vortex Bursting on a Pitching Delta Wing," AIAA Paper No. 88–4334, 1988.

7. LeMay, S. P. et al., "Leading–Edge Vortex Dynamics on a Pitching Delta Wing," AIAA Paper No., 88–2559, 1988.

8. Soltani, M. R., Bragg, M. B. and Brandon, J. M., "Experimental Measurements on an Oscillating 70–degree Delta Wing in Subsonic Flow," AIAA Paper No. 88–2576.

9. Jarrah, M–A. M., "Low–Speed Wind–Tunnel Investigation of Flow about Delta Wings, Oscillating in Pitch to Very High Angle of Attack," AIAA Paper No. 89–0295, 1989.

10. Atta, R., and Rockwell, D., "Leading–Edge Vortices Due to Low Reynolds Number Flow Past a Pitching Delta Wing," AIAA Journal, Vol. 28, pp. 995–1004. 1990.

11. Magness, C., Robinson, O., and Rockwell, D., "Control of Leading–Edge Vortices on a Delta Wing," NASA/AFOSR/ARO Workshop on Physics of Forced Separation, 1990.

12. Brandon, J. M., and Shah, G. H., "Unsteady Aerodynamic Characteristics of a Fighter Model Undergoing Large–Amplitude Pitching Motions at High Angles of Attack, AIAA Paper No. 90–0309, 1990.

13. Herbst, W. B., "Dynamics of Air Combat," Journal of Aircraft, Vol. 20, No. 7, July 1983.

14. McAtee, T. P., "Agility – Its Nature and Need in the 1990s. Society of Experimental Test Pilots Thirty First Symposium Proceedings, 1987.

15. Hamilton, W. L., and Skow, A. M., "Operational Utility Survey, Supermaneuverability," AFWAL–TR–85–3020, September 1984.

16. Nguyen, L. T., and Gilbert, W. P., "Impact of Emerging Technologies on Future Combat Aircraft Agility," AIAA Paper No. 90–1304, 1990.

17. Tobak, M. and Peake, D. J., "Topology of three–dimensional separated flows," Ann. Rev. Fluid Mech., Vol. 14, pp. 61–85, 1982.

18. Peake, D. J., and Tobak, M., "Three–dimensional Separation and reattachment," High Angle–of–Attack Aerodynamics, AGARD/VKI Lecture Series No. 121, Paper No. 1.

19. Hunt, B., "The Role of Computational Fluid Mechanics in High–Angle–of–Attack eerodynamics," High Angle–of–Attack Aerodynamics, AGARD/VGI Lecture Series No. 121, Paper No. 6.

20. Lee, M. and Ho, C.–H., "Lift Force of Delta Wings," Applied Mechanics Reviews," Vol. 43, pp. 209–221, 1990.

21. Taylor, S. L., Kjelgaard, S. O., Weston, R. P., Thomas, J. L., and Sellers III, W. L., "Experimental and Computational Study of the Subsonic Flow about a 75° Swept Delta Wing," AIAA Paper No. 87–2425, 1987.

22. Meyers, J. F. and Hepner, T. E., "Measurement of Leading Edge Vortices from a Delta Wing Using a Three–Component Laser Velocimeter," AIAA Paper No. 88–2024, 1988.

23. Payne, F. M., Ng, T. T. and Nelson, R. C., "Visualization and Wake Surveys of Vortical Flow over a Delta Wing," AIAA Journal, Vol. 26, pp. 137–143, 1988.

24. Kegelman, J. T. and Roos, F. W., "Effects of Leading–Edge Shape and Vortex Burst on the Flowfield of a 70–degree–Sweep Delta Wing," AIAA Paper No. 89–0086, 1989.

25. Nelson, R. C., and Visser, K. D., "Breaking Down the Delta Wing Vortex," AGARD Conference Proceedings, No. 494.

26. Washburn, A. E., "The Effect of Freestream Turbulence on a Vortical Flow Over A Delta Wing," George Washington University, M. S. Thesis, December 1990.

27. Anders, K., "Measurement of velocity distribution in delta wing vortices using laser–Doppler velocimetry," VKI PR 1981–03.

28. Muylaert, J., "Effect of Compressibility on vortex bursting no slender delta wings," VKI PR 1980–21, 1980.

29. Rediniotis, O. K., Hoang, N. T., and Telionis, D. P., "Multi–Sensor Investigation of Delta Wing High–Alpha Aerodynamics," AIAA Paper No. 91–0735.

30. Stewartson, K., and Hall, M. G., "The Inner viscous solution for the core of a leading–edge vortex," J. Fluid Mech., Vol. 15, pp. 306–338.

31. Verhaagen, N. G., and Kruisbrink, A. C. H., "Entrainment effect of a leading–edge vortex," AIAA J., Vol. 25, pp. 1025–1032.

32. Hoang, N. G. and Telionis, D. P., "The Dynamic Character of the Wake of an Axisymmetric Body at an Angle of Attack," AIAA Paper No. 91–3268.

also
Experiments in Fluids
in press

AIAA-93-0185

3-D LDV Measurements Over a Delta Wing in Pitch-Up Motion

N. T. Hoang, O. K. Rediniotis and D. P. Telionis
Department of Engineering Science and Mechanics
Virginia Polytechnic Institute
and State University
Blacksburg, VA 24061-0219

31st Aerospace Sciences Meeting & Exhibit
January 11-14, 1993 / Reno, NV

3-D LDV Measurements Over a Delta Wing in Pitch-Up Motion

N. T. Hoang*, O. K. Rediniotis** and D. P. Telionis***
Department of Engineering Science and Mechanics
Virginia Polytechnic Institute and State University
Blacksburg, VA 24061-0219

Abstract

A detailed investigation of the velocity and vorticity fields over a 75°-sweep delta wing undergoing a ramp-like pitch-up motion is carried out through three-component LDV measurements. The evolution of the flow field in four planes normal to the free-stream is captured at 100 time instants through the wing motion. The delta wing is pitched through angles of attack ranging from 28° to 68°. From the velocity data at each incidence, the corresponding vorticity field is calculated. Hysteresis effects on vortex development and breakdown, with respect to the steady case, are studied through axial velocity and vorticity contours. The topology of streamlines and vortex lines are compared with the corresponding topologies of the steady case. It is found that vortex breakdown can be detected first by a drastic reduction of the axial velocity. In fact, this effect is developing asymmetrically, beginning in the inboard side of the vortex. This is followed by a reduction of the axial vorticity component and finally by a complete reversal of the circumferential vorticity component. Some effects of parameters like Reynolds number, model thickness, non-dimensional pitch-up rate, free-stream turbulence on the developing flow field are addressed.

Introduction

The aerodynamics of modern combat aircraft is dominated by axial vortices emanating from the LEX's, the swept wings, or the canards. The behavior of such vortices at high angles of attack has been vigorously investigated in the past decade. A short literature review and a number of references can be found in an earlier paper of the present authors[1]. Of greater interest to the designers are perhaps the characteristics of such aerodynamic structures evolving in time. Laboratory experiments of dynamic motions involve pitching or rolling oscillations, or ramp-like pitching motions. A collection of over twenty contributions involving maneuvers of a delta wing was included in Ref. 2. This information was collected in the form of a table, listing various parameters for each investigation. A similar but not as complete table appeared in Ref. 1.

The basic aerodynamic characteristics were obtained by most other investigators via flow visualization and the measurement of forces and moments as described in Ref. 1. Very little information is available about the velocity field over a dynamically moving delta wing. Rockwell and his associates[3-5] developed a PIV method and obtained the unsteady velocity field along a plane. This method generates only the components of the velocity contained in a plane which was chosen in Refs. 4-5 to be normal to the wing. The axial velocity component which is very indicative of phenomena like vortex breakdown could not be obtained. The axial component of the vorticity can be calculated in terms of velocity data contained in a plane but again the circumferential component of vorticity can not be derived through PIV measurements. Moreover, in Ref. 4-5 the velocity field was captured during the pitch up motions but only at a specific angle of attack.

Mian et al.[6] employed a laser-Doppler velocimeter to capture the unsteady field developing over a pitching delta wing. However, they were able to obtain only the axial component of velocity and confined their measurements to angles of attack less than 39°. Moreover, these authors do not ensemble average over several realizations of the motion. Instead, they employ filters in order to clean their signals.

The present authors reported on a similar study of the dynamic field over a pitching-up delta wing[1]. Employing a seven-hole prove calibrated for dynamic motions, they were able to measure all three components of the velocity and therefore calculate all components of vorticity. In fact, it was possible to record the entire history of the motion from an initial value of angle of attack α= 28°, up to α = 68°. This technique generated information on all three components of the velocity and vorticity on a tight grid, for a period of the motion. The temporal evolution of these fields thus was recorded. However, the presence of a probe may interfere with the measurements if vortex breakdown is imminent. Such data therefore can be trusted as long as they do not indicate breakdown, because it could not be possible to confirm that this phenomenon is induced by natural causes rather than by the interference of the probe. Moreover, the use of mechanical probes which must be inserted in the flow prohibits measurements over a moving wing. Instead, all measurements reported in Ref. 1. were obtained along planes immediately downstream of the trailing edge of the wing.

In the present paper we employ laser-Doppler velocimetry which is non-intrusive. Moreover, it allows measurements along planes that cut the model and therefore the method can provide unsteady information over the moving wing. This arrangement allows careful documentation in the time domain of all velocity and vorticity components. To the knowledge of the authors, this is the first time that all three components of vorticity were measured over maneuvering delta wings. It is now possible to monitor all criteria for vortex breakdown in the dynamic domain, namely, the vanishing of the axial velocity, the reversal of the circumferential of vorticity and the drastic reduction of the axial component of vorticity in the core of the vortex.

Facilities and Instrumentation

Research was conducted in the Engineering Science and Mechanics (ESM) Water Tunnel. This facility has a test section of 10" × 12" and can achieve speeds up to 9 ft/sec

* Research Associate
** Assistant Professor
*** Professor, Associate Fellow, AIAA

at turbulence levels ranging from 0.6% to 1.5%. A detailed description of this facility and its calibration is included in Refs. 7 and 8.

Measurements were carried out with laser-Doppler velocimetry (LDV). Such systems have been employed in the ESM laboratory for about fifteen years and a few generations of DANTEC and TSI complete units are available. The present data were obtained by a TSI, three-beam two-component LDV system. Two of the beams are shifted at 60 MHz and 40 MHz, respectively. It is thus possible to separate the two components by electronic filters and therefore employ only one photomultiplier.

The original system described in Refs. 8 and 9 was capable of obtaining two velocity components in planes xz parallel to the side walls of the tunnel (the x-direction is aligned with the freestream and the z direction is along the vertical as shown in Fig. 1). Moreover, the design of the traversing system allowed traversing in the directions of x and z. This design was dictated by the need to study nominally two-dimensional flows. In the present effort we modified the LDV components and the traversing system in order to obtain all three velocity components and traverse along planes yz. This is necessary in order to obtain data along planes that cut across the delta wing vortices.

A large optical bench and a more powerful laser (35 mW, Helium-Neon) were purchased. The TSI design was then modified to mount the laser next to the train of optics instead of underneath it. The long side of the optical bench and therefore the direction of the optical beams was positioned normal to the axis of the test section. The same mirror tower was employed for traversing. The tower is now mounted on a precision sliding table to allow traversing in the y direction. The position of the upper mirror of the tower is controlled by a lead screw thus facilitating traversing in the z-direction. Figure 1 displays the LDV system on the optical bench next to the test section. A second set of mirrors was also mounted on traversing brackets and the system allows directing the beams either from the side wall of the tunnel or from the ceiling of the tunnel. In the first case (beams through the front window) the two velocity components measured are along axes x' and y' (or equivalently along x and z, as shown in Figure 1(a)). In this case, following the optics train a pair of mirros project the laser beams through a 250 mm f/4 lens. In the second case, (beams through the top window) the measured velocity components are along axes x'' and y'' (or equivalently along x and y as shown in Figure 1(b)). In this case the optics train is followed by three mirrors that project the laser beams through a 250 mm f/4 lens. In this way, all three components of the velocity can be obtained, although not all simultaneously.

Traversing in the y and z directions is achieved by two stepping motors and monitored by two LVDT's. The latter provide an independent analog feedback to confirm the accurate positioning of the measuring volume. In this way, two-dimensional grids along planes yz can be traversed. The accuracy in positioning the measuring volume is 0.2mm. Phase referencing and instantaneous angle of attack information is obtained through optical methods. The optical encoder used has an accuracy of 0.1°. To obtain data along different yz planes, the entire optical bench is resting on a manual traversing system and can be traversed in the x-direction.

The entire operation is controlled by two serially communicating laboratory computers which are programmed to operate the pitching mechanism and the stepping motors, collect the information on the instantaneous angle of attack, perform the LDV data acquisition, reduce the data and transfer it to a mainframe IBM 3090 for calculations and plotting. The entire data acquisition process is fully automated. The only processes

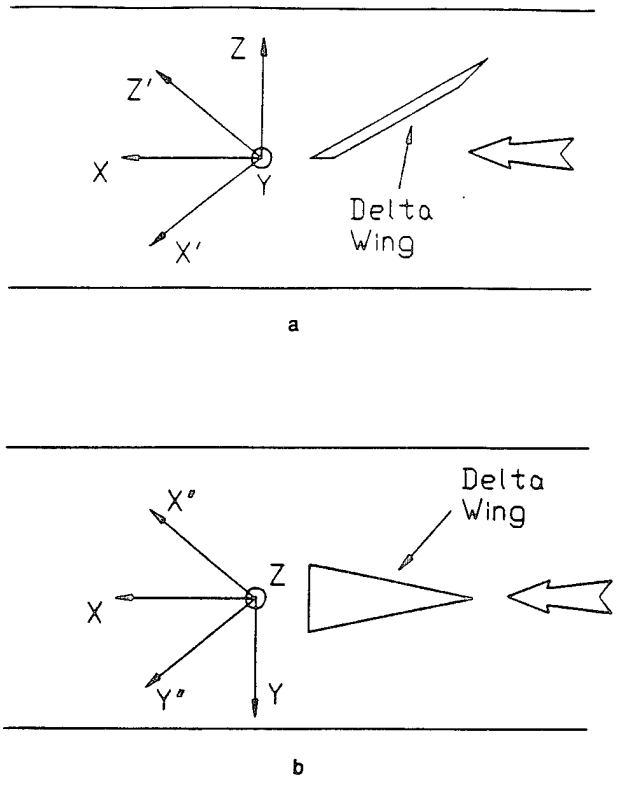

Fig. 1. The coordinate systems used for the LDV measurements: (a) side view, (b) top view.

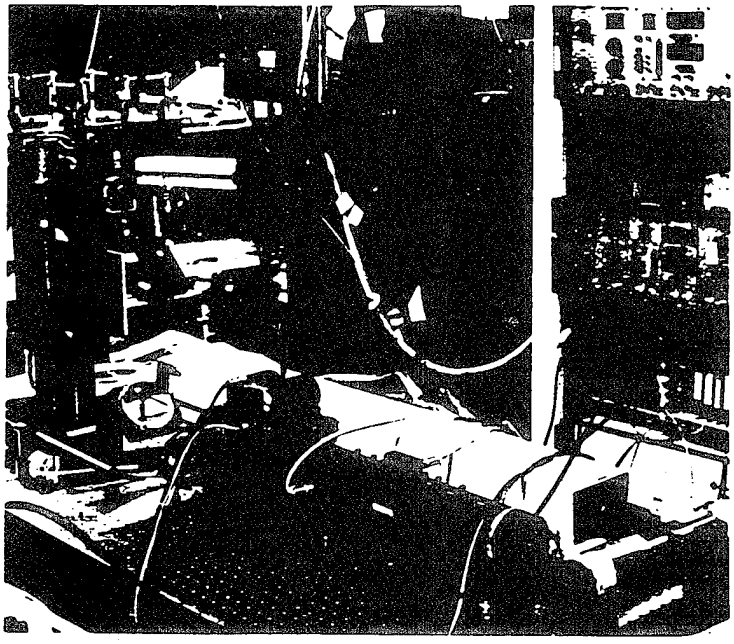

Fig. 2. The LDV system next to the water tunnel test section.

requiring manual operation are traversing in the x-direction (for a different plane of measurement) and seeding the water every about 12 hours.

Models, their Dynamic Motion and Data Acquisition

In this paper we report on the continuation of our effort to study the aerodynamics of delta wings in pitch-up motions. It was therefore imperative to design and construct models similar to the ones employed in our earlier studies[1,10]. The shape of these models was dictated by structural considerations and by needs to mount inside them a traversing mechanism and a LDV fiber-optic probe. The thickness of such models is not negligible as shown in Fig. 3(a). Both, thick (Fig. 3(a)) and thin models (Fig. 3(b)), were used to provide some information on the effect of thickness on the developing flow.

The models were mounted on brackets that allow them to pitch about any axis. We chose to pitch about the apex in order to be able to compare with data obtained in the wind tunnels with our other models. It should be noted that pitching about the apex preserves the conicity of geometry for all angles of attack. Thus the solid surface would not interfere with the conicity of the flow. Any departure from conical flow should be due to nonlinear effects of the flow itself. Pitch-up schedules were chosen to match earlier studies. The angle of attack was given a ramp function as shown in Fig. 4. The above pitch-up schedule, with a free stream velocity of $U_\infty = 0.38m/sec$ and a chord length of $C = 0.142m$ corresponds to an average non-dimensional pitch rate of

$$k_{ave} = \frac{\dot{\alpha}_{ave} C}{2U_\infty} = 0.06$$

where $\dot{\alpha}_{ave}$ is the average pitch-up rate in rad/sec. The Reynolds number was about 5.4×10^4. At each measuring point data were taken and ensemble-averaged for 20 realizations of the motion.

Data were obtained along four fixed vertical planes A through D, as shown in Fig. 5. The planes are arranged in two pairs of neighboring planes thus allowing the calculation of derivatives in the x-direction and therefore the calculation of all three vorticity components. One pair of planes was positioned immediately downstream of the trailing edge to provide data comparable with results obtained earlier. Another pair was positioned over the wing as shown in Fig. 5. Measurements were obtained on planes C, D almost all the

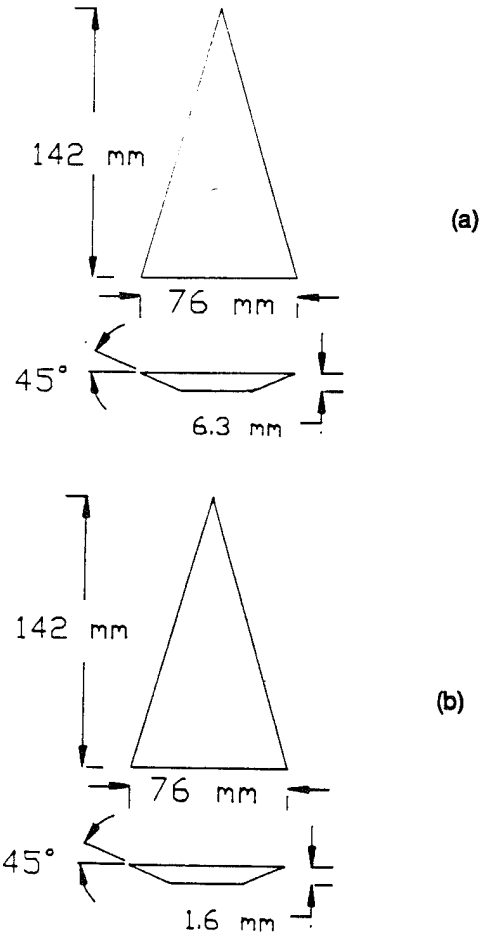

Fig. 3. The delta wing models used: (a) thick model, (b) thin model.

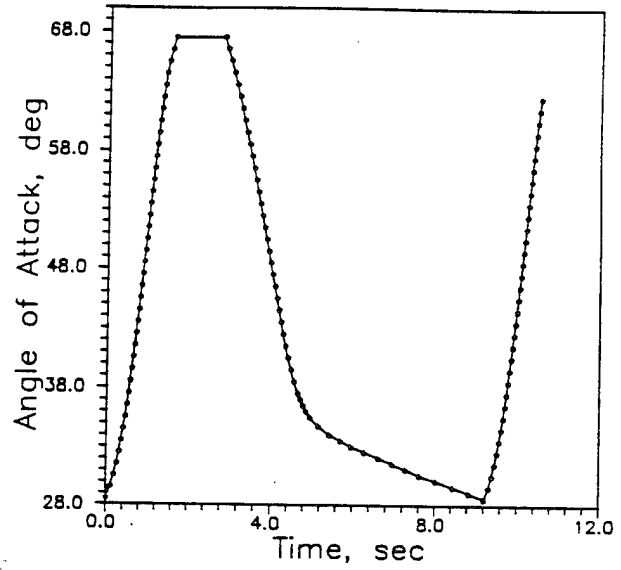

Fig. 4. The dynamic motion of the model, presented as an angle of attack temporal function.

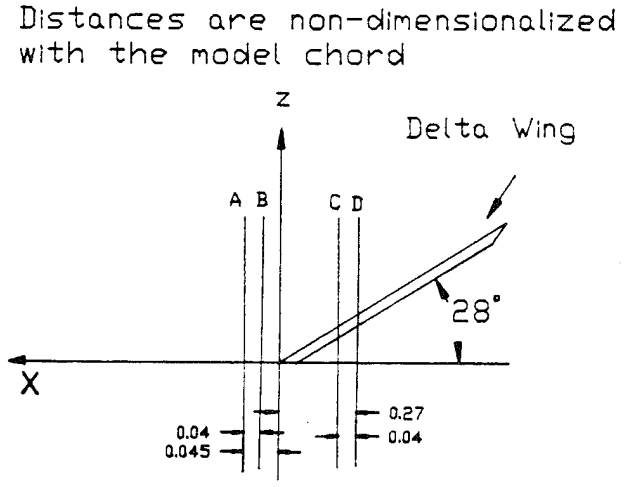

Fig. 5. Definition of the planes along which LDV measurements were performed.

way down to the surface of the model. As time increases, the size of the measuring domain above the surface of the model is therefore increasing.

Results and Discussion

As is usually the case, with modern methods of data acquisition, we obtained an immense amount of data and it is very difficult to present results in a comprehensive way. The complexity is also due to the fact that we have information on two three-dimensional vector fields, the velocity and vorticity fields, defined on the same space. On the other hand, this information is limited to planes normal to the direction of the oncoming flow.

It would be preferable to have data along planes normal to the wing which would be closer to normal to the axis of the developing vortex. But this would require traversing the optical beams together with the wing. This can be done only with a fiber optic probe mounted on the model, which the present team has implemented and plans to use in the near future. For the information obtained here, we present vector components along the plane of measurement and normal to them. We also present components along the axis of the vortex. This requires some calculations because this axis moves with the wing and it is not even fixed in the frame of the wing. The location of the axis is determined by calculating the center of the vortex at each instantaneous position of the wing and then connecting the apex to the center of the vortex. This axis will be denoted in this paper as the η-axis.

In Fig. 6 we present the in-plane velocity vectors and on the same frames we superimpose contours representing the axial component of velocity (left column of Fig. 6), and vorticity (right column), namely the component along the x-axis. In all the plots the velocity components have been non-dimensionalized with the free-stream velocity U_∞ and the vorticity components with the quantity U_∞/C. The vertical axis represents z/S_o where S_o is the wing span: S_o = 76 mm. Each frame presents instantaneous information captured while the wing passes through a specific angle of attack. Data are available at many intermediate positions of the wing. What is presented now are essentially snapshots of a developing phenomenon. The data plotted here present the development of one of the two leading-edge vortices over the delta wing.

The vectors of Fig. 6 indicate the rotational character of the cross-section of the vortex. As the wing suction surface retreats, the vortex follows it in its downward motion. The behavior of the axial velocity component is one of the clear indications of the impending vortex breakdown. Columnar vortices developing inside tubes in laboratory experiments display a well-behaved pattern of vortex breakdown. The axial velocity goes to zero at the core of the vortex and then reverses direction, while the recirculating region spreads away from the center. In the present case, the velocity decrease appears first in the inboard region and moves towards the core of the vortex in an asymmetric fashion. This feature of the flow may be due to the way we define the axial component of the velocity. A more appropriate way may be to present contours of the velocity component along the axis of the vortex itself. This is done in Fig. 7. It now appears that the asymmetry of the developing pattern although still present, is not as pronounced. Moreover, the low-speed region approaches the core from the wing surface. Such asymmetry has previously been observed by other researchers[11] in steady flow.

In the vorticity contour plots the core of the vortex appears as a maximum of the axial vorticity. Well-ordered rings of levels of vorticity indicate a coherent vortex. Breakdown is on the other hand, indicated by an overall reduction of the axial component of vorticity and a level of randomness in its distribution. This is clearly observed in Fig. 6.

In Fig. 8 we present similar data obtained in steady flow with the wing fixed at the same angles of attack. The comparison of Figs. 8 and 6 indicates a familiar time lag which differentiates the truly unsteady from the quasi-steady motion. It is obvious that the delay becomes more pronounced as the angle of attack increases.

Similar data obtained along plane A downstream of the trailing edge of the wing indicate that the vortex is totally broken down from the very first frame (Fig. 9). This does not seem to agree with our wind tunnel tests which indicate a very coherent vortex at the same angle. Wind tunnel tests were obtained via seven-hole probes which may have interfered with the flow to induce breakdown. In fact, to avoid this uncertainty we undertook the present experimental effort. And yet, the seven-hole probe data indicate coherent vortices in the trailing edge region whereas the present LDV data indicate broken down vortices. The above observation gives us the opportunity to address here the influence on the flow of parameters like model thickness and Reynolds number.

To study the effect of model thickness, experiments were conducted with a thin model (Fig. 3(b)). Except for the thickness, all flow parameters were kept the same. Figure 10 presents axial velocity contours on plane D for the thin model, at several time instants. Comparing figures 10 and 6, it is obvious that breakdown is significantly delayed for the thin model case. Moreover, for this case, the axial velocity component attains higher values. The reader should note that the model used in the wind tunnel experiments was significantly thinner than the one used here (the thicker one, Fig. 3(a)). Their non-dimensional thickness is t/C = 0.02 and 0.045, respectively.

To study the Reynolds number effects, steady data were taken over the wind on a plane normal to the free stream for two Reynolds numbers: 3×10^4 and 6×10^4. Figure 11 presents axial velocity contours for the two cases. It is obvious that for the lower Re case breakdown has already been initiated. However, for the higher Re case the vortex is still coherent. This Reynolds number effect might be small (most investigators indicate that breakdown is essentially an inviscid instability). It should be noted here that the wind and water tunnel experiments were conducted at Re = 25×10^4 and 5.4×10^4, respectively.

The effects discussed in the above two paragraphs along with non-dimensional pitch rate (k_{ave} = 0.0089, 0.06 for the wind and water tunnel experiments, respectively) and free-stream turbulence (higher in the water tunnel) could account for the differences observed between the two experiments.

Of greater interest here is the circumferential component of vorticity. Figs. 12 and 13 present in-plane vorticity vectors along planes D and A, respectively. Let us first observe the frames on plane D. At the beginning of the motion the sense of rotation is counterclockwise. This means that the vortex lines follow the same helical sense as the streamlines. However, as breakdown enters the picture, the sense is reversed and the helical angle of the vorticity braid changes sign. The above observation should, in fact, be expected if one recalls Biot-Savart's law and how it relates the circumferential vorticity component to the axial velocity component: if the former has a positive sign (counter-clockwise direction is defined as positive) it induces a positive sign to the latter and vice-versa. In other words, positive circumferential vorticity accelerates the core axial velocity, but negative vorticity slows it down, until stagnation is achieved. On plane A the vortex is broken down even at the first frame. This explains the negative sense of the circumferential vorticity in Fig. 13 as early as $\alpha = 28.5°$. All subsequent frames exhibit the same sense of vorticity direction and therefore are not presented here.

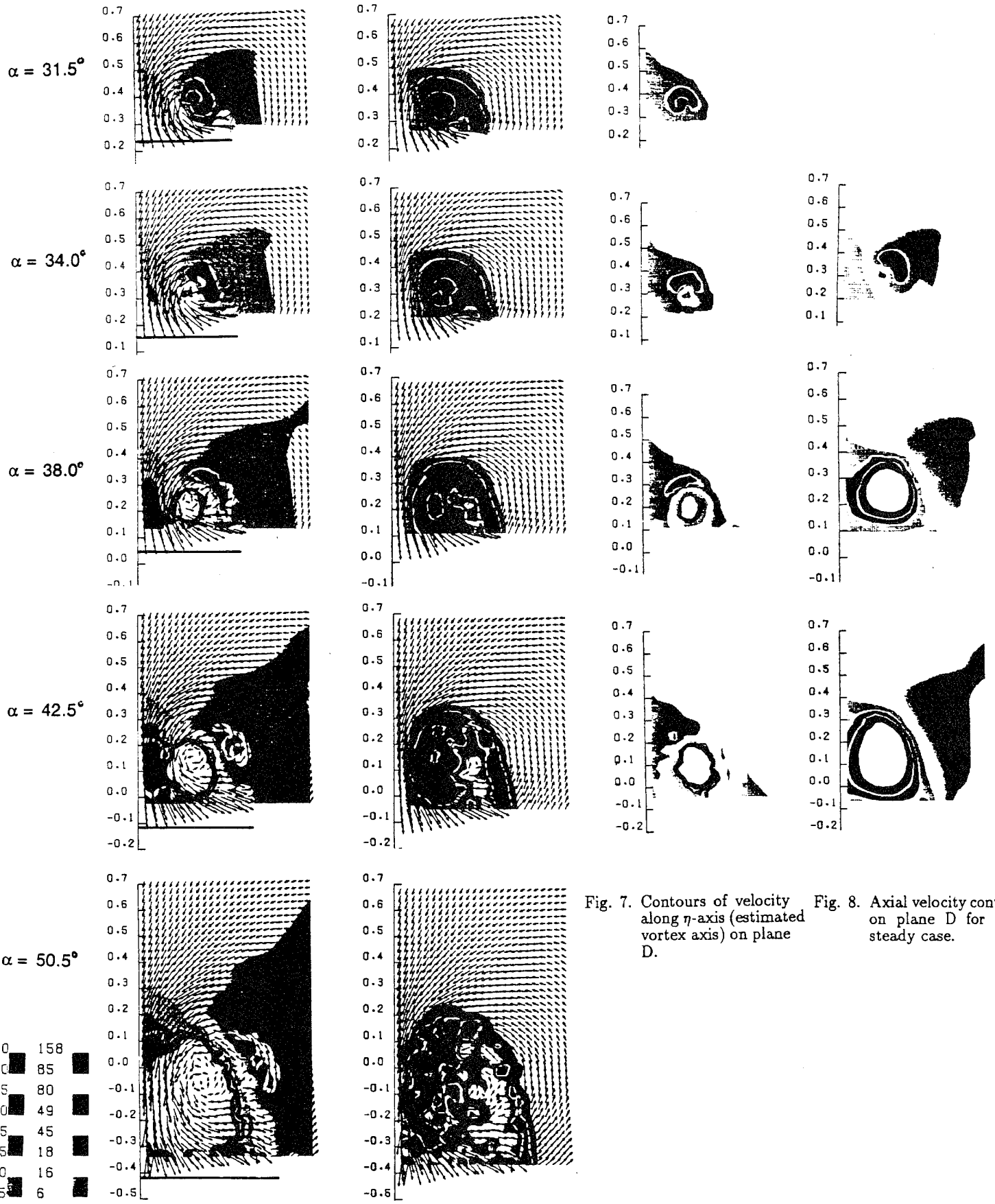

Figure 6. Time history of the flowfield along plane D. Frames present in-plane velocity vectors superimposed on axial velocity (left column) and axial vorticity (right column) contours.

Fig. 7. Contours of velocity along η-axis (estimated vortex axis) on plane D.

Fig. 8. Axial velocity contour on plane D for the steady case.

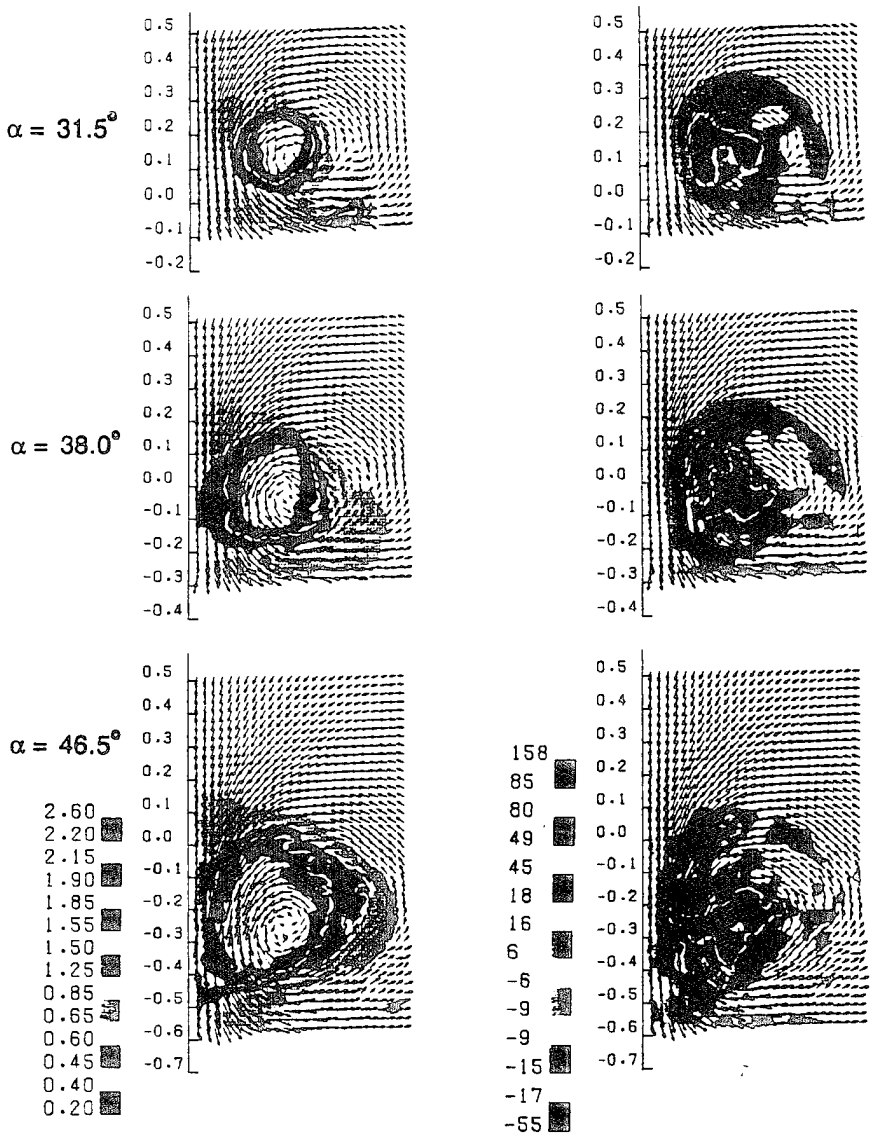

Fig. 9. Flowfield development on plane A. In-plane velocity vectors superimposed on axial velocity contours (left column) and axial vorticity contours (right column).

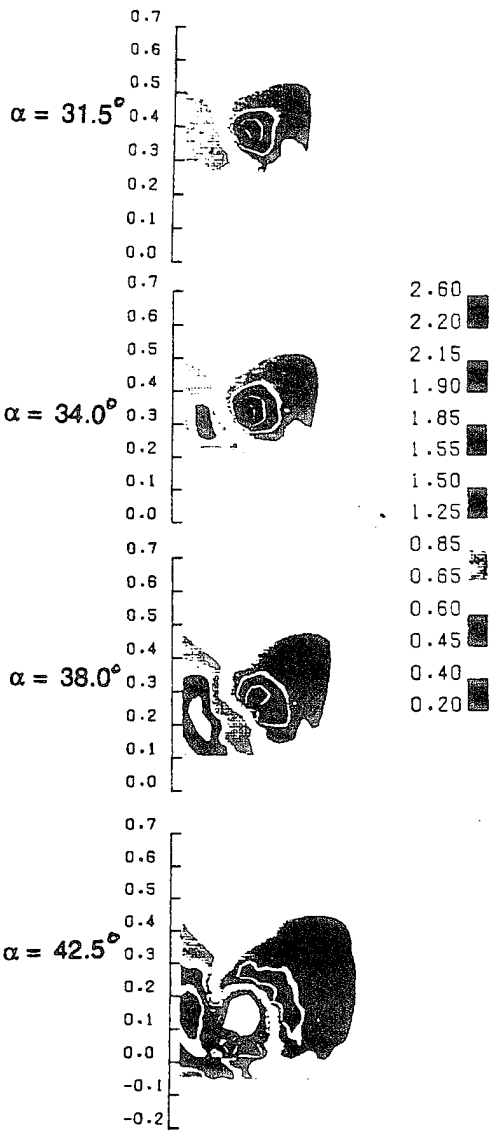

Fig. 10. Axial velocity development along plane D for the thin delta wing case.

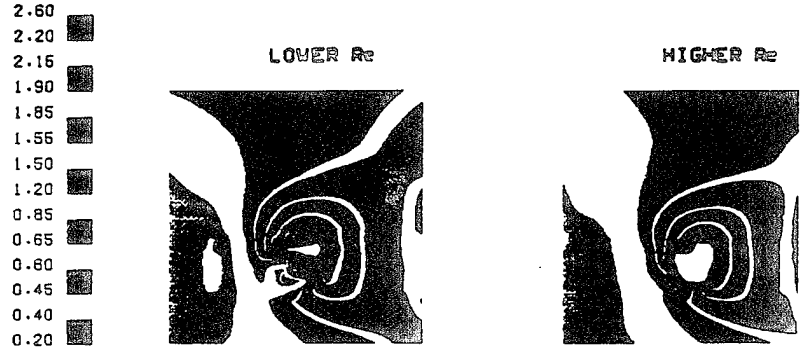

Fig. 11. Steady axial velocity contours along the same plane over the wing at $\alpha = 35°$, for two different Reynolds numbers: 3×10^4 (left), 6×10^4 (right).

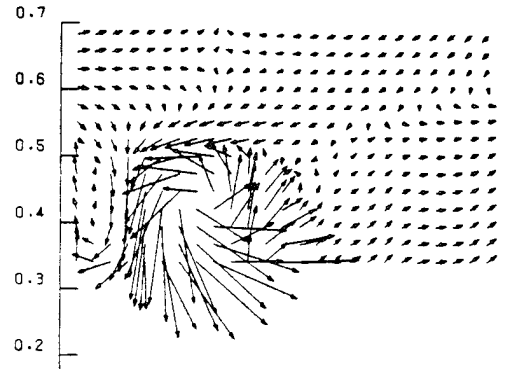

α=28.5°

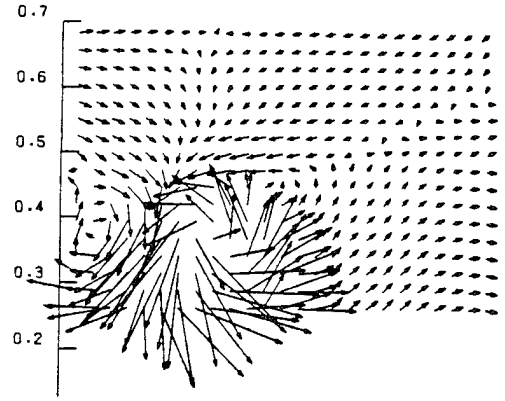

α=31.5°

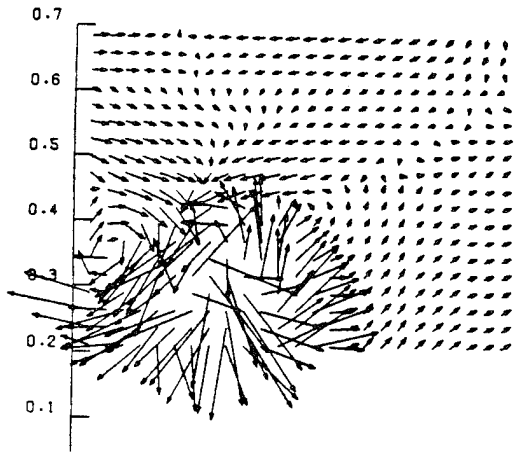

α=34.0°

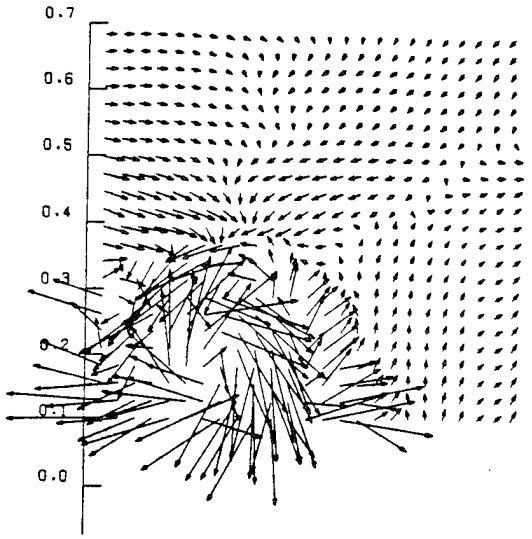

α=38.0°

Fig. 12. Time history of the in-plane vorticity vectors along plane D.

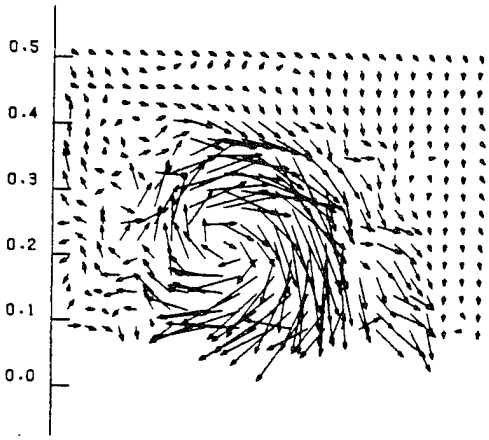

α=28.5°

Fig. 13. In-plane vorticity vectors along plane A.

In steady flow and for moderate angles of attack, the flow over a delta wing is nearly conical. Moreover, streamlines that emanate from the leading edge roll around the conical vortex and spiral inward. Thus, particles released along the leading edge roll around the vortex a few times but eventually reach the core. This behavior can be corroborated experimentally by plotting sectional streamlines along a plane cutting through the vortex. The streamline pattern should have a stable focus[4]. However, during the dynamic motion the flow seems to undergo a topological alteration. The focus of the sectional streamlines becomes unstable. Figure 14 presents such a pattern along plane D at $\alpha = 32^{\circ}$. As shown there the streamlines are spiraling outwards. The lack of saddle points on the symmetry plane in Figure 14 is due to the coordinate system in which the velocity components have been expressed (system xyz). If the velocity components are expressed in a coordinate system aligned with the instantaneous vortex axis (η-axis), the streamline pattern exhibits a saddle point S on the symmetry

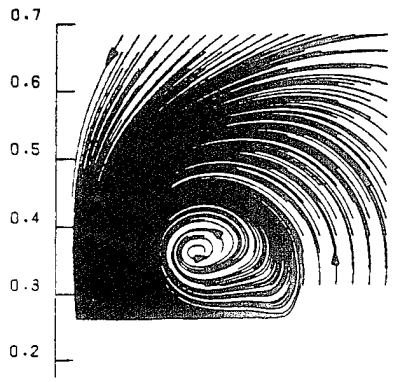

Fig. 14. Sectional streamline pattern on plane D, during pitch-up, at $\alpha = 32°$. Velocity components expressed in xyz system.

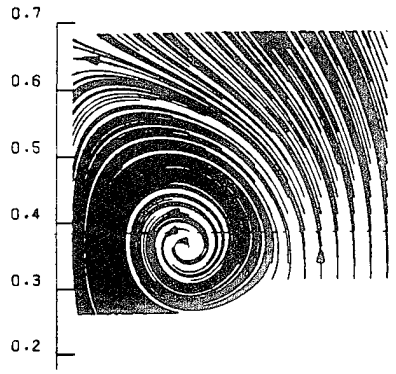

Fig. 15. Sectional streamline pattern on plane D, during pitch-up, at $\alpha = 32°$. Velocity components expressed in a system aligned with the vortex axis.

plane (Fig. 15). There should be another saddle point on the symmetry plane, right above the wing (not shown in the figure).

Conclusions

The development of the velocity and vorticity fields over a 75°-sweep delta wing in pitch-up motion has been investigated in detail through three-component LDV measurements.

It was found that the phenomenon of breakdown develops in an asymmetric fashion. This means that high axial velocity regions coexist with low ones in the vortex core. In fact, it appears the vortex breakdown is signaled by axial velocity reduction a little sooner than by the decrease in vorticity coherence.

The sense of the circumferential vorticity component was found to be closely associated with vortex breakdown. At a certain cross-section of the vortex, in pre-breakdown stages, this sense is positive (counter-clockwise). As the angle of attack increases a negative circumferential vorticity region gradually extends from the wing's inboard region towards the vortex core and finally takes over so that at post-breakdown stages the circumferential vorticity has totally reversed its sign. Cross flow streamline patterns indicate a focus which for unsteady flows proved to be unstable.

Time lag phenomena between the steady and the unsteady cases are obvious and become more pronouced in the later stages of the motion.

Model thickness has a very clear effect on the flow development. The thinner model sustains a coherent leading-edge vortex in pre-breakdown stage up to higher angles of attack and achieves higher levels of axial velocity and vorticity.

Tests are currently being conducted to study the effects of pitch rate and Reynolds number on the evolution of the flow.

References

1. Rediniotis, O. K., Klute, S. M., Hoang, N. T. and Telionis, D. P., "Pitch Up Motions of Delta Wings," AIAA, Paper # 92-0278, Reno, NV, Jan. 1992.
2. Rediniotis, O. K., "The Transient Development of Vortices Over a Delta Wing," Ph.D. Dissertation, VPI & SU, October 1992.
3. Atta, R. and Rockwell, D., "Leading Edge Vortices Due to Low Reynolds Number Flow Past a Pitching Delta Wing," AIAA Journal, Vol. 28, pp. 995-1004, 1990.
4. Magness, C., Robinson, O. and Rockwell, D., "Instantaneous Topology of the Unsteady Leading-Edge Vortex at High Angles of Attack," submitted for publication, August 1991.
5. Magness, C., Robinson, O. and Rockwell, D., "Unsteady Crossflow on a Delta Wing Using Particle Image Velocimetry," Journal of Aircraft, Vol. 29, pp. 707-709, July-August, 1992.
6. Mian, J. J., Chang, R. C., Chou, J. H. and Lin, C. K., "Nonuniform Motion of Leading-Edge Vortex Breakdown on Ramp Pitching Delta Wings," AIAA Journal, Vol. 30, pp. 1691-1702, July 1992.
7. Koromilas, C., and Telionis, D. P., "Unsteady Laminar Separation - An Experimental Study," Journal of Fluid Mechanics, Vol. 94, Part 2, pp. 347-384, 1980.
8. Mathioulakis, D. S., and Telionis, D. P., "Pulsating Flow over an Ellipse at an Angle of Attack," AIAA/ASME 4th Fluid Mechanics, Plasma Mechanics & Lasers Conference, AIAA Paper #86-1106, 1986, also, Journal of Fluid Mechanics, Vol. 201, pp. 99-121, 1989.
9. Mathioulakis, D. S. and Telionis, D. P., "Velocity and Vorticity Distribution in Periodic Separation Flow," Journal of Fluid Mechanics, Vol. 184, pp. 303-333, November 1987.
10. Rediniotis, O. K., Hoang, N. T., and Telionis, D. P., "Multi-sensor Investigation of Delta Wing High-Alpha Aerodynamics," AIAA Paper No. 91-0735, Reno, Nevada, Jan 1991.
11. Kegelman, J. T. and Roos, F. W., "Effects of Leading-Edge Shape and Vortex Burst on the Flowfield of a 70-Degree-Sweep Delta Wing," AIAA Paper No. 89-0086, Reno, NV, Jan. 1984.

AIAA J. in press

FLOW CONTROL OVER A MANEUVERING DELTA WING AT HIGH ANGLES OF ATTACK

by

Sandra M. Klute*, Othon K. Rediniotis† and Demetri P. Telionis††
Department of Engineering Science and Mechanics
Virginia Polytechnic Institute and State University
Blacksburg, VA 24061-0219

Abstract

The possibility of delaying vortex breakdown to higher angles of attack by employing control surfaces is studied experimentally. The effect of an apex flap is tested for fixed and dynamically pitching delta wings. Flow visualization, surface pressure measurements and laser-Doppler velocimetry are employed to map out pressure, velocity and vorticity fields. It is found that a drooping apex flap can delay vortex breakdown by an angle of 8° beyond the steady flow breakdown angle of attack. The apex flap effect is equally pronounced in dynamic maneuvers.

Introduction & Background

At high angles of attack, vortex breakdown dominates the aerodynamics of swept lifting surfaces. The occurrence of this phenomenon is accompanied by drastic changes in the pressure distribution, which in turn strongly affect the attitude of an aircraft. It is desirable to control the onset of vortex breakdown, delay it, or induce it at will. This is particularly needed for controlled flight at high angles of attack.

Various methods have been tested to control vortex breakdown at high angles of attack. Most of the significant work in this area until 1990 was reviewed by Lee and Ho[1]. Recently, attention has been paid to the use of blowing and suction to achieve localized control of the

* Graduate Student
† Assistant Professor
†† Professor, Associate Fellow AIAA

leading edge vortices. Experiments have been performed by Wood and Roberts[2], and Wood, Roberts and Lee[3] in which steady blowing has been utilized to control vortices emanating along curved leading edges. Gad-el-Hak and Ho[4] employed sinusoidal perturbations of a high frequency. For the case of blowing along the leading edge, a delay in the vortex breakdown position has been reported by Wiseer, Iwanski, Nielson, and Ng[5]. Magness, et al.[6,7] and later Gu et al.[8] employed cyclic blowing and suction to delay vortex breakdown and stabilize the flow over delta wings at high angles of attack.

At moderate angles of attack, flaps have been employed to influence forces and moments over delta wings. Lamar[9] experimented with a single trailing-edge aileron, tip-mounted onto a cropped delta wing. This successfully generated a constant rolling moment. In addition, a vortex flow roll-control device was designed to develop flow asymmetries through modification of the planform geometry. Results indicate a potentially useful device in which the effect of increasing the angle of a raked-tip leading edge is to produce an almost linear increase in rolling moment. However, these tests were confined to angles of attack less than 30°. Rao and Campbell[10] discuss several effects of vortical flow generators, including leading-edge vortex flaps which can operate either on the lower or upper surface of a delta wing. It is clear that these devices have potential over various different flight regimes. A detailed description of contributions in this area is included in Ref. 11.

In the present paper we explore the effectiveness of a deployable surface, an apex flap, to control the flow over a delta wing. The emphasis here is on larger angles of attack and therefore the aim is to control, delay or induce vortex breakdown. The present team of investigators has reported on the effectiveness of cavity flaps on vortex breakdown[12]. Results on a few other devices were reported by the present authors in Ref. 13. Other authors[14,15] also reported on the effectiveness of devices such as leading-edge flaps to control vortex breakdown in dynamic wing motions, but considered angles of attack not higher than 35°. Here we very briefly discuss the results with such devices and concentrate on the most effective device, the apex flap, carrying the investigation up to an angle of attack of

50°. Moreover, and for the first time, we explore the effectiveness of such a device on a dynamically developing vortical field. This is the case of a delta wing during a pitching up motion.

Facilities and Instrumentation

Tests were conducted in two different facilities, a $10'' \times 12''$ water tunnel and a wind tunnel with a test section of $20'' \times 20''$. Three-component laser-Doppler velocimetry (LDV) was employed in the water tunnel and surface pressure data were obtained in the wind tunnel. The LDV system is a TSI system operating in backward scatter with a 35 mW Helium-Neon laser. Mirrors, traversing mechanisms and lead screws operated by stepping motors facilitate displacement of the measuring volume. Measuring grids normal to the oncoming stream can thus be automatically traversed. The measuring volume can be positioned on a grid point with an accuracy of $\pm$ 0.1 mm through the use of two LVDT's which are incorporated in a position feedback loop. Two components of the velocity are measured simultaneously from each side of the tunnel and the three-dimensional field is later constructed.

Experiments were conducted with fixed as well as with dynamically pitching models. The motion chosen was a swift pitch up about the apex, followed by a slow return to the initial angle of attack. Data were obtained in the wind tunnel at 100 discrete instances during the pitch up and were ensemble-averaged over 200 realizations of the motion. Only seven realizations were averaged in the water tunnel after tests indicated that the flow was highly repeatable. In both tunnels, a trigger was provided from the driving mechanism. In addition, an encoder recorded the angle of attack at each of the sampling points to monitor the instantaneous position of the model. The ramp-like motion involved a constant angular velocity ω. The dimensionless pitch rate $\omega c/2U_\infty$ was 0.06, where c and U_∞ are the chordlength and the free-stream velocity respectively.

The entire operation was controlled by two serially communicating laboratory computers which are programmed to operate the pitching mechanism and the stepping motors, collect

the information on the instantaneous angle of attack, perform the LDV or pressure data acquisition, reduce and ensemble-average the data and transfer them to a mainframe IBM 3090 for calculations and plotting.

Two delta wing models with 75° sweep angle were employed with sizes designed to achieve approximately the same blockage ratio in both facilities. The models were mounted on dynamic struts which can position them at a fixed angle of attack, or alternatively, carry them into pitch-up motions with arbitrarily described schedules. Both models had a thickness-to-chord ratio of 0.042 and a bevel angle of 45° on their windward side. They were geometrically similar to the models employed earlierly by the present group[16–18]. The model employed in the wind tunnel is shown in Fig. 1a. The front portion of both models was hinged and could be drooped as shown in Fig. 1b. The angle of droop is denoted by the symbol B. The upper surface of the model was equipped with pressure taps connected to a miniature PSI pressure scanner along an axis approximately beneath the vortex axis. The location of this axis was determined by earlier studies[16–18] of the present group to be 6.4° inboard of the leading edge. The model employed in the water tunnel was geometrically similar but was not equipped with pressure transducers. Both models could be tested in their basic shape, as well as with a drooping apex flap.

LDV data were obtained along two fixed vertical planes, denoted as planes I and II as shown in Fig. 1b. At the initial angle of attack, $\alpha = 28°$, these two planes intersect the wing section at chordwise locations of 0.7 and 1, respectively. The second plane corresponds to the trailing edge at $\alpha = 28°$. During pitch up about an axis passing through the undeflected apex, plane I cuts the wing planform at locations corresponding to even higher chordwise locations.

An extensive uncertainty analysis for the present experimental rig was carried out. The reader can find details in Ref. 19. The laser-Doppler velocimeter is sensitive to the velocity component given by $V = f_D \frac{\lambda}{2 \sin k}$, where f_D is the Doppler frequency, λ is the wavelength

of the laser light, and κ is half the beam crossing angle. Using $w_f = 0.01 f_D$ as a worst case for the uncertainty on the frequency, and $w_k = 0.25\kappa$ for the beam alignment uncertainty, a velocity uncertainty of $w_v = 0.027 U_\infty$ (20:1) is calculated. In the wind tunnel the combined inaccuracy of the pressure transducers, transducer calibration, amplifiers, and data acquisition board is estimated as $\pm 0.0347 C_p$ at $U_\infty = 12 m/s$ (20:1).

Results and Discussion

The flow over a delta wing is dominated by two leading edge vortices. Such vortices are characterized by high axial velocity and vorticity, but these features may suddenly change if the vortices break down[1,11]. The axial velocity then goes to zero and subsequently reverses direction while vorticity diminishes significantly. Vortex breakdown creeps up from downstream and at a certain angle of attack reaches the trailing edge of the wing. This condition is often referred to as the onset of breakdown. With further increases of the angle of attack, breakdown moves up over the wing and towards the apex, until the vortex is broken down along the entire chord. The wing is then stalled. The development of breakdown is monitored in our experiments via pressure and LDV measurements.

Steady flow experiments were conducted first in the wind tunnel. Mean and RMS values of pressure over an unmodified model at various angles of attack are displayed in Fig. 2. Data are presented in terms of the nondimensionalized distance from the apex of the model along the axis of the wing. In this figure we also display selected data from Ref. 20 for comparison. In general, results compare well, both at the apex and trailing edge. Some differences occur as the half-chord region is appraoched, which may be due to the fact that the model employed by these authors had a double-beveled edge.

As the angle of attack increases, the static pressure decreases monotonically, until breakdown enters the domain over the wing. The location of vortex breakdown is characterized by a local slight increase of the streamwise pressure distribution. This increase appears as a cross-over of the pressure distribution over the curve corresponding to the smaller angle

of attack. For example, in figure 2a, the pressure line of $\alpha = 34°$ crosses that of $\alpha = 32°$ at $x/c = 0.59$. Flow visualization was conducted and the results confirmed this to be an accurate streamwise breakdown position for $\alpha = 34°$. Further increase in the angle of attack involves a further lowering of the pressure over the entire region of measurement. A purely phenomenological observation made in every test is that the curvature of the streamwise pressure distribution changes sign at the breakdown angle of attack.

Breakdown can also be detected by a drastic increase in the RMS level. Figure 2b shows that at $\alpha = 34°$, a slight increase in the RMS occurs at the pressure port nearest the trailing edge. A drastic increase in the RMS follows for $\alpha = 36°$, with values as high as 0.32 at the trailing edge. It is interesting to note that the loss in pressure magnitude always slightly precedes the increase in its RMS.

A number of control surfaces in the form of fences or flaps attached on the windward or leeward side of the wing were tested. However, their effectiveness in controlling the vortices at high angles of attack was surpassed by the apex flap. Data on the performance of such devices were included in Ref. 13. Here we confine our discussion to the results obtained with an apex flap.

Results obtained with the apex flap are presented in Figs. 3-5 for drooping apex flap angles of $B = 8°$, $12°$ and $18°$, respectively. A considerable delay of breakdown is now observed. For B = 8°, Fig. 3a shows clearly that at $\alpha = 36°$, the pressure over the entire wing is still decreasing beyond the level corresponding to smaller angles of attack. It is not until $\alpha = 38°$ that the pressure suddenly rises. RMS measurements in Fig. 3b confirm this delay in breakdown. Data are next presented in Fig. 4 for B = 12°. A further delay in breakdown is observed. Pressure remains low for $\alpha = 38°$ and suddenly rises for $\alpha = 40°$. Between $\alpha = 38°$ and $\alpha = 40°$, the breakdown position has moved from the trailing edge to a position forward of $x/c = 0.45$.

The apex flap was next positioned at B = 18°. The RMS pressure distribution presented

in Fig. 5b shows low values until $\alpha = 42°$. Before breakdown, both in Fig. 4b and Fig. 5b, RMS values seem to be higher at the first pressure port and then decrease towards the trailing edge. This could result from turbulence created by the vortex bending around the corner of the apex flap and main wing. In Fig. 5a the pressure for $\alpha = 42°$ crosses that of $\alpha = 40°$ at x/c = 0.45 This is almost the maximum delay in vortex breakdown observed for any deflection angle of the apex flap. Tests were conducted at seven deflection angles between 6° and 18°. These results are not shown here due to lack of space but indicated that the optimal deflection angle, *i.e.*, the maximum breakdown delay corresponds to B = 15°.

Next, we considered the corresponding pressure and velocity field during dynamic pitch-up motions. Pressures taken on the unmodified model, at a reduced pitch up rate of 0.06 display a characteristic delay in breakdown[4,17,18,21–24]. Well-behaved, coherent vortices exist up to an angle of attack $\alpha = 45°$ (Fig. 6). Breakdown appears for $\alpha = 46.5°$ and has already moved upstream of the trailing edge, up to $x/c = 0.66$. Making use of the encouraging results obtained with the apex flap in our steady work, the flap was deployed at B = 15° during a pitch-up maneuver. Results are plotted in Fig. 7 for comparison against those in Fig. 6. Here breakdown has been delayed to 52.5°.

To further verify these findings, three-component LDV data were obtained in the water tunnel and are presented in Figs. 8-11. In Fig. 8, velocity vectors in the crossflow plane are plotted along with axial velocity contours over the wing for the unmodified wing and the wing with the apex flap deployed*. Note that here the measuring plane is fixed and corresponds to $x/c = 0.70$ at the initial angle of attack of $\alpha = 28°$. The wing actually maneuvers through this fixed plane, so that for $\alpha = 50.5°$, the plane of measurement corresponds to $x/c = 0.96$. The position of this plane is marked as plane I in Fig. 1. Data along a second fixed plane,

* In the CD-ROM version of this paper, Figs. 8 and 9 present in color instantaneous frames at $\alpha = 28°, 34°, 38°$, 42.5°, 46.5°, and 50.5°. The files of the actual experimental data are also included.

plane II (Fig. 1) were also obtained and will be presented in Fig. 9.

As the wing retreats, a larger domain becomes available for measurement on its upper surface and thus the area populated by data appears growing in each of the frames of the figures that follow. The lowest line of data defines the intersection of the measuring plane and the wing surface. Moreover, the projection of the trailing edge to the plane of data is also marked by a horizontal line. Figure 8a presents data with an unmodified wing while Fig. 8b contains data obtained with an apex flap deployed at an angle $B = 15°$. Breakdown characterized by an axial flow stagnation region develops over the plain wing and spreads from the inboard region towards the center of the core. This behavior may be a little misleading, because our axial component is along the free-stream direction and not along the instantaneous axis of the vortex. However, the behavior of the velocity component along the vortex axis is not much different as pointed out by Hoang et al[16].

The zero velocity region approaches the core from the wing and therefore in violation of the axisymmetric nature of the flow. This feature was also observed and reported earlier for steady flow by Kegelman and Roos[25]. For the unmodified wing, breakdown along the plane of measurement is initiated at $\alpha = 38°$ and dominates the flow field at $\alpha = 42.5°$*. On the other hand, the core of the vortex over the wing with a deployed apex flap contains much higher values of velocity and for much larger angles of attack. In Fig. 8b, it appears that breakdown does not develop until $\alpha = 50.5°$. In fact, these data indicate that the axial velocity increases in the core of the vortex even up to $\alpha = 46.5°$.

In Fig. 9 we display similar results obtained along plane II (Fig. 1). The flow over the unmodified wing is totally broken down, and yet some coherence and axial velocities larger than U_∞ can be observed over the droop-nosed wing, even up to $\alpha = 38°$*.

Vorticity contours are presented for the two stations I and II (Fig. 1) over the droop-nosed wing in Fig. 10 and 11, respectively. Again, it appears that the modified wing retains vorticity coiled in a nearly axisymmetric pattern up to $\alpha = 46.5°$ at the $x/c =$

* These are shown only in the CD-ROM version of the paper.

0.70 station. Opposite sense of vorticity, representing secondary vortices can be observed near the wing surface. A comparison of the vorticity contours in Fig. 10b with the axial velocity contours of Fig. 8b also indicates that vorticity retains a coherent distribution, consistent with the ordered circumferential distribution of the velocity. In other words, vorticity contours nearly coincide with the circumferential streamline loops as conjectured by the circumferential velocity components. Vortex sheets are therefore nearly coincident with stream tubes. On the other hand, the axial velocity distribution is skewed. The low speed region is approaching from the inboard region. A significant delay in loss of vorticity is also observed in Fig. 11b where we present the results obtained along plane II.

Conclusions

Breakdown is characterized by loss of static pressure suction which is followed by an increase in the RMS of pressure. Breakdown develops asymmetrically. The low velocity region penetrates the core from the wing. The deployment of an apex flap in a drooping position proved to delay the appearance of breakdown over the wing to an angle of attack of about 8° beyond the corresponding value of the unmodified fixed wing. The most efficient drooping angle for the apex flap was found to be 15 degrees. The same configuration appears to be equally efficient in controlling breakdown during pitch-up maneuvers. This basic design may prove to be a practical mechanism for the control of aircraft at very high angles of attack. In that case, the concept of the apex flap could be evidenced as a modified LEX or canard.

Acknowledgement

This work was supported by the Air Force Office of Scientific Research, Project No. AFOSR-91-0310, and was monitored by Major Daniel Fant.

References

1. Lee, M. and Ho., Chih-Ming, "Lift Force of Delta Wings," *Applied Mechanics Review*, Vol. 43, 1990, pp. 209-221.
2. Wood, N. J. and Roberts, L., "The Control of Vortical Lift on Delta Wings by Tangential Leading-Edge Blowing," AIAA Paper 87-0158, Jan. 1987.

3. Wood, N. J., Roberts, L., and Lee, K. T. "The Control of Vortical Flow on a Delta Wing at High Angles of Attack," AIAA Paper 87-2278, 1987.

4. Gad-el-Hak, M. and Ho, C.-M., "Unsteady Vortical Flow Around Three-Dimensional Lifting Surfaces," *AIAA Journal*, Vol. 24, No. 5, 1986, pp. 713-721.

5. Wisser, K., Iwanski, K. T., Nelson, R. C. and Ng, T. T., "Control of Leading-Edge Vortex Breakdown by Blowing," AIAA Paper 88-0504, 1988.

6. Magness, C., Robinson, O., and Rockwell, D. "Control of Leading-Edge Vortices on a Delta Wing," AIAA Paper No. 89-0999, No. 1989.

7. Magness, C., Robinson, O. and Rockwell, D., "Control of Leading-Edge Vortices on a Delta Wing," presented at the NASA/AFOSR/ARO Workshop on Physics of Forced Separation, April 1990.

8. Gu, W., Robinson, O. and Rockwell, D., "Control of Vortices on a Delta Wing by Leading-Edge Injection," *AIAA Journal*, Vol. 31, No. 7, 1993, pp. 1177-1186.

9. Lamar, J. E., "Nonlinear Lift Control at High Speed and High Angle of Attack Using Vortex Flow Technology." AGARD$-R-$740 Special Course on Fundamentals of Fighter Aircraft Design, 1986.

10. Rao, D. M., and Campbell, J. F., "Vortical Flow Management Techniques," *Progress in Aerospace Sciences*, Vol. 24, 1987, pp. 173-224.

11. Rediniotis, O. K., Hoang, N. T. and Telionis, D. P., "Multi-sensor Investigations of Delta Wing High-Alpha Aerodynamics," AIAA Paper 91-0735, January 1991.

12. Schaeffler, N. W., Hoang, N. T., and Telionis, D. P., "Controlling of Delta Wing Vortices with Vortex Cavity Flaps," 1993 ASME Winter Annual Meeting, Paper No. 93-WAM/NCA-27, 1993.

13. Klute, S. M., Rediniotis, O. K., and Telionis, D. P., "Flow Control Over Delta Wings at High Angles of Attack," AIAA Paper No. 93-3494, Aug. 1993.

14. Srinivas, S., Gursul, I. and Batta, G., "Active Control of Vortex Breakdown over Delta Wings," AIAA Paper No. 94-2215, June 1994.

15. Gursul, I., Yang, H. and Deng, Q., "Control of Vortex Breakdown with Leading Edge Devices," AIAA PAper No. 95-06761, Jan. 1995.

16. Rediniotis, O. K., Hoang, N. T. and Telionis, D. P., "Multi-sensor Investigation of Delta Wing High-Alpha Aerodynamics," AIAA Paper No. 91-0735, Jan. 1991.

17. Rediniotis, O. K., Klute, S. M., Hoang, N. T., and Telionis, D. P., "Pitch-up Motions of Delta Wings," *AIAA Journal*, Vol. 32, No. 4, 1994, pp. 716-725.

18. Hoang, N. T., Rediniotis, O. K., and Telionis, D. P., "The Temporal Evolution of a Pair of Streamwise Vortices," *Experiments in Fluids*, in press.

19. Wilder, M. C., "Airfoil-Vortex Interaction adn the Wake of Oscillating Airfoil," Ph.D. Dissertation, Virginia Polytechnic Institute and State University, February 1992.

20. Thompson, S. A., Batill, S. M. and Nelson, R. C., "Delta Wing Surface Pressures for High Angle of Attack Maneuvers," AIAA Paper No. 90-2813, August 1990.

21. Atta, R., and Rockwell, D., "Leading Edge Vortices Due to Low Reynolds Number Flow Past a Pitching Delta Wing," *AIAA Journal*, Vol. 28, No. 6, 1990, pp. 995-1004.

22. Magness, C., Robinson, O. and Rockwell, D., "Unsteady Crossflow on a Delta Wing Using Particle Image Velocimetry," *Journal of Aircraft*, Vol. 29, July-August, 1992, pp. 707-709.

23. Magness, C., Robinson, O. and Rockwell, D., "Instantaneous Topology of the Unsteady Leading-Edge Vortex at High Angle of Attack," *AIAA Journal*, Vol. 31, No. 8, 1993, pp. 1384-1391.

24. Magness, C., Robinson, O., and Rockwell, D., "Laser-Scanning Particle Image Velocimetry Applied to a Delta Wing in Transient Maneuver," *Experiments in Fluids*, Vol. 15, No. 3, 1993, pp. 159-167.

25. Kegelman, J. T., and Roos, F. W., "Effects of Leading-Edge Shape and Vortex Burst on the Flowfield of a 70-Degree-Sweep Delta Wing," AIAA Paper No. 89-0086, Jan. 1989.

Fig. 1. A Delta wing model with a drooping apex flap. (a) planform (dimensions in inches), (b) the pitch up motion and the planes of measurement.

Fig. 2. Steady flow over the basic configuration. (a) Mean pressure, (b) RMS of pressure.

Fig. 3. Pressure distribution on suction surface, with drooping apex flap at $B = 8°$, (a) mean pressure, (b) RMS.

Fig. 4. Pressure distribution on suction surface with drooping apex at B=12°, (a) mean pressure, (b) RMS.

Fig. 5. Pressure distribution on suction surface with drooping apex at B=18°, (a) mean pressure, (b) RMS.

Fig. 6. Unsteady axial pressure distribution during pitch up with B=0°.

Fig. 7. Unsteady axial pressure distribution during pitch up with B=15°.

Fig. 8a. Axial velocity contours and crossflow velocity vectors over an unmodified delta wing (plane I) performing a pitch-up motion at a rate of $\omega c/2U_\infty = 0.06$.

Fig. 8b. Axial velocity contours and crossflow velocity vectors over a delta wing (plane II) with an apex flap deployed at $B = 15°$ performing a pitch-up motion.

Fig. 9a. Axial velocity contours and crossflow velocity vectors in the wake of an unmodified delta (plane II) wing performing a pitch-up motion.

Fig. 9b. Axial velocity contours and crossflow velocity vectors in the wake of a delta wing (plane II) with an apex flap deployed at $B = 15°$ performing a pitch-up motion.

Fig. 10a. Vorticity contours and crossflow velocity vectors (plane I) over an unmodified delta wing performing a pitch-up motion.

Fig. 10b. Vorticity contours and crossflow velocity vectors over a delta wing (plane I) with an apex flap deployed at $B = 15°$ performing a pitch-up motion.

Fig. 11a. Vorticity contours and crossflow velocity vectors in the wake (plane II) of an unmodified delta wing performing a pitch-up motion.

Fig. 11b. Vorticity contours and crossflow velocity vectors in the wake (plane II) of a delta wing with an apex flap deployed at $B = 15°$ performing a pitch-up motion.

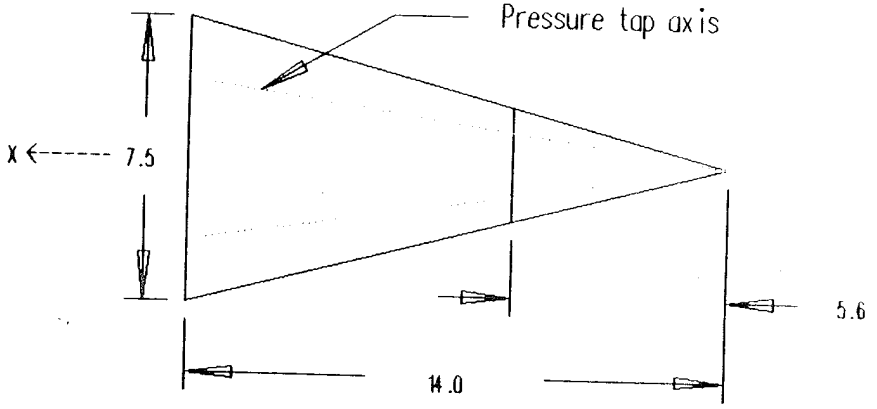

Fig. 1a.

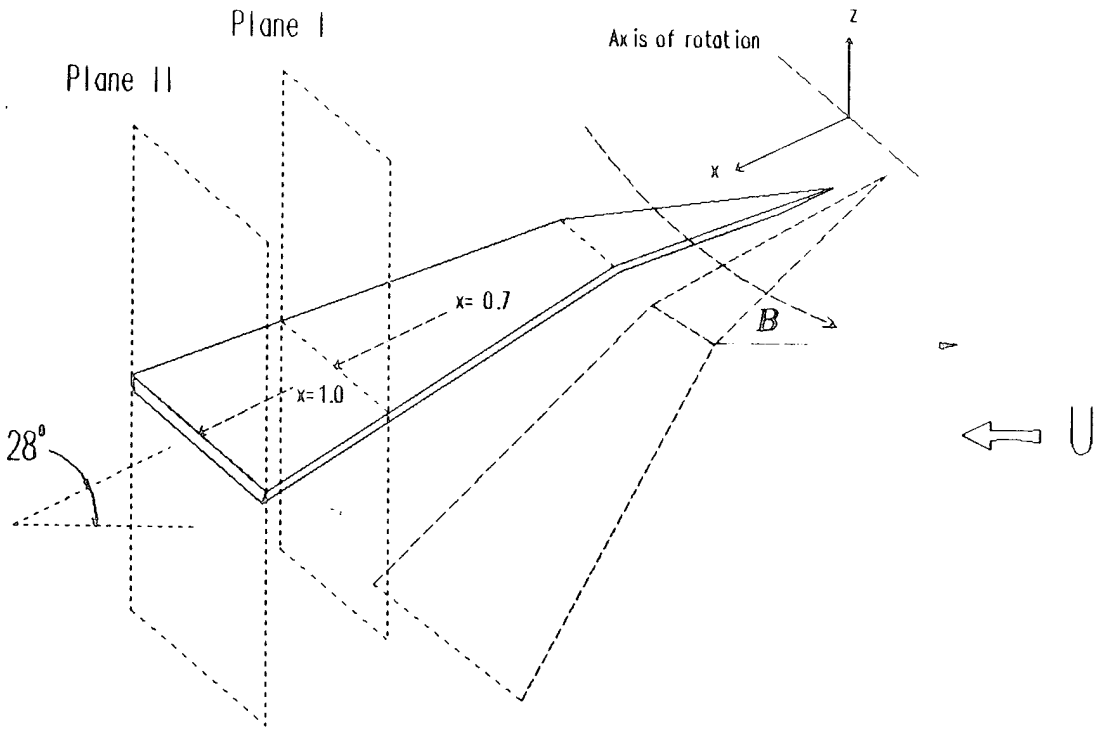

Fig. 16.

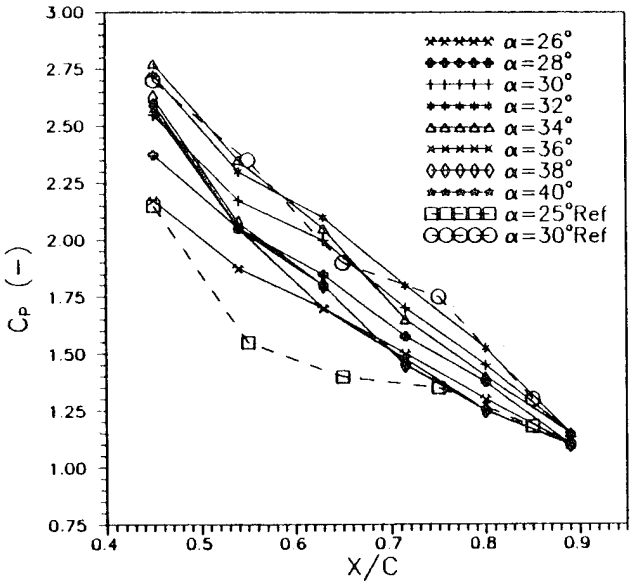

~~Fig. 4.1. Axial pressure distribution.~~

Fig. 2a

~~Fig 4~~ Fig. 2b. (these will need to be sized to match 2a ... or 2a enlarged)

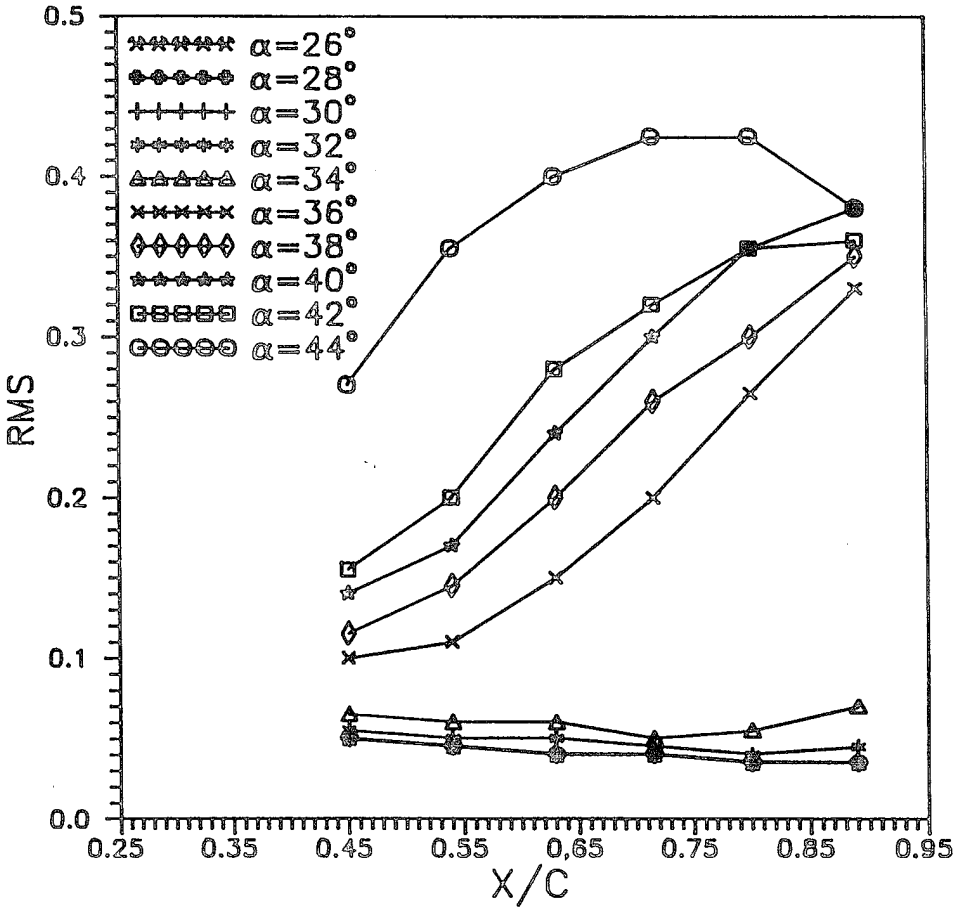

Fig. 4.2. Axial RMS distribution.

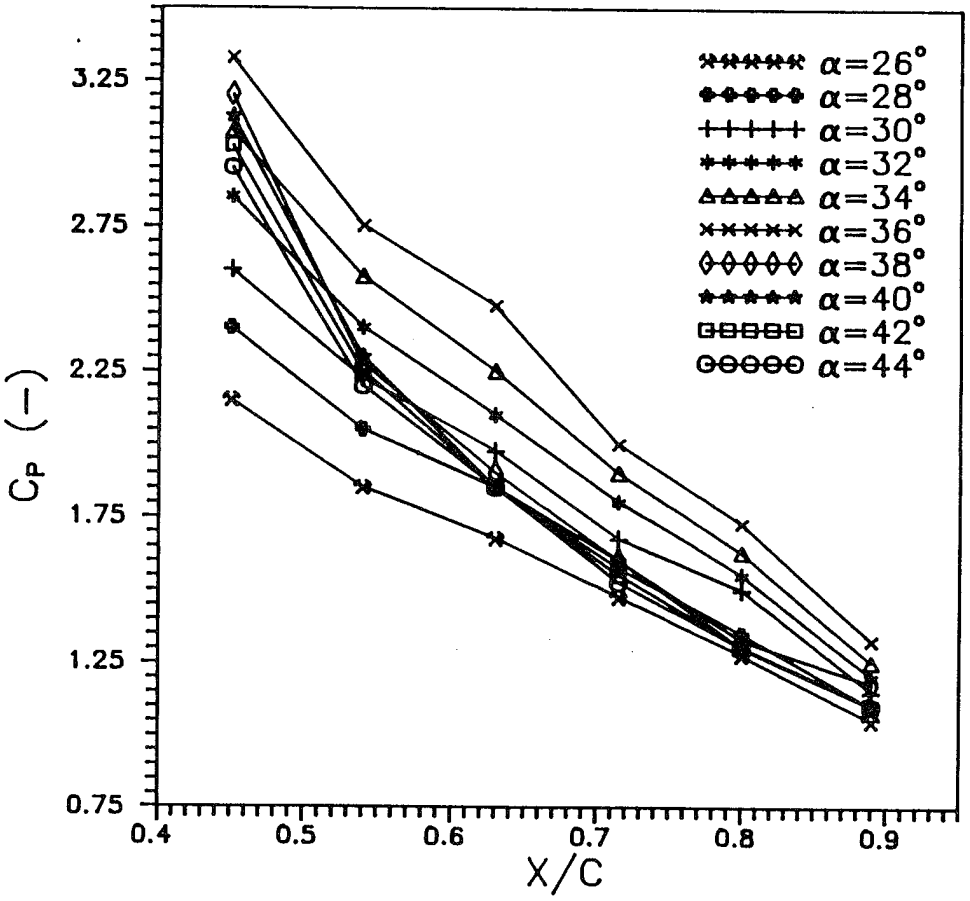

Fig. 7.1. Pressure distribution on model with B=8°.

Fig. 7.2

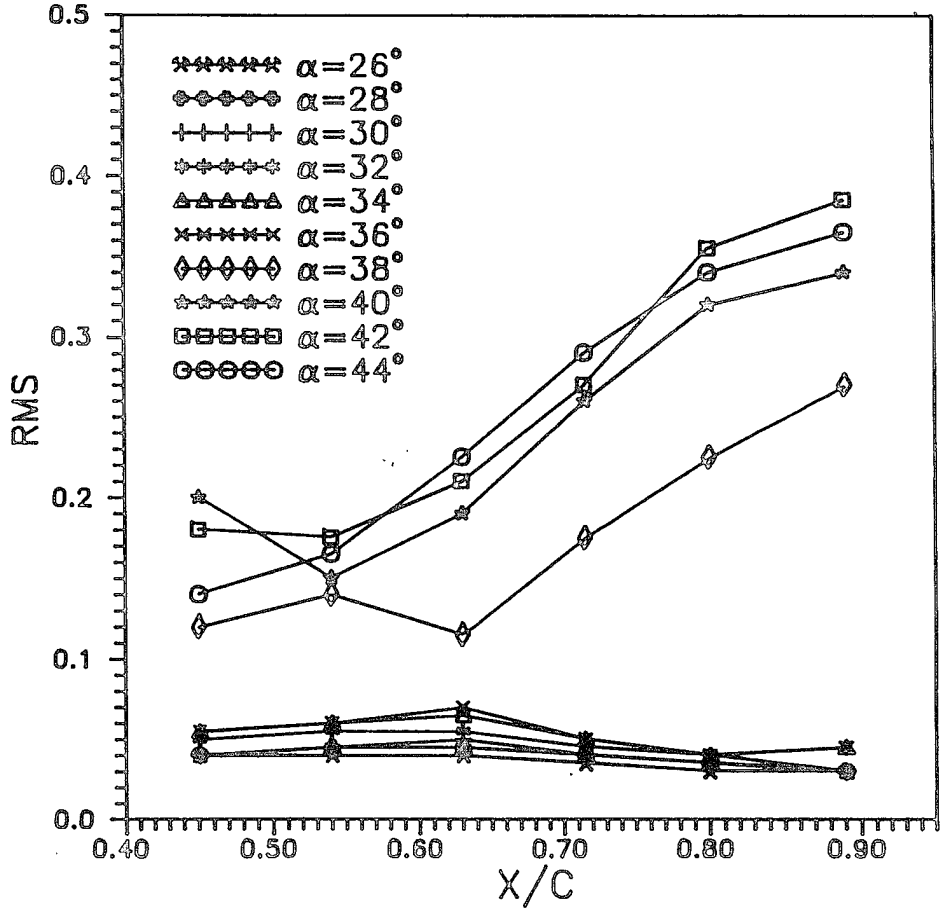

Fig. 7.2. Axial RMS distribution on model with $B=8^{o}$.

Fig 4a

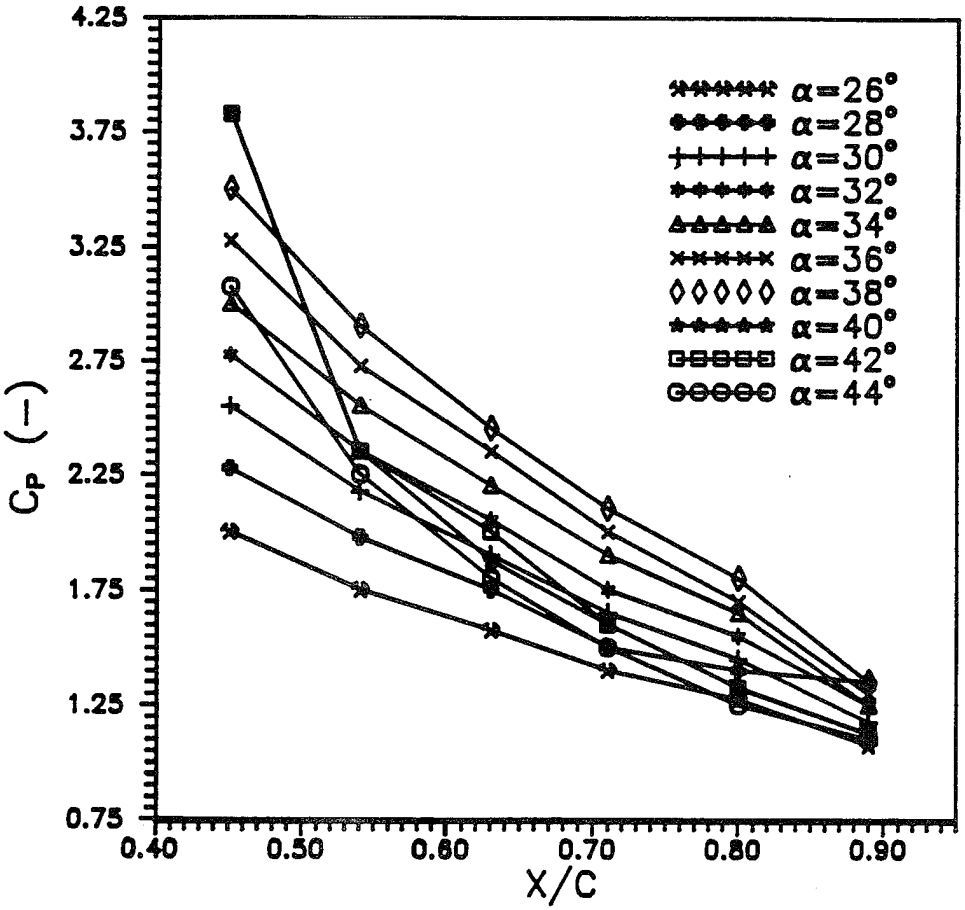

Fig. 8.1. Pressure distribution on model with B=12°.

Fig 4b

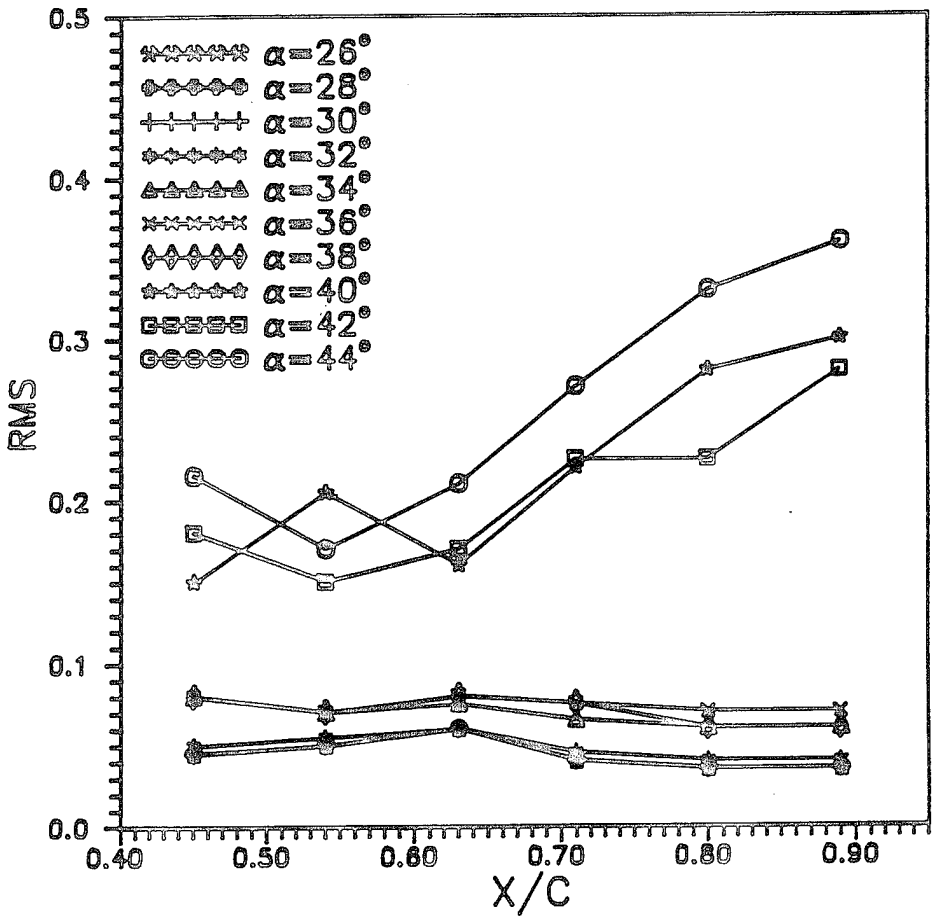

Fig. 8.2. RMS distribution on model with B=12°.

Fig 5a

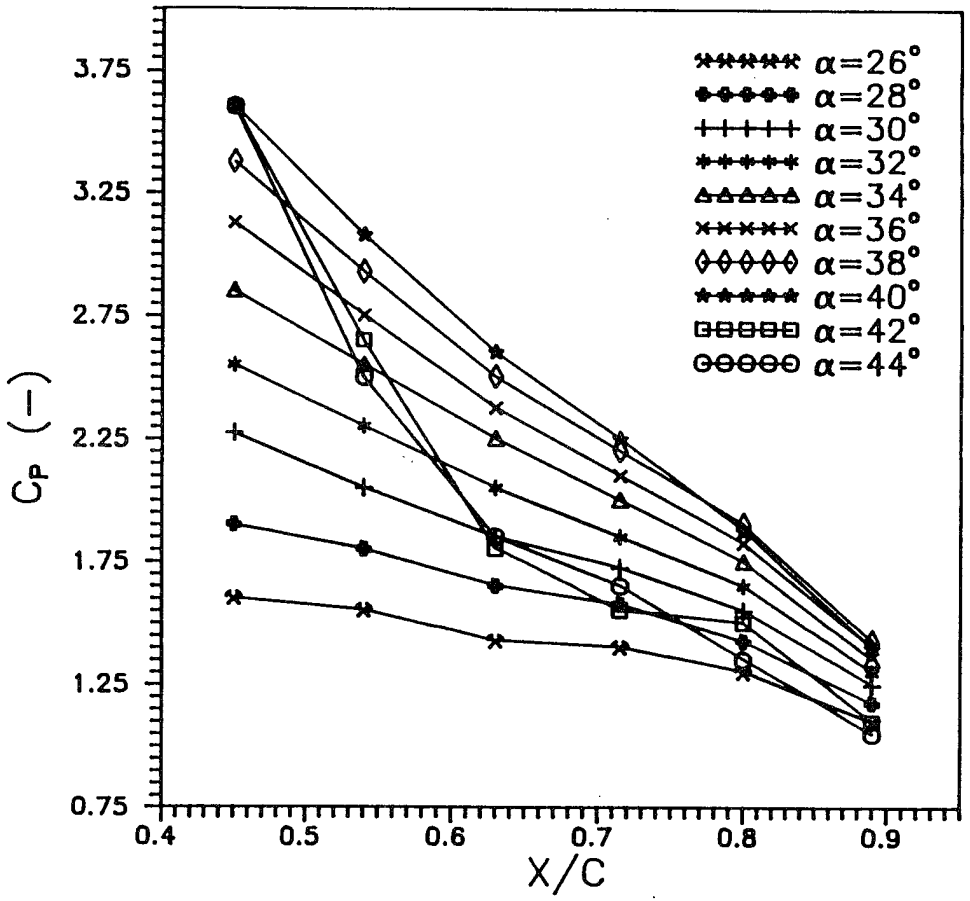

Fig. 9.1. Pressure distribution on model with B=18°.

Fig 5b

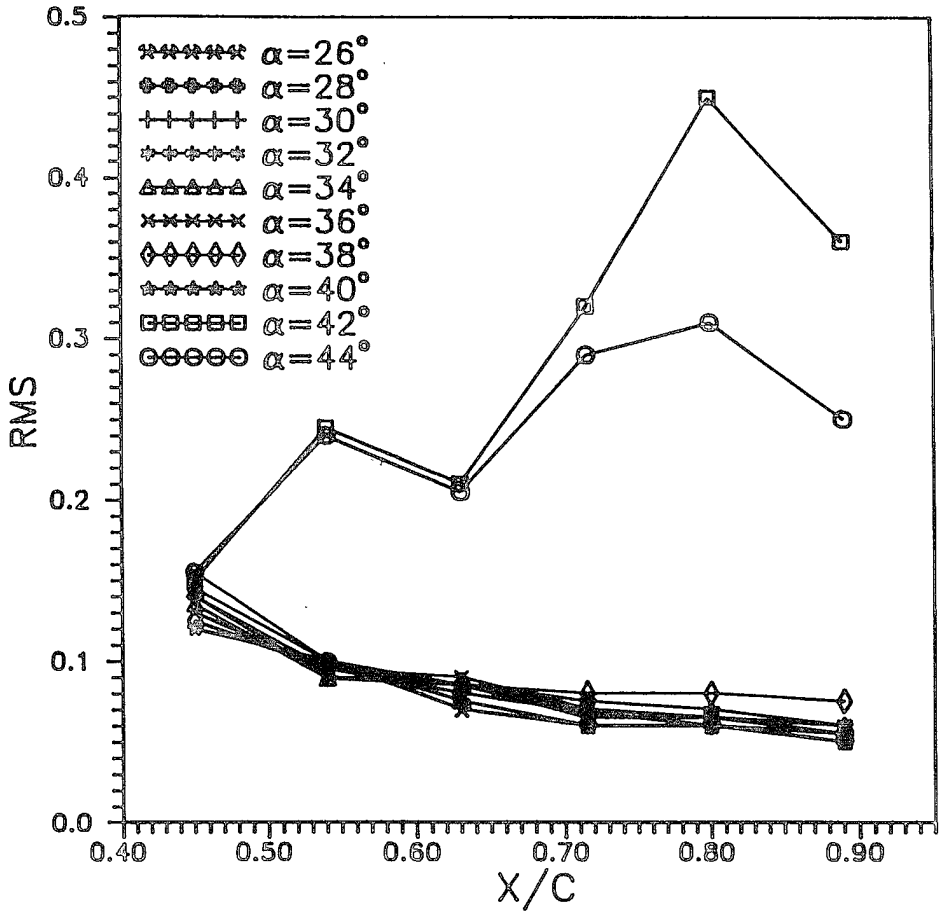

Fig. 9.2. Axial RMS distribution on model with B=15°.

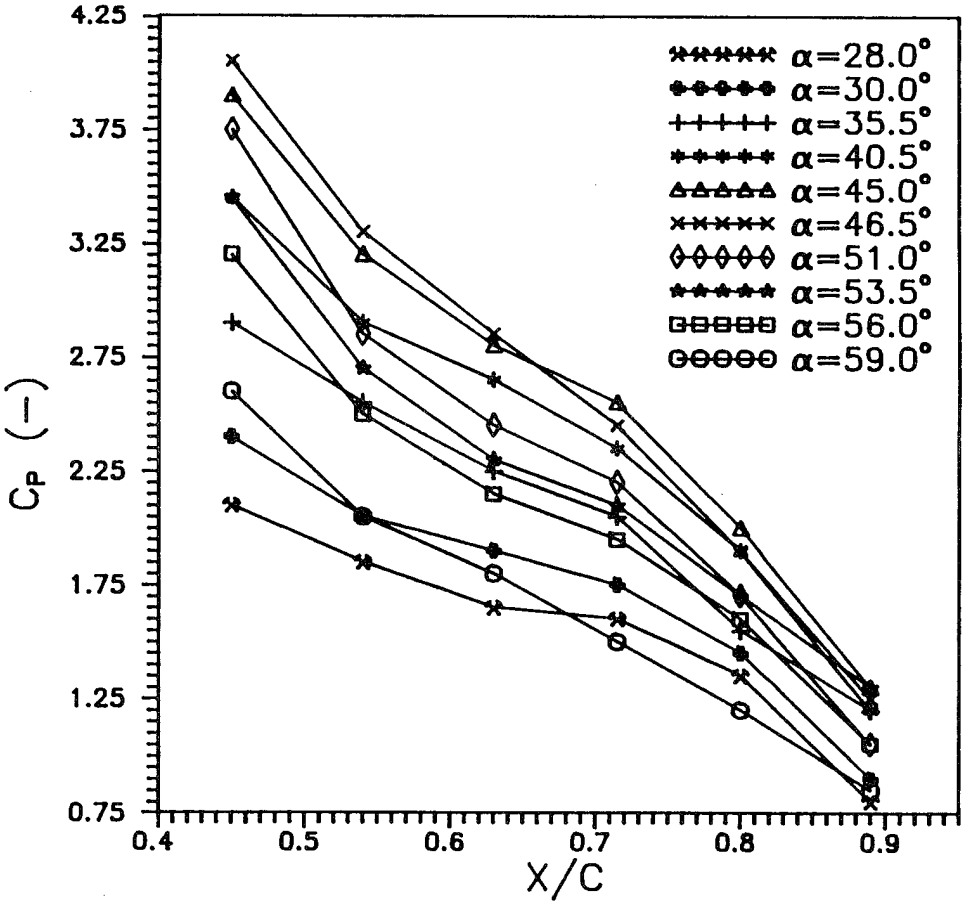

Fig. 10. Unsteady axial pressure distribution on model with B=0°.

Fig. 7

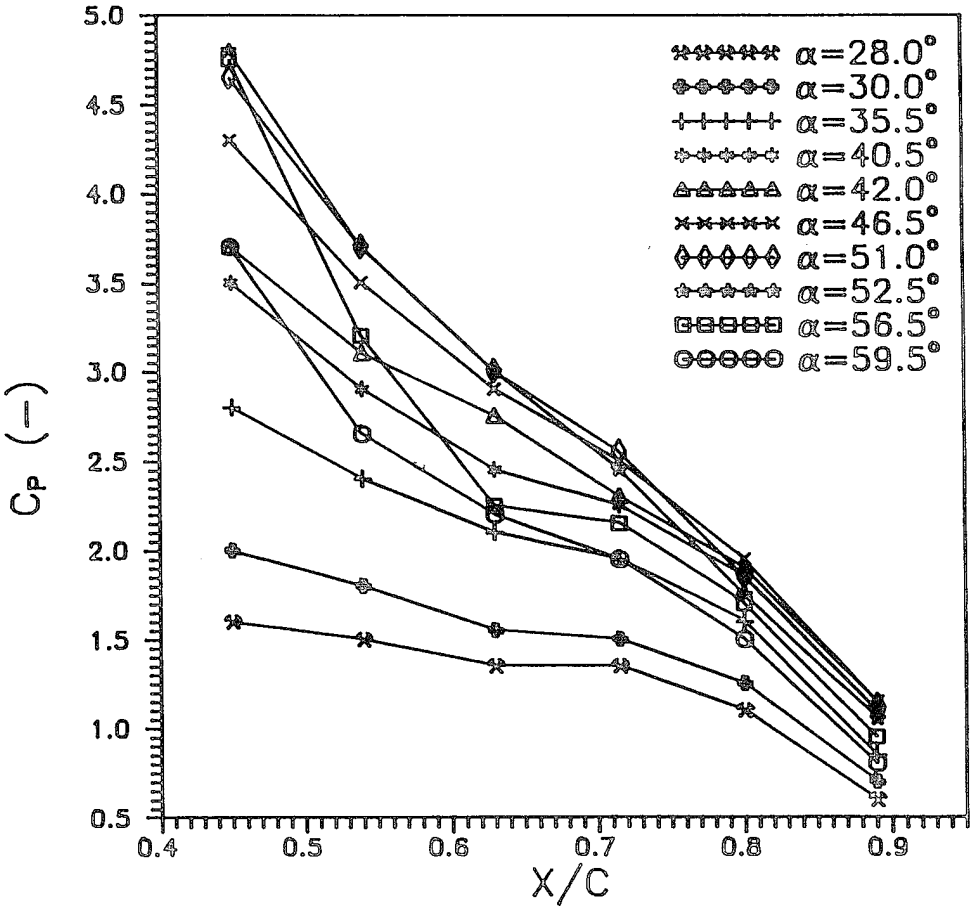

Fig. 11. Unsteady axial pressure distribution on model with B=15°.

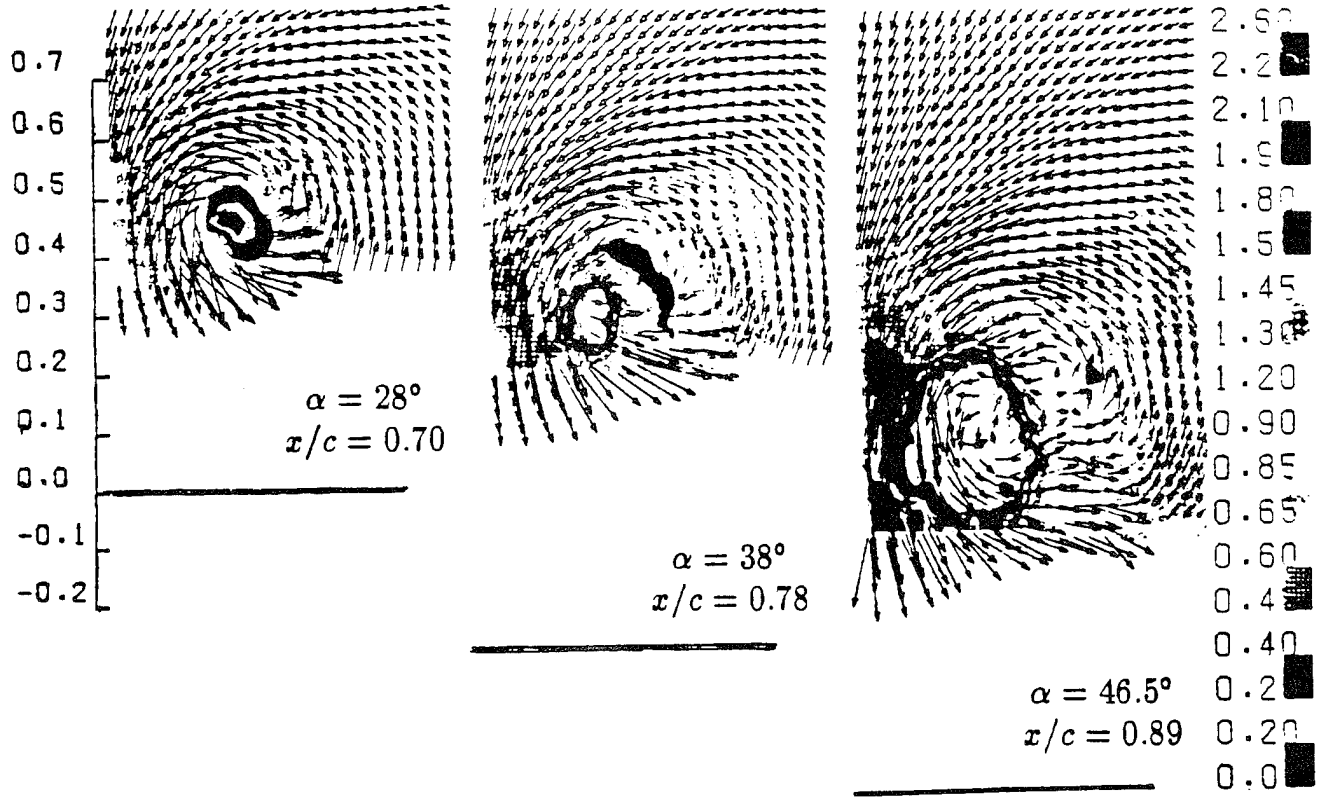
0.7
0.6
0.5
0.4
0.3
0.2
0.1
0.0
-0.1
-0.2
$\alpha = 28°$
$x/c = 0.70$
$\alpha = 38°$
$x/c = 0.78$
$\alpha = 46.5°$
$x/c = 0.89$
2.60
2.2
2.10
1.9
1.80
1.5
1.45
1.30
1.20
0.90
0.85
0.65
0.60
0.4
0.40
0.2
0.20
0.0

Fig. 8a ↑ Fig. 8b. ↓

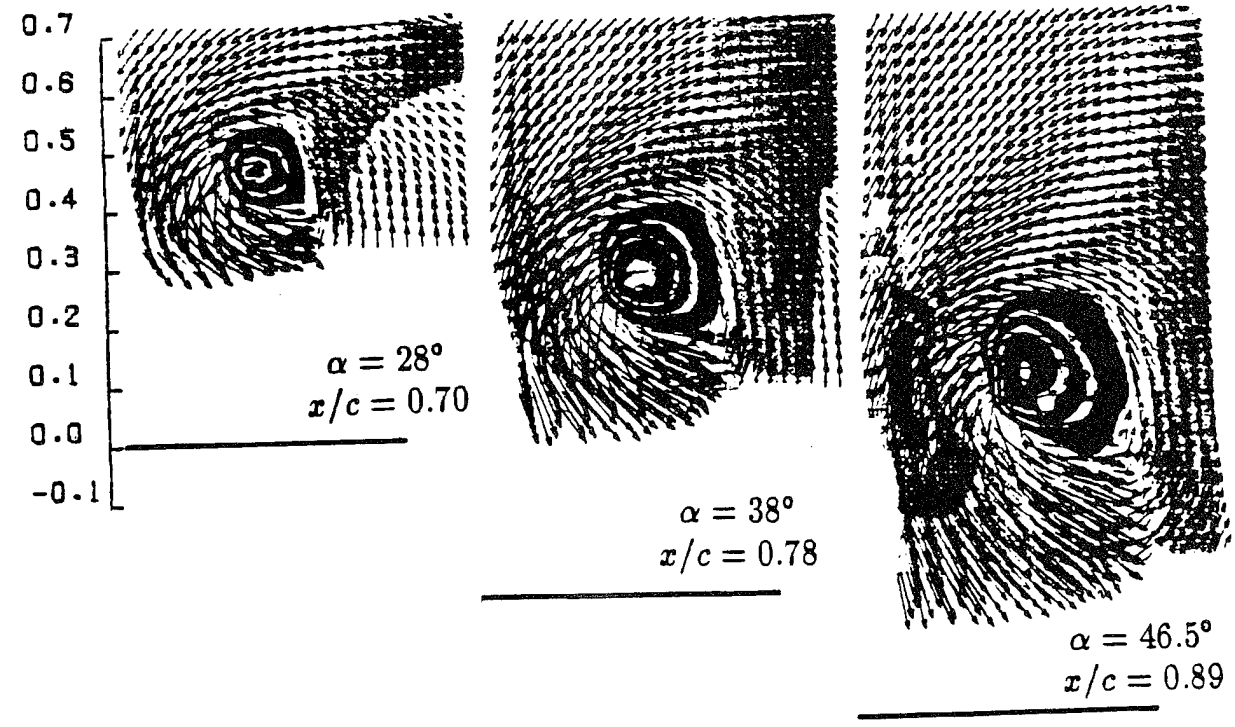
0.7
0.6
0.5
0.4
0.3
0.2
0.1
0.0
-0.1
$\alpha = 28°$
$x/c = 0.70$
$\alpha = 38°$
$x/c = 0.78$
$\alpha = 46.5°$
$x/c = 0.89$


$\alpha = 50.5°$
$x/c = 0.96$

Fig 8b

Fig. 9a

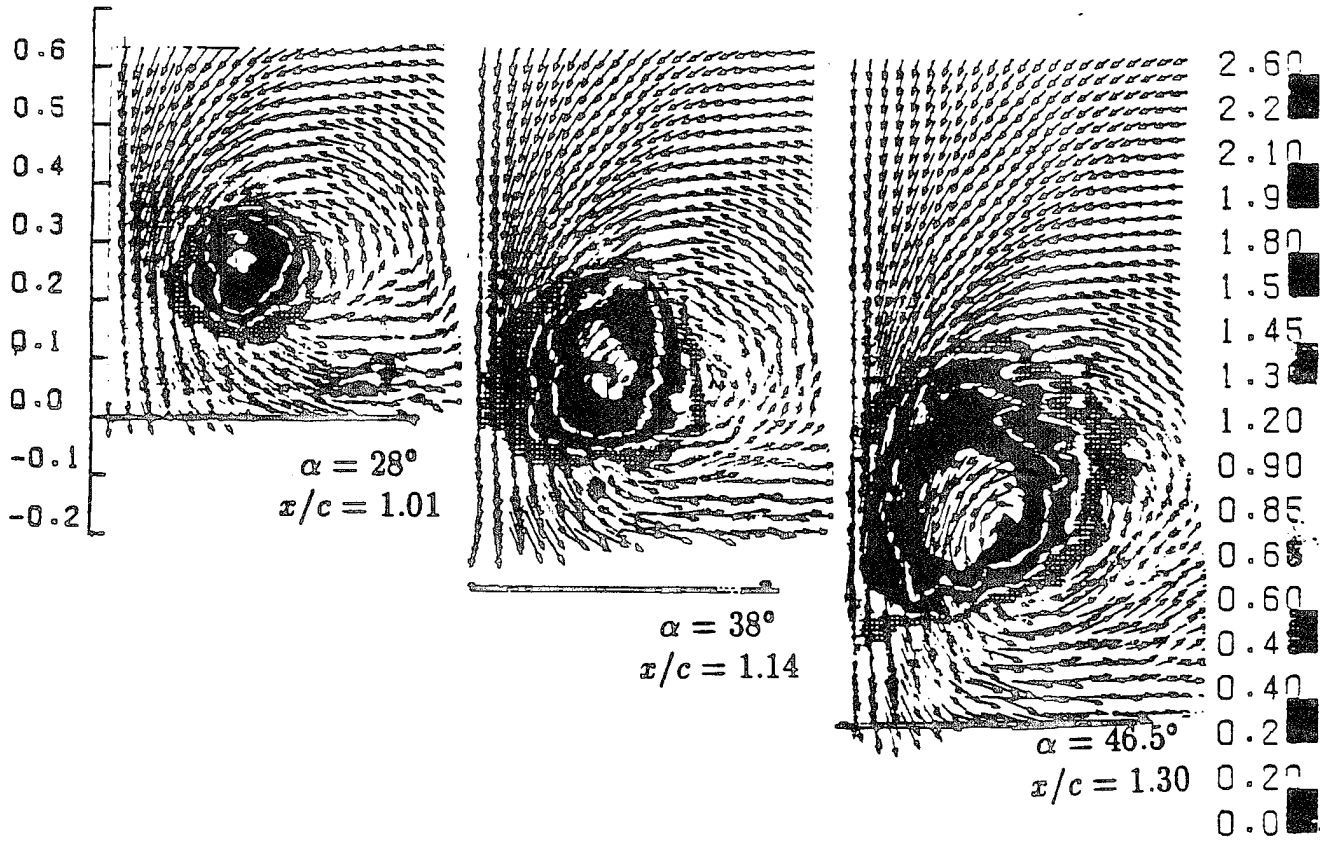
0.6
0.5
0.4
0.3
0.2
0.1
0.0
-0.1
-0.2
$\alpha = 28°$
$x/c = 1.01$
$\alpha = 38°$
$x/c = 1.14$
$\alpha = 46.5°$
$x/c = 1.30$
2.60
2.2
2.10
1.9
1.80
1.5
1.45
1.3
1.20
0.90
0.85
0.60
0.40
0.2
0.0

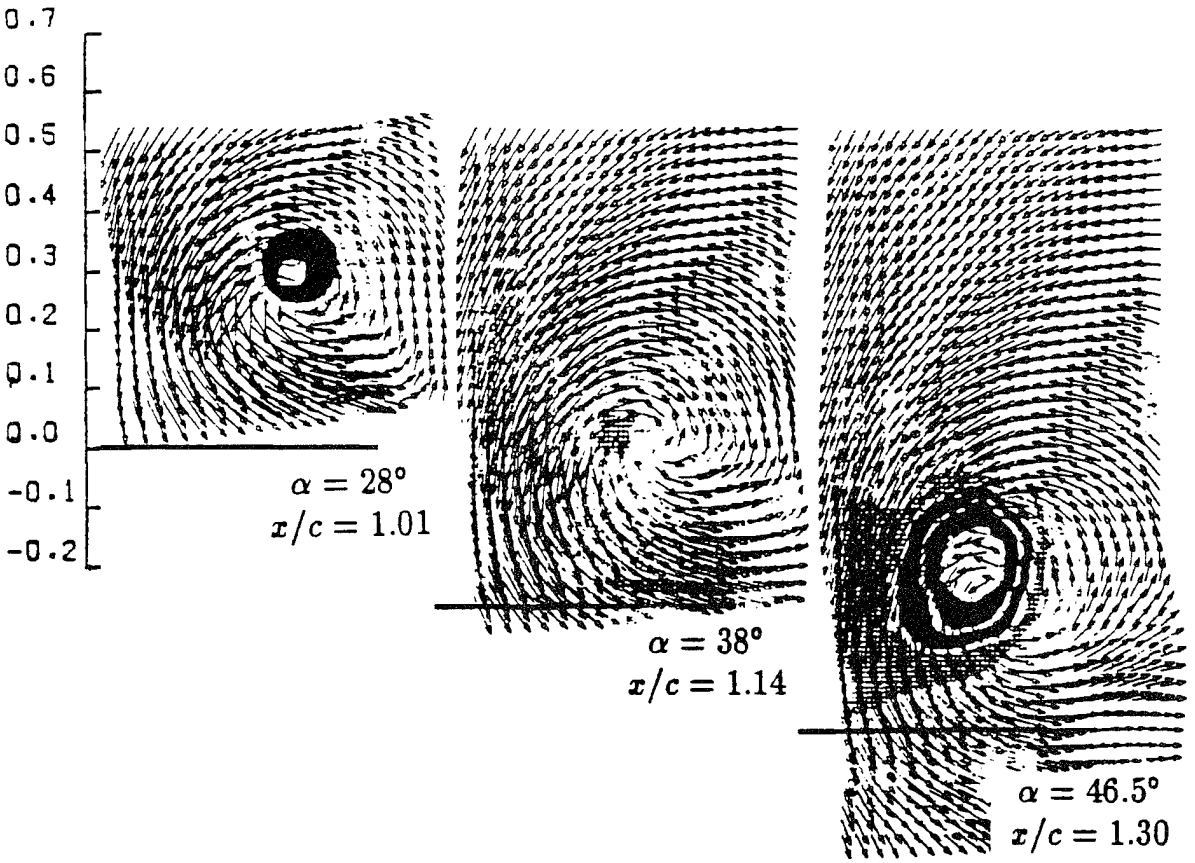

Fig. 9b.

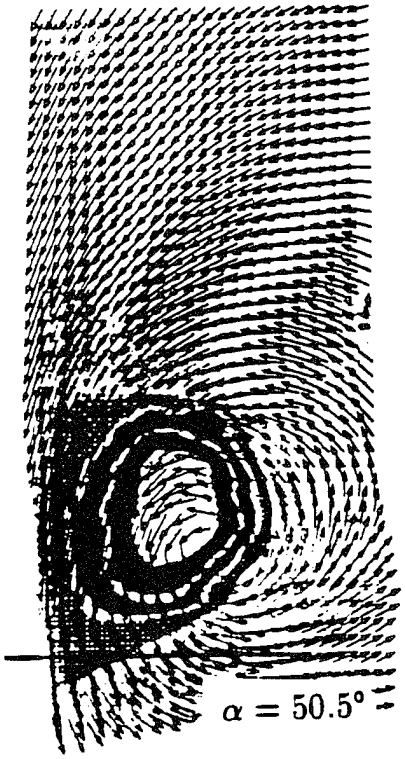

Fig. 9b. cont'd

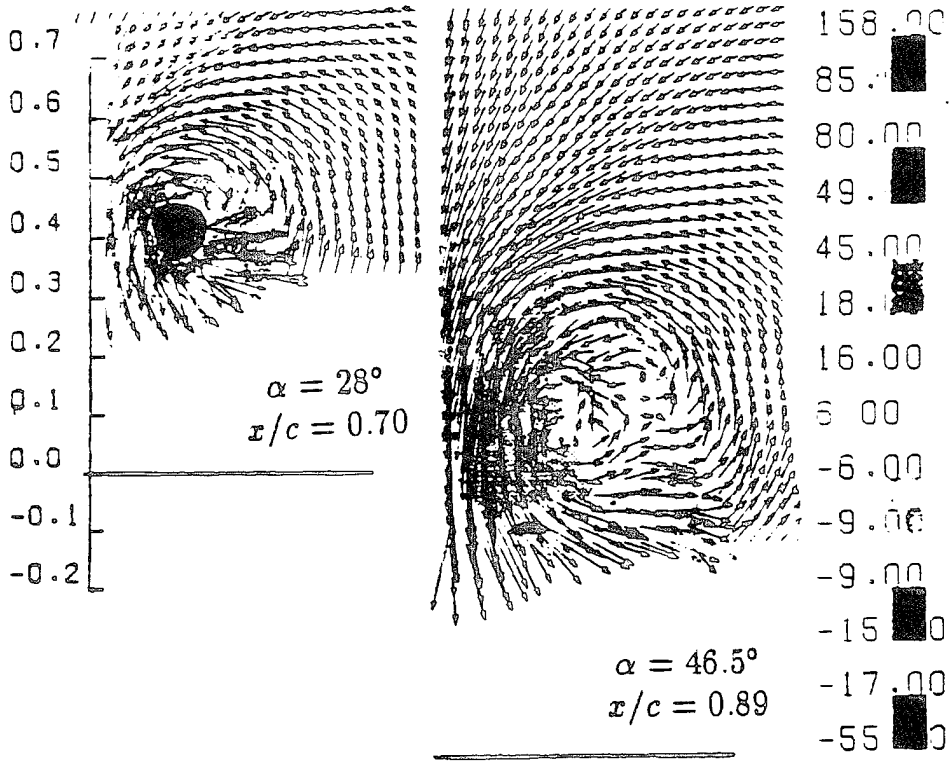

Fig. 10a

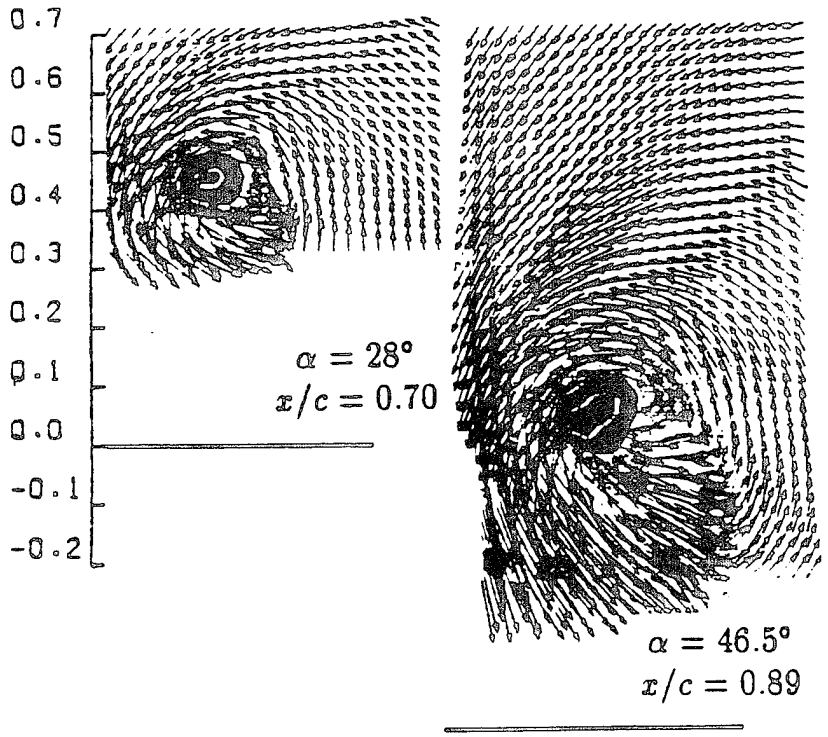

Fig 10b

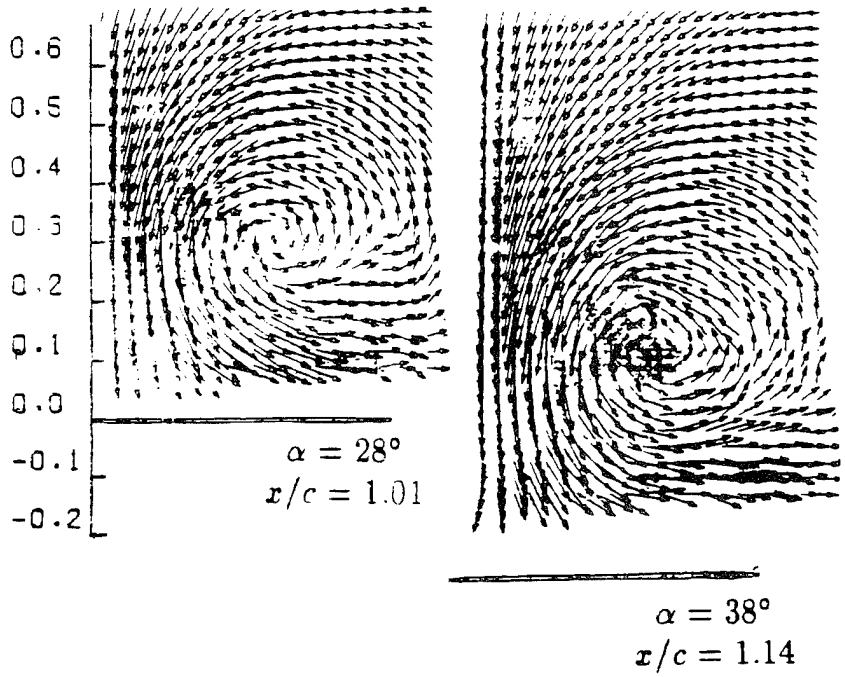

Fig. 11a

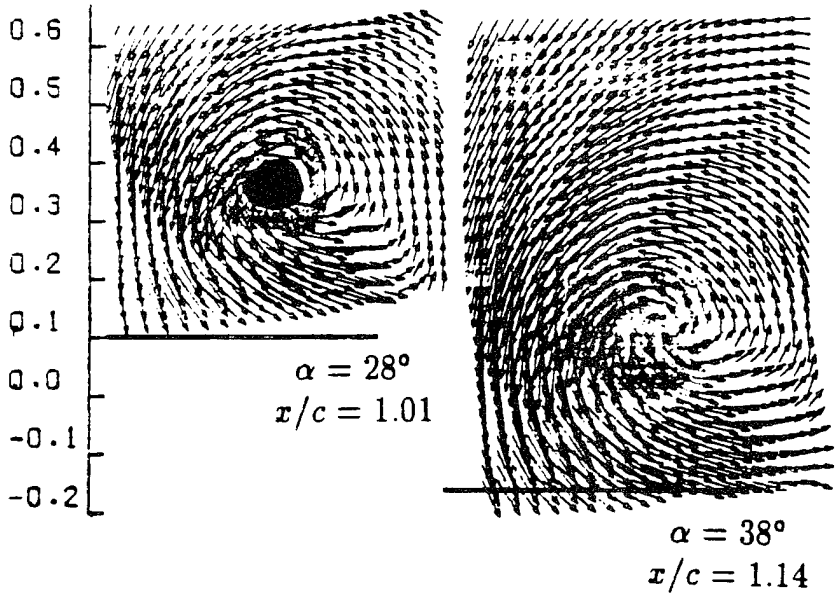

Fig. 11b

THE AMERICAN SOCIETY OF MECHANICAL ENGINEERS
345 E. 47th St., New York, N.Y. 10017

93-WA/NCA-27

4

CONTROLLING OF DELTA WING VORTICES WITH VORTEX CAVITY FLAPS

N. W. Schaeffler, N. T. Hoang, and D. P. Telionis
Department of Engineering Science and Mechanics
Virginia Polytechnic Institute and State University
Blacksburg, Virginia

ABSTRACT

The ability of vortex cavity flaps to delay vortex breakdown over the planform of a delta wing at high angles of attack is investigated. Surface pressure measurements were made over a range of angles of attack to determine when vortex breakdown occurs over the planform with the flap deployed. Laser-Doppler velocimetry is used to map out the flow field over the delta wing at an angle of attack of 35°. The effect of vortex cavity flaps on the structure of leading edge vortices is documented. It was found that for a 70° swept delta wing, cavity flaps can delay the appearance of vortex breakdown over the wing to higher angles of attack than could be otherwise realized.

INTRODUCTION

The requirements for a high performance "super-maneuverable" fighter aircraft calls for a blend of high-supersonic cruise ability and optimal low speed control. The former demands, for reasons of aerodynamic efficiency at high Mach numbers, that a delta wing be chosen as the wing planform. The latter requires a wing with excellent low Mach number flight characteristics, a well known weakness of delta wings. In order to enhance these characteristics, especially to higher angles of attack, a number of deployable control surfaces have been extensively studied in the last decade.

Among these, leading-edge flaps, also referred to as leading-edge vortex flaps, have received considerable attention. In this control surface configuration, the entire leading edge of the wing is hinged to deflect up or down. When deflected down, the effect is to have the leading edge vortex reattach to the flap itself and not the wing. This decreases the effective angle of attack, which is advantageous at high angles of attack. When deflected up, the angle of attack appears larger, thus increasing lift at low angles of attack. Rao (1979, 1980), Marchman (1981, 1981) and Reddy (1981) investigated the effect of these flaps on the performance of delta wings and demonstrated that the two configurations can lead to controlled increases and decreases in drag and could also generate a component of the lift vector in the direction of flight, thus producing a thrusting effect. Broader discussions of advanced control devices can be found in Lamar and Campbell (1983) and in Rao and Campbell (1987).

An alternative design of a control surface was introduced and originally investigated by Rao (1985). In this configuration, a flap is extended from underneath the wing, inclined at an angle to the wing, with the leading edge of the flap parallel to the leading edge of the wing. Rao termed this configuration a vortex cavity flap. It is expected that the vortex flap will help modify and control the onset, growth and shedding characteristics of large-scale vortices but in Rao (1985) data is presented only on the effects of cavity flaps on lift and drag.

In this paper we explore the potential of employing cavity flaps to control the aerodynamic characteristics of the leading edge vortices and therefore the stability characteristics of delta wings at high angles of attack. A first step in this direction for angles of attack as high as 50 degrees was reported by Rao (in press) who demonstrated that the thrust and drag influence of flaps remain effective well beyond the stall regime. All the work conducted so far on flows over flapped delta wings was based on force and moment measurements and in some cases, on flow visualization. At best, one can therefore only offer conjectures as to what exactly happens in the development of vortical structures over swept lifting surfaces. In the present

Presented at the ASME Winter Annual Meeting

paper we present velocity data obtained with a laser-Doppler velocimeter (LDV) and surface pressure data. Both the surface pressure data and the velocity measurements were obtained with and without the cavity flaps.

FACILITIES AND INSTRUMENTATION

This work was carried out in two facilities. The surface pressure measurements were done in the VPI & SU Stability Wind Tunnel. This tunnel is a continuous, closed jet, single return subsonic wind tunnel with a $6' \times 6'$ cross-section. Speeds of up to 220 ft/sec with an extremely low maximum turbulence level of 0.05% can be achieved.

The LDV measurements were done in the Engineering Science and Mechanics (ESM) Water Tunnel. This facility has a test section of $10" \times 12"$ and can achieve speeds up to 9 ft/sec at turbulence levels ranging from 0.6% to 1.5%. A detailed description of this facility and its calibration is included in Koromilas and Telionis (1980), and Mathioulakis and Telionis (1987, 1989).

For the LDV measurements, a TSI, three-beam, two-component, single color LDV system equipped with a 35 mW Helium-Neon laser was employed. Two of the beams are shifted at 60 MHz and 40 MHz, respectively, thus making it possible to separate the two components by electronic filters and therefore employing only one photomultiplier. The LDV system, with its laser mounted along side the system instead of underneath, is mounted upon an optical bench and positioned so that the optical train is normal to the axis of the tunnel. Directly in front of the optical train, a mirror tower is used to bring the beams into the focusing optics and also to traverse the measuring volume. Two mirror towers were used depending upon if the data was being taken from the side or the top of the tunnel. Figure 1 shows the relationship between the measured velocity components and the test section. When data is being taken from the side, the measured velocity components are along the x' and y' axes, or equivalently along x and z, as shown in Figure 1(a). Two mirrors are used to bring the beams through the focusing optics and into the test section. Moving the two mirrors as a unit facilitates traversing in the y direction. Moving the two mirrors relative to one another, accomplishes the z traversing. When data is taken from the top, the measured velocity components are along the x'' and y'' axes, or equivalently, along x and y as shown in Fig. 1b. Three mirrors are required to bring the beams through the focusing optics and into the test section. Moving all three mirrors as a unit accomplishes the y traverse, while moving the top two relative to the bottom one provides movement of the measuring volume in z. In each case, a 250 mm $f/4$ lens focuses the beams into a measuring volume. This arrangement allows the same plane, which is normal to the flow, to be traversed from the top and from the side therefore allowing all three components of the velocity be obtained, although not all simultaneously.

Traversing in the y and z directions is automated by two stepping motors and monitored by two LVDT's. The latter provide an independent analog feedback to confirm the accurate positioning of the measuring volume. Two-dimensional grids in planes parallel to the yz plane can be traversed. The accuracy in positioning the measuring volume is 0.2mm. To obtain data along different yz planes, the entire optical bench is mounted upon a manual traversing system and can be traversed in the x-direction. The entire data acquisition process is fully automated. The only processes requiring manual operation are traversing in the x-direction (for a different plane of measurement) and seeding the water about every 12 hours.

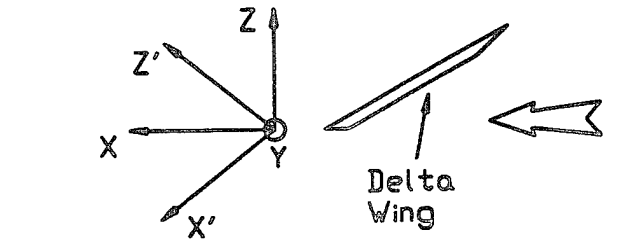

(a) Side View

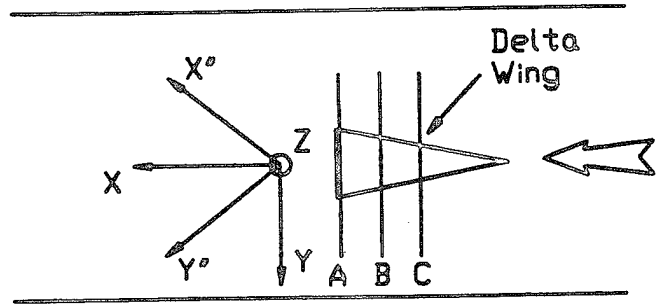

(b) Top View

Fig. 1. The coordinate system used for the LDV measurements: (a) side view, (b) top view.

The pressure instrumentation consisted of an ESP 32-channel electronic pressure scanner and an IBM PS/2 Model 60 equipped with a Data Translation DT 2905 data acquisition board. The ESP is a pressure scanner with 32 individual and independent pressure transducers multiplexed to a single analog output. The module itself is compact enough (1″ × 2.5″ × 1.8″) to be mounted inside the model. A cable connects the ESP to support circuitry outside the tunnel which is responsible for switching of the ports. The maximum rate at which the ports can be scanned is 20,000 readings/sec. The range of the ESP is ±37.350 Torr (1 Torr = 1 mm Hg) with an accuracy of ±0.026 Torr.

MODELS AND DATA ACQUISITION

The present group has been involved with delta wing aerodynamics work for quite some time. In the present effort we employ a water tunnel model which is geometrically similar to the model used in the wind tunnel. The wind tunnel model has been used extensively in earlier studies by this group (Rediniotis, et al. (1989), Rediniotis, et al. (1992), Hoang et al. (1993)). A schematic of the models is shown in Fig. 2. Geometrically similar cavity flaps were attached to each model and tests were conducted with and without flaps. The flaps had a chord equal to the width of the inclined surface of the edge, as shown in Fig. 3.

For the wind tunnel model, 27 pressure taps were installed along an axial line on the upper surface of the wing, as shown in Fig. 4. The taps have an opening diameter of 0.033″ and a spacing of 0.019, when non-dimensionalized by the chord of the model. The ESP is connected to the pressure taps by tubing of no more than 12 inches in length. Roughly equal lengths of tubing were used to connect each pressure tap to the ESP. Pressure measurements were taken for angles of attack from 28° to 44° in 2° increments.

For the LDV measurements, the model was placed in the water tunnel at an angle of attach α = 35°. Measurements were obtained along three vertical planes normal to the stream and located at distances $x/c = 0, 0.25$, and 0.50 which were named planes A, B and C, respectively, as shown in Fig. 1. In each plane a two-dimensional grid was defined with spacing $\Delta y = \Delta z = 1.25$ mm.

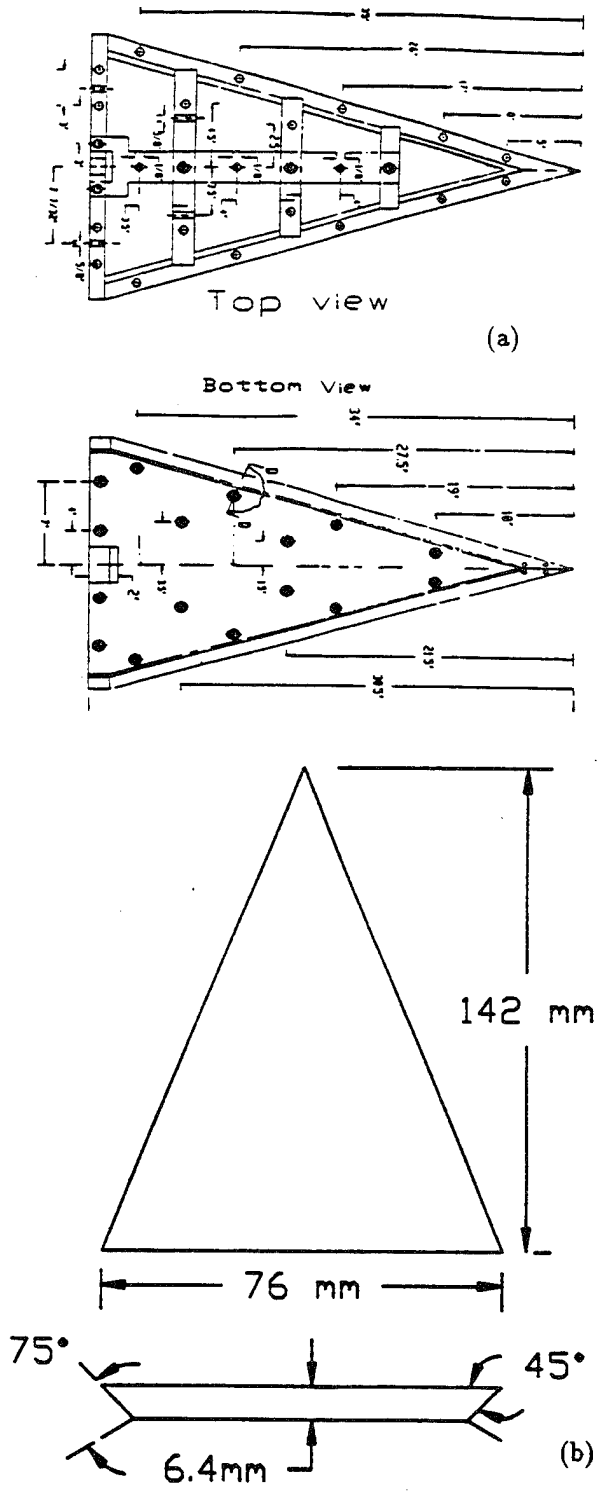

Fig. 2. The delta wing models. (a) The wind tunnel model, (b) The water tunnel model with flaps installed.

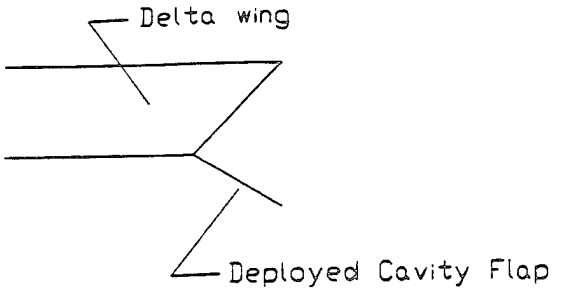

Fig. 3. Schematic of cavity flap configuration.

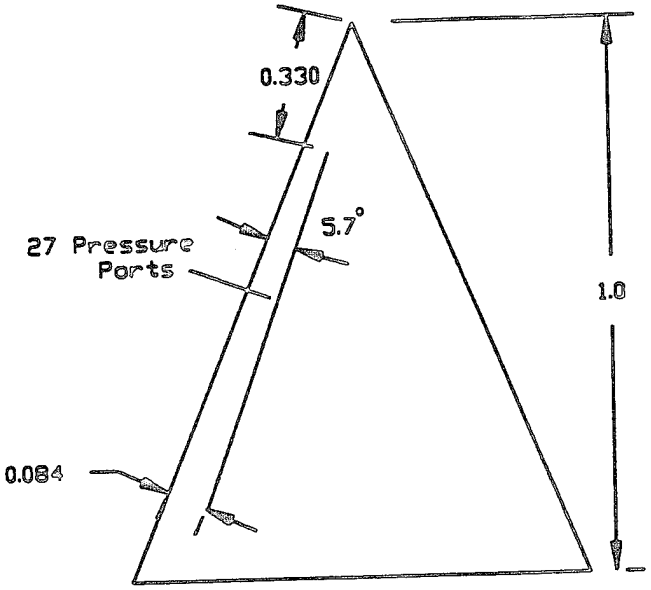

Fig. 4. Location of the axial line of pressure taps on the wind tunnel model. All distances non-dimensionalized with respect to the chord of the model.

RESULTS AND DISCUSSION

In the placement of the line of pressure taps, an assumption was made about the conical nature of the flow over a delta wing. For the pressure measurements over the plain wing, this assumption was valid. As shown in Fig. 5a, the pressure coefficients vary in a roughly linear fashion as the measurement station moves towards the trailing edge. For the wing equipped with flaps, this is not the case. The pressure distribution, as shown in Fig. 5b, does not have the linear distribution of Fig. 5a. It looks as if the core of the primary vortex is shifted over when the flaps are deployed. The LDV measurements should be able to shed light on this. What is clear from the pressure distribution, however, is that, without flaps, breakdown occurs over the planform of the wing at around 30° angle of attack. With flaps, its occurrence is delayed until about 36°.

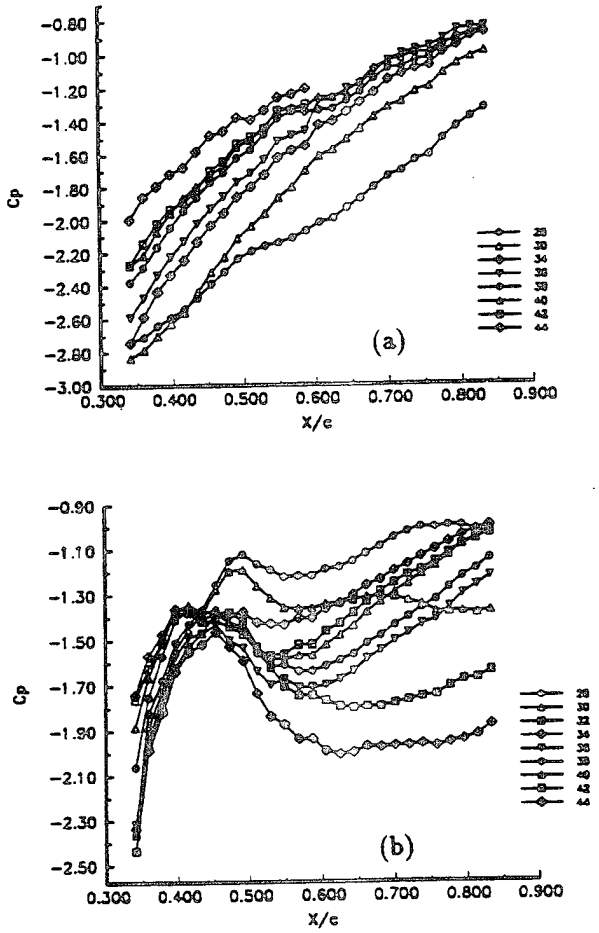

Fig. 5. Pressure coefficients as a function of non-dimensional axial distance. (a) Without flaps, (b) with flaps.

The axial component of the velocity is a strong indication of the location of leading edge vortices. This is because the vorticity wrapping around the vortex sheet induces an axial component of the velocity which, on many occasions, can reach values as high as three times the free stream velocity. Axial velocity contours for a plane wing are plotted in Fig. 6a,b and c along planes A, B and C, respectively. Figure 6c presents evidence of a coherent vortex with a maximum axial velocity $u/U_\infty \simeq 2.5$. However, the contours of Fig. 6b indicate clearly that the vortex

core has broken down. The velocity decreases towards the center of the core and it is possible that a stagnated region exists. The pattern is asymmetric and in the outboard region a pocket of high axial velocity exists. This pocket persists up to the trailing edge as shown in Fig. 6a. The conical character of the pattern is apparent but in plane A, it appears that the core of the vortex is already lifting to align itself with the free stream.

Data obtained with cavity flaps are presented in Fig. 7. It now appears that at this angle of attack, the flaps are capable of sustaining a coherent vortex. Axial components as high as 1.6 are observed even at the trailing edge of the wing. Moreover, it appears that the vortex is displaced somewhat in the inboard direction.

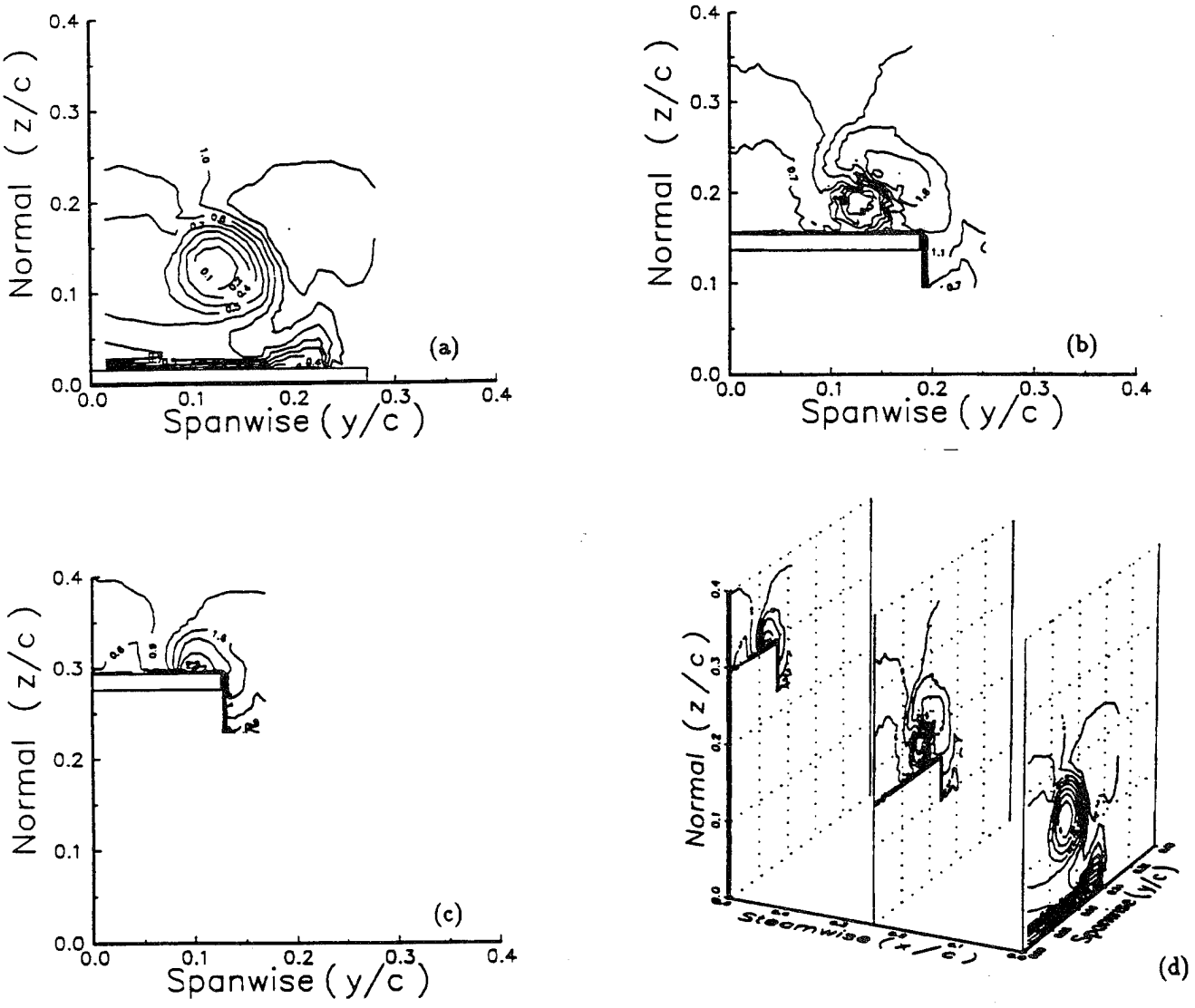

Fig. 6. Axial velocity contour over the delta wing (no flaps) at an angle of attack $\alpha = 35°$. (a) Plane A, (b) Plane B, (c) Plane C, (d) Composite view showing the three planes and their orientation in the streamwise direction.

Velocity vectors of the components contained in the planes of grid measurement are presented in Fig. 8. The fact that the leading edge vortex displaced further inboard is now corroborated. Moreover, it appears that along the trailing edge a second coherent vortex emerges a little further outboard.

CONCLUSIONS

Vortical flows over delta wings are very sensitive to external disturbances which could trigger vortex breakdown. The velocity data presented here were obtained by an unobtrusive method to provide such information for the first time on the effect of vortex

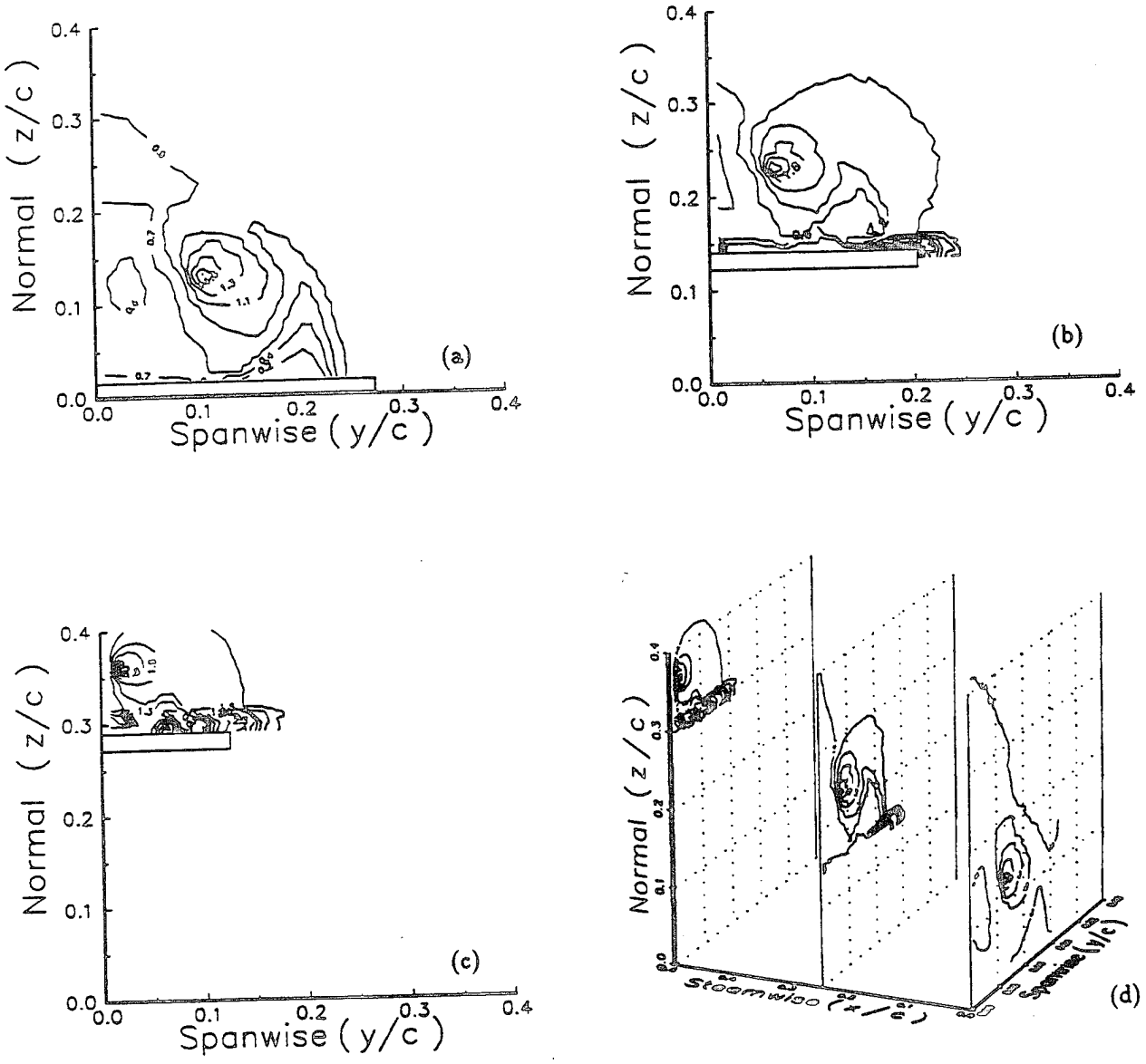

Fig. 7. Axial velocity contours over the delta wing with cavity flaps deployed. (a) Plane A, (b) Plane B, (c) Plane C, (d) Composite view showing the three planes and their orientation in the streamwise direction.

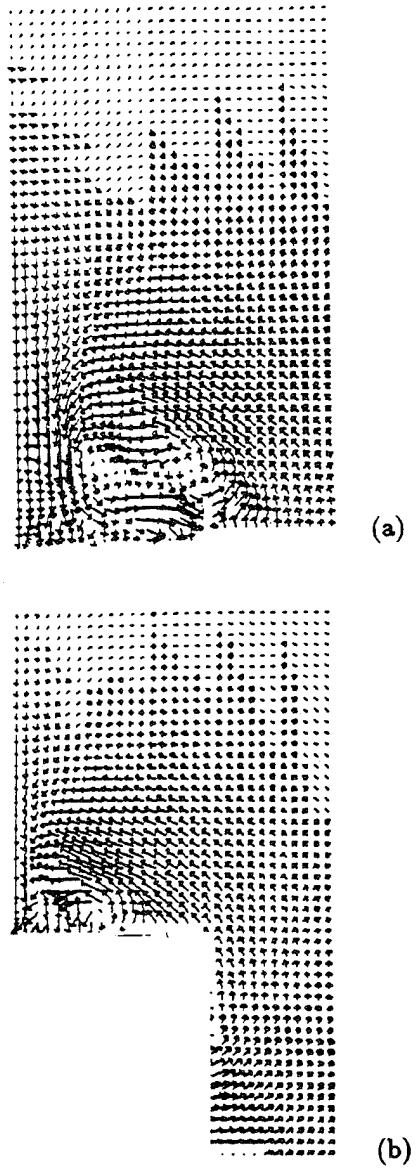

Fig. 8. Cross flow velocity vectors corresponding to (a) Plane B, (b) Plane C.

cavity flaps. Cavity flaps were employed and it was found that their deployment results in displacement of the vortices in the inboard direction. Moreover, the flaps prevent the vortices from breaking down for the angle of attack of $\alpha = 35°$. It therefore appears that for a fixed planform area, cavity flaps could be a useful tool for controlling the vortices developing over delta wings. It is planned to employ such flaps in order to control the flow field at higher angles of attack and in dynamic motions simulating aircraft maneuvers.

ACKNOWLEDGEMENTS

This work was supported by the Air Force Office of Scientific Research, Project No. AFOSR-91-0310 and was monitored by Major Daniel Fant. The authors would like to thank Dr. O. K. Rediniotis for his assistance in this investigation.

REFERENCES

Hoang, N. T., Rediniotis, O. K., and Telionis, D. P., 1993, "Three-D LDV Measurements Over a Delta Wing in Pitch-Up Motion," AIAA Paper No. 93-0185.

Koromilas, C. and Telionis, D. P., 1980, "Unsteady Laminar Separation, an Experimental Study," *Journal of Fluid Mechanics*, Vol. 94, pp. 347-384.

Lamar, J. E. and Campbell, J. F., 1983, "Recent Studies at NASA-Langley of Vortical Flows Interacting with Neighboring Surfaces," AGARD, CP-342, Paper No. 10.

Marchman III, J. F., 1981 "Effectiveness of Leading-Edge Vortex Flaps on 60 and 75 Degree Delta Wings," *J. Aircraft*, Vol. 18, pp. 280-286.

Marchman III, J. F., 1981, "Aerodynamics of Inverted Leading-Edge Flaps on Delta Wings," *J. Aircraft*, Vol. 18, pp. 1051-1056.

Mathioulakis, D. S. and Telionis, D. P., 1987, "Velocity and Vorticity Distributions in Periodic Separation Flow," *Journal of Fluid Mechanics*, Vol. 184, pp. 303-333.

Mathioulakis, D. S. and Telionis, D. P., 1989, "Pulsating Flow over an Ellipse at an Angle of Attack," *Journal of Fluid Mechanics*, Vol. 201, pp. 99-121.

Rao, D. M. and Campbell, J. F., 1987, "Vortical Flow Management Techniques," Prog. Aerospace Sci., Vol. 24, No. 3, pp. 173-244.

Rao, D. M., 1979, "Leading Edge Vortex Flap Experiments on a Delta Flap Wing," NASA CR-159161.

Rao, D. M., 1980, "Leading Edge Vortex Flaps for Enhanced Subsonic Aerodynamics of Slender Wings," Proceedings of the 1980 International Council of Aeronautical Sciences, Munich, Germany.

Control of the Transient Development of Leading Edge Vortices by Vortex Cavity Flaps

AIAA-94-1857-CP

by

N. W. Schaeffler*, O. K. Rediniotis† and D. P. Telionis††
Department of Engineering Science and Mechanics
Virginia Polytechnic Institute and State University
Blacksburg, VA 24061-0219

Abstract

A dynamic mount is employed to drive a delta wing into dynamic pitch up motions. Flow visualizations and surface pressure measurements are obtained. The effect of deploying cavity flaps is found to be significant in steady flows for angles as high as 42°. In unsteady flows it appears that the benefits of cavity flaps are more pronounced at even higher angles of attack.

Introduction

The new generation of fighter aircraft will be expected to execute maneuvers which will involve very high angles of attack. The control of such aircraft in the post-stall domain is a great challenge to the aerodynamicist. The flow fields over the lifting surfaces of such aircraft involve the transient development of large vortical structures and the stability of the vehicle hinges critically on our ability to control such structures. In this paper we explore the possibility of controlling vortical structures at high angles of attack by deploying control surfaces. We investigate the effect of control surfaces in two cases. (i) the wing at fixed angles of attack and (ii) the wing performing dynamic pitch ups.

Leading-edge flaps, often also referred to as leading-edge vortex flaps (LEVF) have been employed to improve delta wing aerodynamic characteristics at low speeds. Rao[1,2], Marchman[3,4] and Reddy[5] investigated the effect of LEVF's on the performance of delta wings and demonstrated that positive or negative deflections can lead to increase or decrease of drag. Broader discussions of advanced control devices can be found in Lamar and Campbell[6] and in Rao and Campbell[7]. These studies are based mostly on force and moment measurements and some flow visualizations.

In this paper we explore the potential of an alternative configuration of a control surface to control the aerodynamic characteristics of vortices and therefore increase the stability characteristics of delta wings at high angles of attack. This is the vortex cavity flap. A first step in this direction for angles of attack as high as 50° was reported by Rao[8] who demonstrated that the thrust and drag influence of flaps, both leading edge and vortex cavity flaps, remain effective well beyond the stall regime. The cavity flap was introduced and originally investigated by Rao[9]. This configuration is attractive for fundamental work because it does not change the nominal area of the wing and therefore any changes that occur are due only to the deployment of the flap and not to increase in wing planform. It is expected that the cavity flap will help modify and control the onset, growth and shedding characteristics of large-scale vortices but in Ref. 9 data were presented only on the effects of cavity flaps on lift and drag. The present group has employed laser-Doppler velocimetry to study the effects of cavity flaps on vortex breakdown in steady flow[10]. In the present study we present pressure distributions and extend this work to unsteady flow and to higher angles of attack.

Facilities and Instrumentation

The present research was conducted in the VPI & SU Stability Wind Tunnel. This tunnel has a 6′ × 6′ test section and an excellent quality of flow. The tunnel has been recently equipped with a dynamic strut which was given the acronym DyPPiR for "Dynamic-Plunge-Pitch-Roll" mechanism. The design construction, and calibration of this facility involved many faculty at VPI&SU, under the direction of Dr. Roger Simpson and six years of intensive work. A discussion of the main elements of the design can be found in Ref. 11 and the accompanying instrumentation employed by the present team in Ref. 12. More information on the actual performance of the DyPPiR is included in Ref. 13.

The DyPPiR can provide simultaneous plunging, pitching and rolling of models the order of 150 lb in weight, at frequencies of up to 10 Hz, depending on the amplitude of the motion. These motions can be independently controlled by software. Any

* Graduate Student
† Assistant Professor
†† Professor, Associate Fellow AIAA

combination of arbitrary motions is possible. In this case, ramp pitch up motions are executed. Such motions have been tested earlier in two much smaller facilities[14,15], a wind tunnel and a water tunnel and at Reynolds numbers the order of 10^4.

A schematic of the DyPPiR is shown in Fig. 1. A high pressure (3,000 psi) hydraulic system is employed to control the motion of the model. The plunge actuator is situated underneath the test section. This is a heavy unit, capable of driving the carriage and the model which together with the roll and pitch actuators weigh over 500 lb. The carriage is constrained by two round-way bearing tracts to run in the vertical direction. The pitch and roll actuators are mounted at the upstream end of the carriage. A sting is employed to position the model upstream of the DyPPiR. Active control of all three motions is possible and the three schedules can be defined independently. Plunging and rolling oscillation frequencies of up to 7 Hz are possible for amplitudes of 16″ and ±5° respectively. Rolling oscillation of up to 5 Hz at an amplitude of 122.5° can also be achieved.

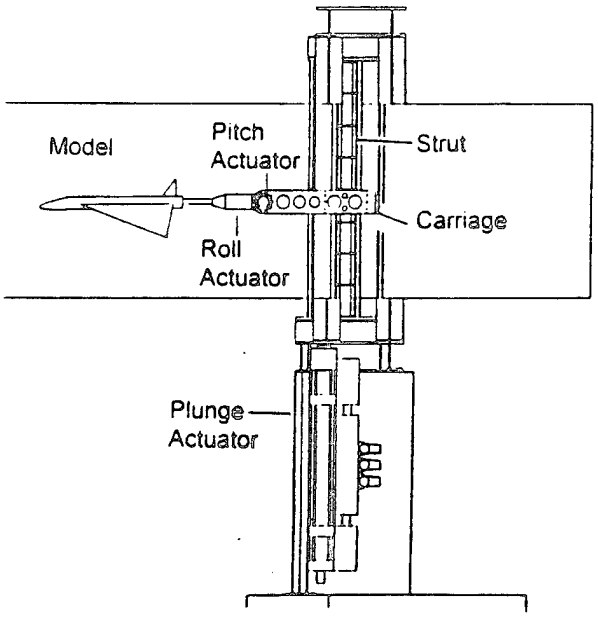

Fig. 1. The Dynamic-Plunge-Pitch-Roll mechanism (DyPPiR).

Simultaneous plunging of the DyPPiR carriage and pitching of the pitch actuator induces pitching of the model about its quarter-chord axis. The aim here is to control the leading edge vortices and delay breakdown, while pitching up to high angles of attack. This is pursued by deploying cavity flaps.

In the present experiments we employ a 75° sweep-3′ chord delta wing model (Fig. 2) which has been tested extensively in this facility in steady flow[13]. The flaps are hinged on the lower edge of the wing and are deployed as shown in Fig. 3. The model is hollow to provide space for instrumentation. This is an in-

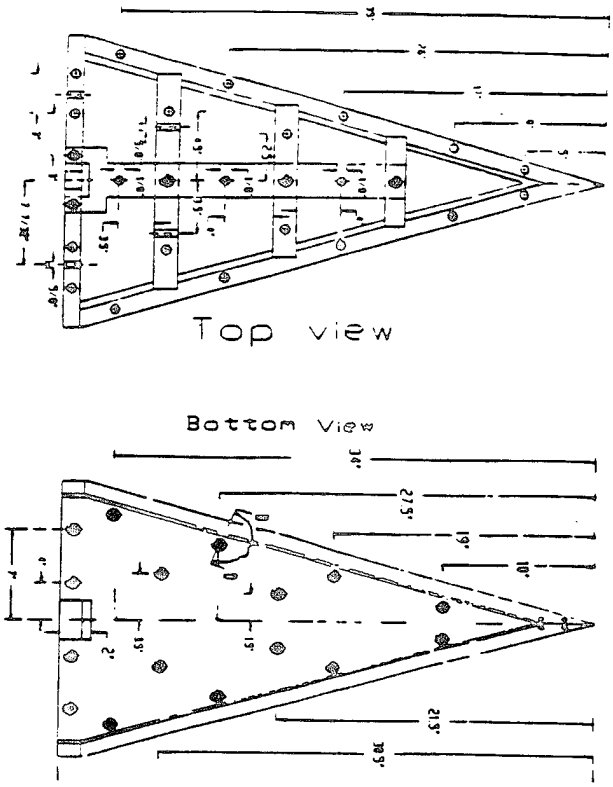

Fig. 2. The Delta wing model.

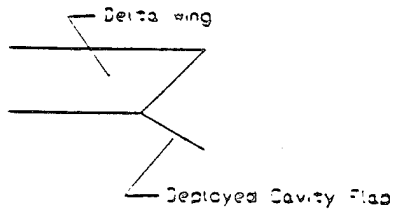

Fig. 3. The schematic of cavity flap configuration.

novating design allowing for fiber-optic laser-Doppler anemometry and traversing mechanisms to be operated from inside the model. To facilitate this type of operation, the upper surface of the model is a removable piece of high optical quality acrylic. The LDV optics can thus direct beams through the model wall from anywhere inside the model. The top surface of the model is equipped with many rows of pressure taps.

Pressure transducers are positioned beneath the instrumented surface to provide unsteady pressures with high frequency response.

Steady Flow Results

The effect of cavity flaps on the steady flow over a delta wing has been previously investigated by the present group[10]. In that investigation, Laser Doppler Velocimetry (LDV) measurements were made at low Reynolds number and it was shown that deployment of the flaps could prevent vortex breakdown from occurring over the planform of the wing for an angle of attack of $\alpha = 35°$. To compliment those data, surface pressure measurements were made at high Reynolds number over a wide range of angles of attack. Figure 4 shows the steady surface pressure distribution along an axial line on a plain delta wing under steady flow conditions. The line of data is a radial line emanating from the apex and traversing the wing beneath the core of the vortex as determined by earlier experiments. Results are shown in Fig. 4 for eight angles of attack, ranging from 28° to 44° in increments of 2°. This will serve as a baseline for the pitchup

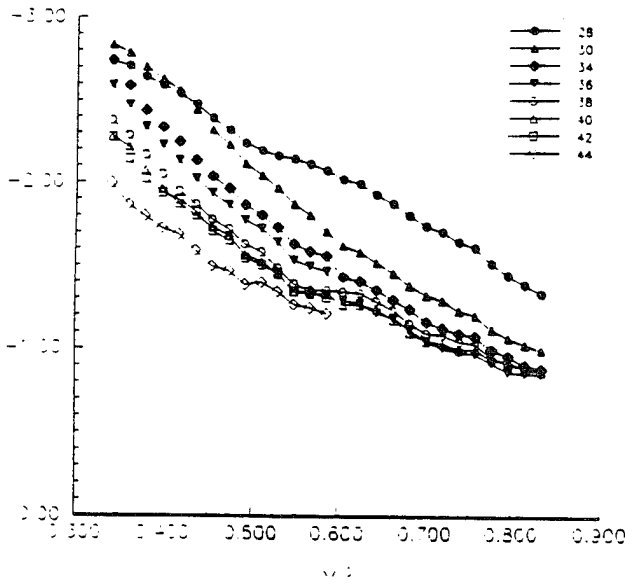

Fig. 4. Surface Pressure Distribution along an Axial line. Steady Flow. Plain Delta wing.

maneuvers to be discussed later. It also illustrates the ability of the DyPPiR to carry out automated steady flow measurements.

The data shown in Fig. 8 illustrate the classic behavior of the delta wing as the angle of attack increases. The curve for $\alpha = 30°$ is below the curve for $\alpha = 28°$, but as we approach the apex, the two curves cross at approximately $x/L = 0.45$. At higher angles of attack, the curves switch positions due to the presence of vortex breakdown over the planform of the wing. The resulting loss of vortex lift can be seen in the fact that subsequent angles of attack have numerically higher pressure coefficients. Figure 5 shows the same pressure distribution for a delta wing equipped with cavity flaps. An interesting distribution is observed. The data were obtained along the same physical line as the data of Fig. 4 but, it appears that the flaps have displaced the vortex, resulting in a trough in the pressure distribution. It can be observed, however, that as the angle of attack is increased the pressure coefficients continue to rise indicating an increase in

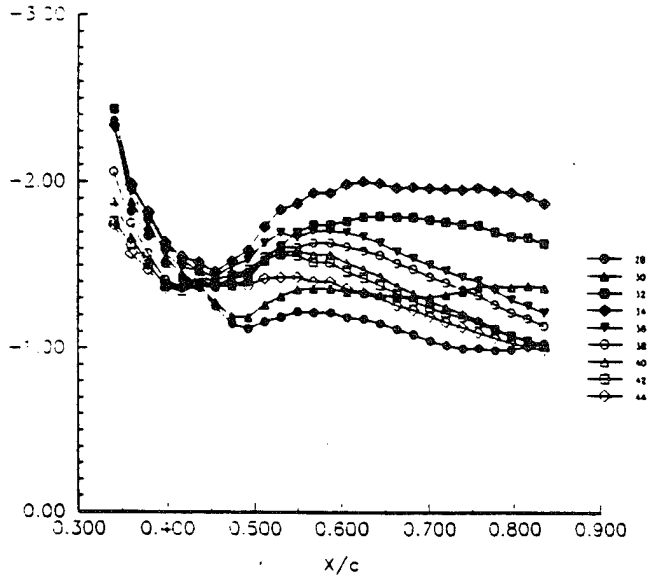

Fig. 5. Surface Pressure Distribution along an Axial line. Steady Flow. Delta wing with Cavity Flaps.

vortex lift. It is not until an angle of attack of 36° that the remaining curves begin to drop. The peculiar trough in the domain $0.25 < x < 0.55$ may be due to a displacement of the core in the inboard direction and therefore away from the line of measurement.

Flow visualization was achieved by releasing Helium bubbles from a hole near the apex of the wing. At the edge of the wing, the bubbles find themselves inside the vortex sheet and some tend to roll with the sheet but most of them are quickly sucked to the core where the pressure is minimum. The core of the vortex is thus clearly visualized in the form of a line populated densely by bubbles. At breakdown the core opens up and the bubble region expands.

In Figs. 6 through 10, we present flow visualization for angles of attach α = 28°, 30°, 36° and 40° respectively. At the top frame of each figure we display visualizations obtained with the plain wing, while at the bottom, we show results obtained over a wing with deployed cavity flaps. In Fig. 6 we observe that the core vortex is coherent all the way to the trailing edge of the wing, although at that location, the vortex over the plain wing is breaking down. Figures 7 and 8 indicate clearly the effect of the cavity flaps. Vortex breakdown in both cases is displaced downstream by about a distance of a third of the chord. A most interesting phenomenon is observed in Fig. 9. At this angle of attack, the flow over the plain wing is clearly broken down. The cavity flaps at this angle of attack induce a rather coherent vortex although the size of the core is considerably longer than the core observed over the wing at $\alpha = 28°$. Halfway down the wing, breakdown is observed again.

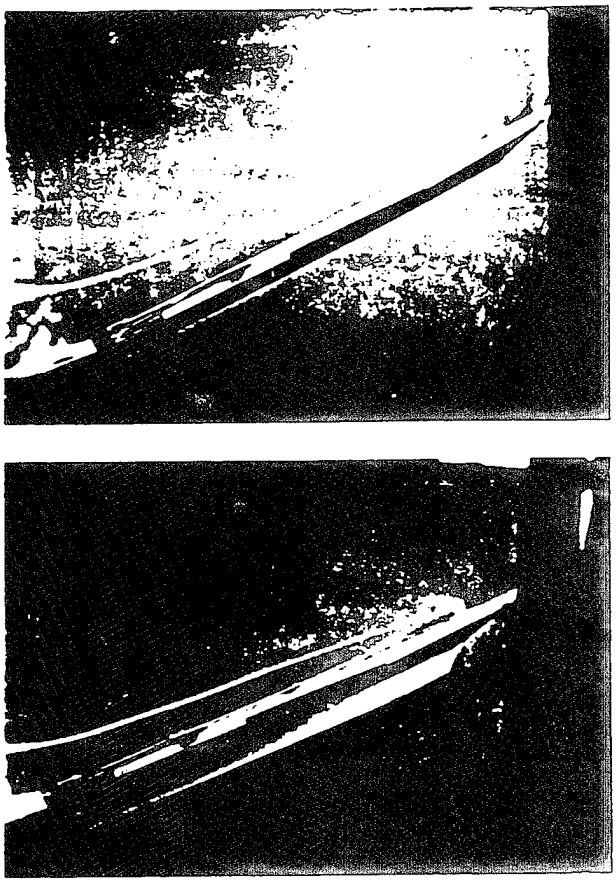

Fig. 6. Flow visualization over the wing at $\alpha = 28°$, (a) plain wing, (b) cavity flaps deployed.

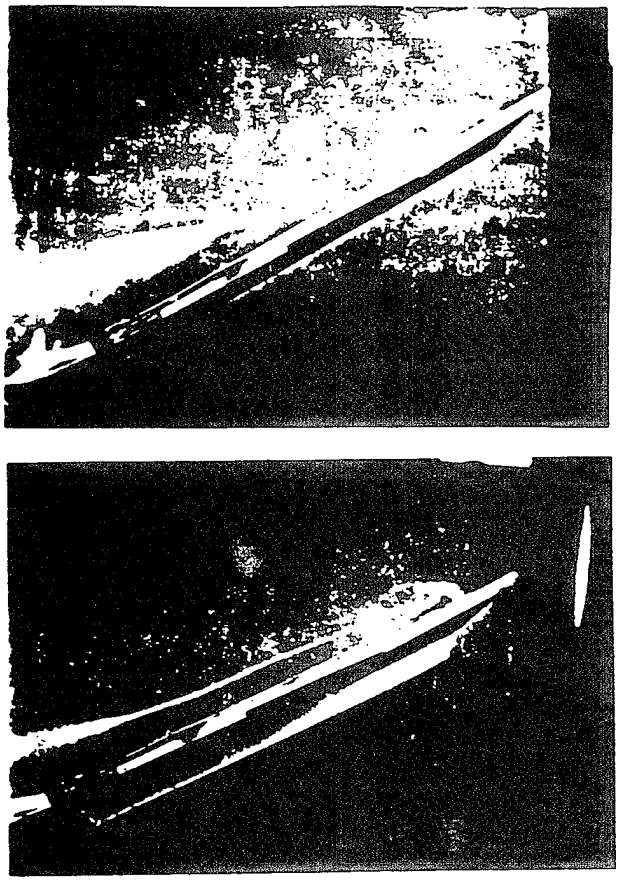

Fig. 7. Flow visualization over the wing at $\alpha = 30°$, (a) plain wing, (b) cavity flaps deployed.

Dynamic Motion Results

To study the effect of cavity flaps on transient development of the leading edge vortices, a pitchup maneuver was executed on the DyPPiR. In order for pitch up motions to be accommodated, the DyPPiR must execute high speed maneuvers with high accuracy. For pitchup motions, the DyPPiR must plunge down and pitch up simultaneously. As an extreme example of what the DyPPiR is capable of doing, a pitchup motion was executed from 0 to 30° in 0.3 seconds. During this test motion, the pitch goes from 0° angle of attack to 30°, while the plunge drops 23 inches, all in one third of a second. The solid lines in this Figure represent the actual trajectories obtained by linear variable differential transducers (LVDT) and the dashed lines represent the electronic command for

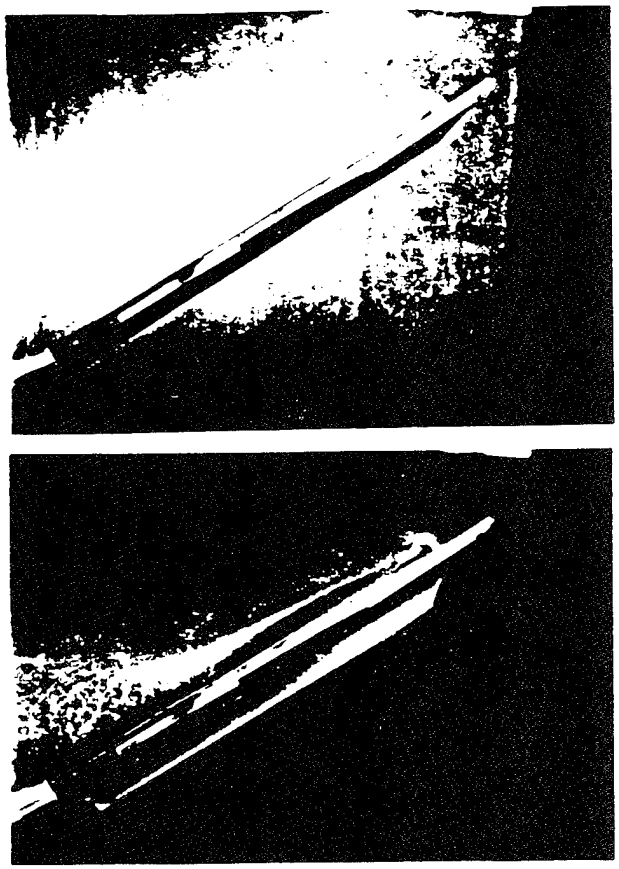

Fig. 8. Flow visualization over the wing at $\alpha = 36°$, (a) plain wing, (b) cavity flaps deployed.

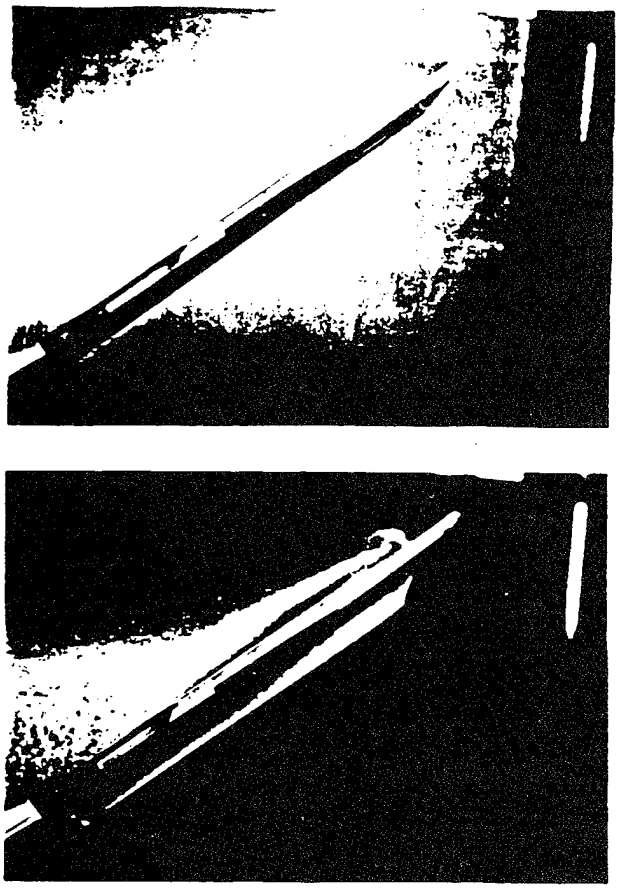

Fig. 9. Flow visualization over the wing at $\alpha = 40°$, (a) plain wing, (b) cavity flaps deployed.

the motion. The response of the DyPPiR to this maneuver is shown in Fig. 10. The pitch up schedule used in the present experiment is shown in Fig 11. It consists of a ramp function from approximately 28° to 42° angle of attack in three-quarters of a second. Again, surface pressure measurements were taken at 900 time instances during the pitch up motion and a resting period at the maximum angle of attack.

Figure 12 again shows the same distribution as Fig. 4 but for an unsteady pitchup maneuver. As the angle of attack increases, the pressure coefficients continuously drop, illustrating the influence of the unsteady nature of the flow. It is not until an angle of attack of 42.78°, the end of the motion schedule, that the curves begin to indicate a leveling of the pressure. There are two lines of data for that angle, one at motion's end, the other is the steady flow distribution obtained after the resting period, a time equal to two periods of the pitchup motion. Fig. 13 is an unsteady version of Fig. 9, obtained over the delta wing with cavity flaps. Here the curves never switch direction, each has lower pressure coefficient than the previous, all the way to the highest angle of attack.

In Fig. 14 we display data for a pitchup motion, but for the surface pressure distribution in a cross flow plane located at x/L = 0.61, for a plain delta wing. The same trend is evident. The curves show evidence of a loss of vortex lift near the end of the motion. Figure 15 presents similar data for a wing with cavity flaps. Again there is no evidence of any loss of vortex lift. The curves never reverse as the angle of attack increases.

Finally, Fig. 16 presents the same data shown in Figs. 14 and 15, but in a different format. In Figs. 14 and 15, data were selected from the 900 time instances sampled during the motion so that the data correspond to when the wing is at an integral, even angle of attack. Ten curves are selected to examine what happened during the time the 900 samples were taken. In Fig. 16 every third data set during the pitchup motion is represented. A matrix of values was created, containing pressure port versus angle of attack. The pressure coefficient is assigned a color based upon its value. The resulting image shows the

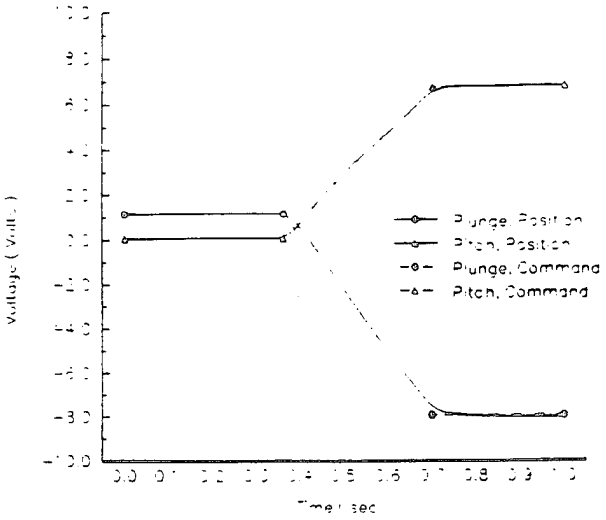

Fig. 10. Response of the DyPPiR to a Pitchup motion of duration of 0.3 seconds.

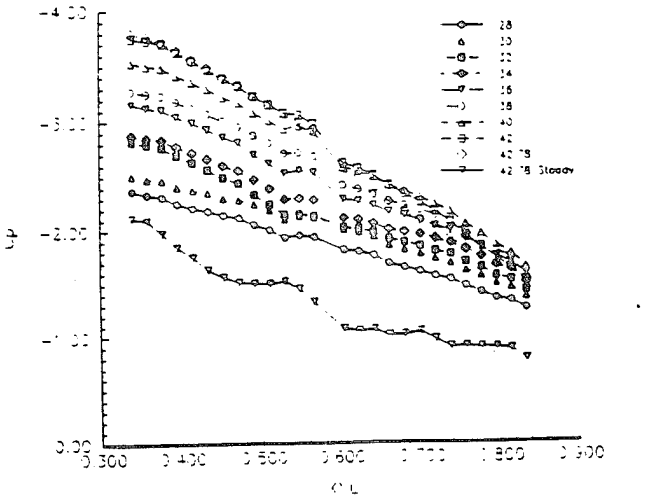

Fig. 12. Surface Pressure Distribution along an Axial line. Unsteady Flow. Plain Delta wing.

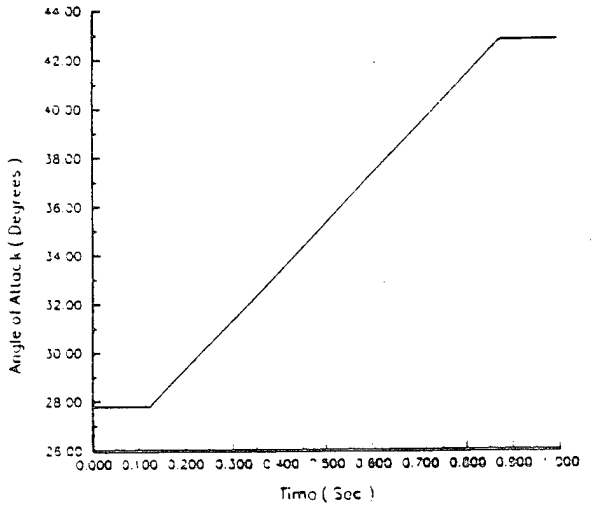

Fig. 11. Pitchup Schedule utilized in the experiment.

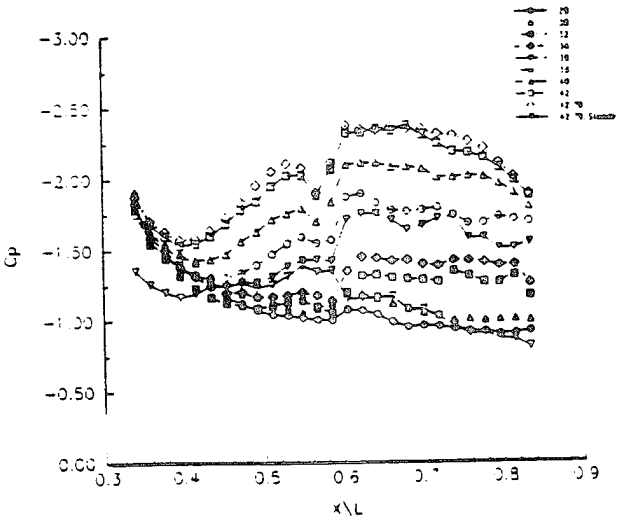

Fig. 13. Surface Pressure Distribution along an Axial line. Unsteady Flow. Delta wing with Cavity Flaps.

evolution of the surface pressure as a function of angle of attack, or as a function of time. The fact that the pressure coefficient in the plain-wing case has peaked and is beginning to decay is shown as the "island" of red in the upper left hand corner. In the case of the wing with deployed flaps the two yellow sections show evidence of merging and a new peak just beginning to form as the motion ends.

Conclusions

The experimental data presented here indicate that cavity flaps can delay considerably vortex breakdown in steady flow. In the range of angles of attack 28° to 42°, for each fixed angle, flaps can displace vortex breakdown downstream by about a third to a half of a chord length. For unsteady flow, the situation is quite different, at least for the angles of attack tested

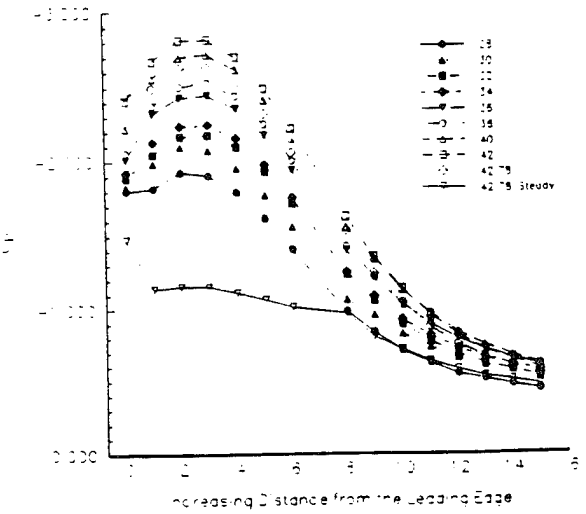

Fig. 14. Surface Pressure Distribution in a Cross-flow Plane at x/L = 0.61. Unsteady Flow. Plain Delta wing.

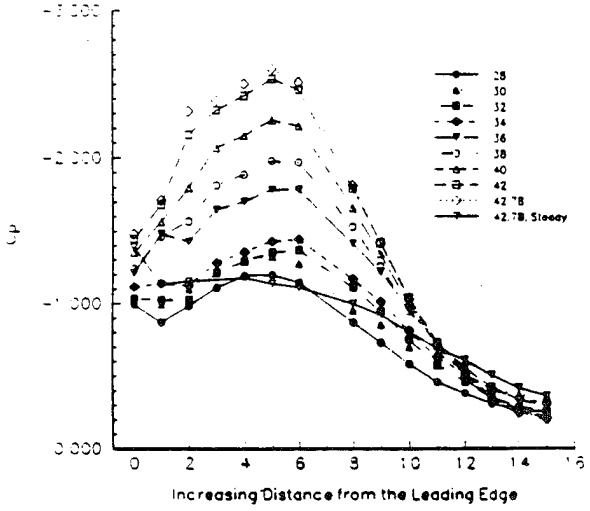

Fig. 15. Surface Pressure Distribution in a Cross-flow Plane at x/L = 0.61. Unsteady Flow. Delta wing with cavity flaps.

here. The dynamic maneuver is allowing the leading edge of the wing to generate vorticity which feeds directly into the vortex and sustains its coherence. In the present study with a dynamic motion terminating at $\alpha - 42°$, our pressure data indicate that right at the end of the motion to pressure seizes to drop and reverses direction. The effect of cavity flaps in the dynamic case is not as pronounced, but this may be

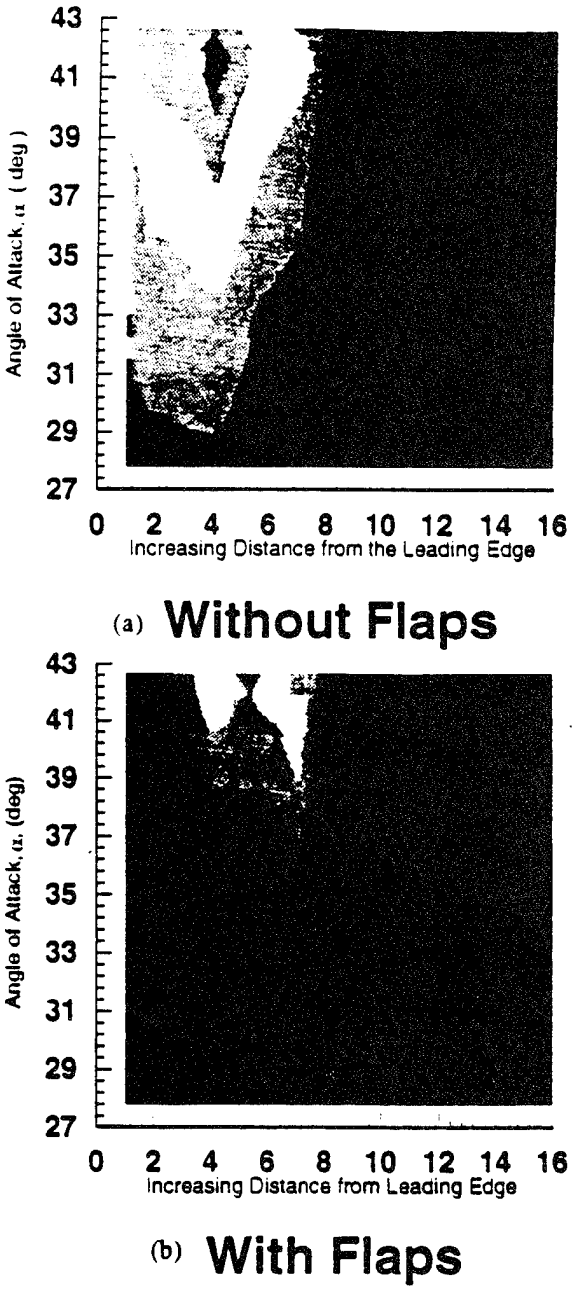

Fig. 16. Surface Pressure Distribution in a Cross-flow Plane at x/L = 0.61. Unsteady Flow.

due to the fact that there is little room for further improvement. Indeed it appears that the minimum in the low pressure over the plain wing is reached at about 40°. On the other hand, cavity flaps appear to delay the appearance of the minimum and essentially shift the behavior to higher angles of attack. Cavity flaps should therefore offer a stabilizing effect to the vortical structures. In fact our results indicate that in dynamic motions, it would be more efficient to deploy the cavity flaps only after the initial stage of the motion.

Acknowledgements

This work was supported by the Air Force Office of Scientific Research, Project No. AFOSR-91-0310 and was monitored by Major Daniel Fant.

References

1. Rao, D. M., "Leading Edge Vortex Flap Experiments on a Delta Flap Wing," NASA CR-159161, 1979.

2. Rao, D. M., "Leading Edge Vortex Flaps for Enhanced Subsonic Aerodynamics of Slender Wings," Proceedings of the 1980 International Council of Aeronautical Sciences, Munich, Germany, Oct. 16, 1980.

3. Marchman III, J. F., "Effectiveness of Leading-Edge Vortex Flaps on 60 and 75 Degree Delta Wings," *J. Aircraft*, Vol. 18, pp. 280-286, 1981.

4. Marchman III, J. F., "Aerodynamics of Inverted Leading-Edge Flaps on Delta Wings," *J. Aircraft*, Vol. 18, pp. 1051-1056, 1981.

5. Reddy, C. S., "Effect of Leading-Edge Vortex Flaps on Aerodynamic Performance of Delta Wings," *J. Aircraft*, Vol. 18, pp. 796-798.

6. Lamar, J. E. and Campbell, J. F., "Recent Studies at NASA-Langley of Vortical Flows Interacting with Neighboring Surfaces," AGARD, CP-342, Paper No. 10, 1983.

7. Rao, D. M. and Campbell, J. F., "Vortical Flow Management Techniques," Prog. Aerospace Sci., Vol. 24, No. 3, pp. 173-244, 1987.

8. Rao, D. M., "Po[illegible]ial of Segmented Vortex Flaps for Post-Stall Controllability," NASA High-Angle-of-Attack Technology Conference, 1990.

9. Rao, D. M., "Towards an Advanced Vortex Flap System - the Cavity Flap." (in press).

10. Schaeffler, N. W., Hoang, N. T., and Telionis, D. P., "Controlling of Delta Wing Vortices with Vortex Cavity Flaps," ASME Winter Annual Meeting, Nov. 1993.

11. Ahn, S., Choi, K.-Y., and Simpson, R. L., "The Design and Development of a Dynamic Plunge-Pitch-Roll Model Mount," AIAA Paper No-89-0048, 1989.

12. Rediniotis, O. K., Hoang, N. T., and Telionis, D. P., "Multisensor Investigations of Delta Wing High-Alpha Aerodynamics," AIAA Paper No. 91-0735, 1991.

13. Hoang, N.T., Wetzel, T.G. and Simpson, R.L., "Unsteady Measurements Over a 6:1 Prolate Spheroid Undergoing a Pitch Up Maneuver," AIAA Paper No. 94-0197, 1994.

14. Rediniotis, O. K., Klute, S. M., Hoang, N. T., and Telionis, D. P., 1992, "Pitch Up Motions of Delta Wings," AIAA Paper No .92-0278, 1992, also *AIAA Journal*, in press.

15. Hoang, N. T., Rediniotis, O. K., and Telionis, D. P., "Three-D LDV Measurements Over a Delta Wing in Pitch-Up Motion," AIAA Paper No. 93-0185, 1993.

AIAA-95-2308

Instabilities of Vortex Breakdown; Their Structure and Growth

L. W. Traub and O. K. Rediniotis
Aerospace Engineering Department
Texas A&M University
College Station, TX

S. M. Klute, C. T. Moore and D. P. Telionis
Department of Engineering Mechanics
Virginia Polytechnic Institute and State University
Blacksburg, VA

26th AIAA Fluid Dynamics Conference
June 19-22, 1995/San Diego, CA

Instabilities of Vortex Breakdown; Their Structure and Growth

L. W. Traub† and O. K. Rediniotis*
Aerospace Engineering Department
Texas A&M University
College Station, Texas

S. M. Klute†, C. T. Moore† and D. P. Telionis**
Department of Engineering Mechanics
Virginia Polytechnic Institute and State University
Blacksburg, Virginia

Abstract

Periodic and quasi-periodic phenomena associated with the post-breakdown flowfield over slender delta wings are investigated. In particular, the structure of the helical mode instability as the source of these phenomena is researched through flow visualization, digital particle image velocimetry and hot-wire anemometry. Evidence is provided to further support the conjecture that the rotation of the helical structure originating at breakdown with a spiraling sense opposite to that of the vortex rotation, is responsible for the quasi-periodic oscillations that appear in the form of distinct peaks in the velocity and surface pressure spectra. Two regions of the helix with different growth rates and non-dimensional frequencies were identified and the coherence and path of the disturbance were quantified.

Introduction

The flowfield associated with the two leading-edge vortices over a delta wing exhibits four types of organized periodic phenomena. Their physical mechanisms do not seem to be related and their frequency ranges are distinctly different. A brief description of each follows.

(a) Kelvin-Helmholtz instabilities developing in the leading-edge shear layer. Experimental work[1,2] as well as numerical simulations[3] have documented the existence of such sub-structures, their formation at or above the leading edge, their convection with the shear layer and their roll-up into the leading-edge vortex. However, discrepancies regarding their unsteady character seem to exist between experiments and computations. Although both approaches yielded Strouhal shedding frequencies of the same order of magnitude (St=fC/U=10 to 30, where C is the wing chord and U is the freestream velocity), the computations predict a Strouhal frequency that decreases almost linearly with chordwise location, while the experiments detect a single frequency along the leading edge. Experiments also document a frequency variation with the inverse square root of the Reynolds number. Although such a relation indicates a dependence of the phenomenon on viscous effects, an inviscid, two-dimensional, spatial, linear stability analysis for shear-layer flows correctly predicts the frequency of the instabilities[4].

(b) Fluctuations of the breakdown location in the chordwise direction. Gursul and Yang[5] observed periodic oscillations of the breakdown location over a 70° -sweep delta wing at a non-dimensional (St) frequency of St=fC/U=0.2 or below. Payne et. al.[6] observed similar "wandering" of the breakdown location, which for a very slender wing (Λ=85°) and low speeds was described as random. For the same wing and high speed, the "wandering" disappeared. For a range of sweep angles (Λ=70°-85°) and speeds they also observed low-amplitude, high-frequency breakdown-location oscillations, although the frequency was not quantified.

(c) Periodic oscillations in the breakdown region of the leading-edge vortices, manifested in the velocity and surface pressure power spectra[7-12]. Although the database of measured[7-11] and calculated[12] frequencies seems to be consistent, a consensus as to the origin of the

† Research Assistant
* Assistant Professor, Member AIAA
** Professor, Member AIAA

oscillations has not entirely been reached. Some researchers[7-10] have attributed these periodic oscillations to non-axisymmetric structures that rotate with the vortex in the breakdown region and in particular[9] to the helical mode instability of the breakdown wake flow, while others[11] suggested that the helical structure only contributes to the phenomenon and that the real origin is a "waving" motion of the streaklines on the surface of the wing. The nature and features of this periodic behavior will be further addressed in the present paper.

(d) Vortex shedding off the wing leading edges[9,13]. At angles of attack equal or larger than the angle of attack for which the breakdown location reaches the wing apex, the shear layers emanating from the wing leading edges do not roll up over the wing. Instead they convect downstream for a distance on the order of the wing chord and roll into vortices which then shed off to form a Karman vortex street pattern. Symmetric as well as alternate vortex shedding patterns are possible with the latter dominating as the wing aspect ratio decreases. Vortex shedding has little Reynolds number dependence and, for a 75°-sweep delta wing, exhibits a non-dimensional Strouhal frequency (St=fC/U) around 0.2.

From the above, it is obvious that the flow over a delta wing exhibits a wealth of dynamic characteristics. Their properties and interactions are yet to be understood. In the present work we address the periodic behavior of type (c) above, for a 75°-sweep delta wing.

Facilities and Experimental Techniques

Experiments were conducted at the Aerospace Engineering Department of Texas A&M University and the Engineering Mechanics Department of Virginia Tech. The techniques employed at Texas A&M include flow visualization and Digital Particle Image Velocimetry (DPIV) while the problem was investigated through Hot Wire Anemometry at Virginia Tech.

A schematic of the experimental layout at Texas A&M is shown in Fig. 1. The investigation was conducted in the Aerospace Engineering 2' x 3' water tunnel. This facility has a maximum test section velocity of 0.91 m/sec (3 ft/s) and a two-dimensional contraction ratio of 6:1. At the free-stream velocities of the present tests the turbulence intensities in the test section do not exceed 0.3%. The tunnel is of the free surface configuration and all three test-section sides are made out of glass. A plexiglass delta wing with a 75° leading edge sweep angle and a chordlength of C=198 mm was used in the tests. In order to enforce flow separation, and thus reduce sensitivity to Reynolds number effects, the leading edges were beveled at 45° on the windward side. The tunnel is equipped with a dynamic pitch-yaw model mount system with position feedback. However, for the purposes of the present work, the system was employed in its static mode of operation. The model angle of attack was varied within the range of angles for which vortex breakdown occurs over the wing (α=30° - 50°), although most of the experimental data were taken at α=40°.

Another one of the tunnel's features employed in this work was its six-color flow visualization system. To visualize the flow field over the wing, dye was injected at the wing apex, and was thus entrained into the two vortex cores. The flowfield was illuminated by a laser sheet generated by a 2-W argon-ion laser. Most such tests were run at a free-stream velocity of 5.3 cm/sec.

In order to further characterize the flowfield downstream of breakdown, the DPIV technique was also employed. The technique is ideal for temporally characterizing quasi-periodic phenomena for which accurate phase referencing is not available. This limitation rules out the use of point measurement and ensemble averaging techniques to extract global temporal information on the flow. In fact, the use of these techniques would, at best, provide the time-averaged velocity distribution. The seed particles were 45-120 μm neutrally buoyant fluorescent spheres. Illumination was provided by a 2W argon-ion laser. A 3.5x beam expander was used to expand the laser beam diameter to 6mm. A lens was then used to expand the beam to a sheet which was then suitably orientated. Series of images were captured and digitized using a combination of a Panasonic CCD camera and a Data Translation DT 2861 frame grabber at a rate of 30 frames/sec. This camera-frame grabber combination yields an image size of 512 x 480 pixels. Instantaneous planar velocity distributions are derived from two captured images, separated by a known time interval, by cross-correlating corresponding sampling windows in the two images. To accelerate the data reduction process, the two windows are first fast-Fourier transformed, the corresponding Fourier coefficients are multiplied and the result is inversely transformed to obtain the cross-correlation[14]. The temporal evolution of the flowfield can be captured by processing, in pairs, a series of captured images. DPIV tests were run at a nominal velocity of 4.6 cm/sec (0.15 ft/s), with a corresponding Reynolds number of about 9100 based on the wing root chord. Since the tests were performed at a low freestream velocity, no laser light pulsing was needed to avoid particle streaking due to the finite CCD integration time. For the same reason, i.e. low freestream velocity, the image pairs processed by the data-reduction software did not necessarily consist of consecutive images.

Experiments were also conducted in the ESM wind tunnel at Virginia Tech which is an open-circuit facility with a 0.508 x 0.508 m test section. The turbulence level in the test section ranges between 0.3% and 0.5%. A 75°-sweep delta wing model with a chordlength of C=303 mm was tested at α=40°. The free-stream velocity was 10.6 m/sec and the Reynolds number based on the wing chord was Re=210,000. Measurements were obtained with a pair of hot wires in order to allow the calculation of power spectra and phase differences. Such methods were employed for flows over delta wings by Rediniotis et al [13] and later by Hubner and Komerath[15]. The experimental setup is shown in figure 2. Measurements were performed at the right leading-edge vortex. One wire (wire A) was fixed very near the plane of symmetry at X/C=0.916, Y/s=0.09 and Z/s=1.08, where X measures from the apex along the chordwise direction, Y measures from the wing symmetry plane, Z measures from the wing surface along the wing normal and s is the local semi-span. The other wire (wire B) was mounted on a traversing scale which in turn was attached to a second traversing scale. This facilitated traversing of the hot wire along a plane normal to the wing surface and at a fixed X/C. The entire rig was mounted on a frame which kept scales and traversing mechanisms outside the tunnel to reduce interference but allowed the entire system to rotate thus facilitating changes of the angle of attack. Traversing was achieved by stepper motors which were controlled by a laboratory computer. The process was automated so that wire B covered a prescribed measuring grid, at each plane. Data were obtained along five planes, at X/C=0.916, 0.958, 1.0, 1.042 and 1.084. At each grid point the signal was self-triggered and ensemble-averaged over 20 realizations. A Hewlett Packard signal analyzer (HP 5420A) was employed to reduce the data and generate auto- and cross-spectra, coherence functions and phase differences.

Results and Discussion

Flow Visualization

Interpretation of flow visualization should be done with caution. When dye or particle identifiers in general are injected at a point in the flow, the visualized patterns are streaklines. These patterns are usually interpreted as representing vorticity concentrations, which might not always be the case. For a streakline or a finite-thickness fluid marker to represent a vortex filament or a vortex tube, respectively, several conditions have to be satisfied. For example, in 2-D unsteady shear flows, the fluid marker has to be introduced at a location where the fluctuating vorticity is negligible and the linearized inviscid theory has to hold[16]. In the present experiments, the marker was injected immediately underneath the apex and was entrained in the vortex cores of the two leading-edge vortices. Figure 3 presents a typical core visualization. The laser sheet is aligned so that it illuminates the half of the helical structure closer to the wing. It is suggested here that, downstream of breakdown, the marker visualizes the vorticity lines, for at least a limited length

Consider the vorticity transport equation:

$$\frac{\partial \Omega}{\partial t} + V\cdot\nabla\Omega = \Omega\cdot\nabla V + \nu\nabla^2\Omega$$

where Ω and V are the vorticity and velocity vectors respectively. If the viscous diffusion is negligible compared to the convection and stretching terms the above equation reduces to Helmholtz's equation:

$$\frac{\partial \Omega}{\partial t} + V\cdot\nabla\Omega = \Omega\cdot\nabla V$$

from which it follows that fluid particles that are part of a vortex tube (or a vortex line) at some instant are part of it for all times. Upstream of breakdown, an order-of-magnitude analysis of the axial components of the convection and viscous diffusion terms $V\circ\nabla\Omega$ and $\nu\nabla^2\Omega$ respectively, revealed that at the edge of the viscous core the former term is at least an order of magnitude larger than the latter. The calculations were based on the velocity distributions of figure 4 taken from Ref. 17. Even inside the core the convection is larger than the viscous diffusion. Similar conclusions were drawn for the case of the 2-D vortices in the wake of a pitching airfoil[18]. Even in their core, the viscous time scales are about fifteen times the convective time scales, i.e., the ratio of the times vorticity takes to diffuse and convect, respectively, over a fixed length, is about fifteen.

. In the case of spiral breakdown, as previously shown[12], there is no 3-D stagnation point corresponding to a saddle. Downstream of breakdown the spiral is displaced away from the axis, to areas with considerable convective velocities. By now it is a well-documented fact that away from the vortex axis, the velocity distributions are not dramatically affected by breakdown. There, axial and azimuthal velocities on the order of the free-stream velocity still exist. The existence of high convection levels is corroborated by the lack of dye accumulation. The continuous dye supply from upstream

is efficiently convected downstream without considerable thickening of the dye trace for at least two helix wavelengths downstream of breakdown. Therefore, although not rigorously proven, we believe that, for at least that length, convection dominates viscous diffusion and that Helmholtz's equation holds. In Visbal[12], a numerically calculated iso-vorticity surface for the case of spiral breakdown exhibits obvious resemblance to the flow visualization.

Flow visualization was performed for a range of angles of attack between 30° and 50°. The breakdown location thus varied from X/C=0.18 to X/C=1.0, where C is the wing root chord and X measures from the apex along the chord. The free-stream velocity was 5.3 cm/sec. For each angle of attack, several consecutive frames were recorded and analyzed. For all cases spiral breakdown was observed. Spiral breakdown was very stable as far as maintaining a fixed location. No excursions of the breakdown location were observed. However, brief changes of breakdown to bubble type occurred in a rather random fashion, although this observation was purely visual and has no statistics associated with it. This transformation to bubble type breakdown was always associated with an upstream shift of the breakdown location by about 7% to 10% of the chord. The original breakdown location was restored when breakdown transformed back to spiral type. Bubble type breakdown occupied only about 10% of the total observation time, while the spiral type persisted for the remaining 90% of the time. Figures 5(a) and (b) present flow visualizations of spiral and bubble breakdown respectively. The flow is from left to right and the laser sheet illuminated the half of the vortex close to the wing. As seen in figures 3 and 5(a), a spiral structure originates at breakdown and extends downstream with an increasing diameter. It is interesting to notice that the spiral structure exists even in figure 5(b), although the original breakdown is of the bubble type.

The spiral structure rotates with the leading-edge vortex although the sense of the helix is opposite to the vortex rotation. The rotation of the structure and its frequency, for at least the first two wavelengths, was very repeatable. The frequency of rotation was measured at the first three wave peaks, as shown in figure 6, by counting the number of frames per revolution (1/30 sec between consecutive frames). Frame counts per revolution varied from 6 to 30, depending on the location of breakdown. To increase the resolution and accuracy of the measurements we took advantage of the repeatability of the motion. The number of frames for several revolutions was counted and was then divided by the number of revolutions. The error in period estimation was thus kept below 5%. It was interesting to find that for a fixed breakdown location, the three frequencies associated with the three wave peaks were equal, within our error margin. Over such a short distance (15% of C) and for the low free-stream velocity the experiments were conducted at, any expected frequency differences would be on the order of a fraction of 1 Hz. Such differences would manifest themselves as an accumulation of the phase difference between the two points of interest, over several revolutions. Such relative phase shift could not be observed over several revolutions of the structure. This observation, at first glance, seems inconsistent with previous experiments[7-10] as well as with the hot-wire measurements reported in a later section of the present work. Figure 7 is a plot of the non-dimensional Strouhal frequency $St=fX_{bd}/U$, where U is the free-stream velocity, versus non-dimensional breakdown location X_{bd}/C. As seen in this figure the non-dimensional frequencies vary from 2.7 to 5.6. Similarly, high non-dimensional frequencies (St around 2.8) were numerically calculated in Ref. 19 for a 75°-sweep delta wing and for X_{bd}/C around 0.8. These values, however, would not be expected according to previous experiments[9]. There[9], for a range of sweep angles and angles of attack, the frequency was measured at several chordwise locations downstream of breakdown and was non-dimensionalized with the chordwise distance, X, of the measurement location from the apex and the free-stream velocity (fX/U). For fixed sweep angle and angle of attack this non-dimensional frequency was found to be nearly constant and independent of the measurement location. For a 75°-sweep delta wing and an angle of attack of 40°, this value was around 1. If this value is a constant for all points downstream of breakdown, to the limit it should also be the value for fX_{bd}/U. However our experiments for a=40° yield a value of about 3.2. Moreover, in our experiments, for the first two helix wavelengths (covering a ΔX of about 15% of the chord C), f X/U is not constant, since the measured f is the same for the first three wave peaks but X changes. Although the Reynolds numbers of the two sets of experiments were different (11,000 here versus 100,000 in Gursul[9]), we feel the discrepancy should not be attributed to this difference. By now, it is a rather well established fact that the phenomenon has very little dependence on Reynolds number. Moreover, LDV measurements previously performed by Rediniotis and Schaeffler[10] at Reynolds numbers around 40,000 yielded frequencies that are in accord with Gursul[9]. However these measurements were taken at chordwise locations significantly downstream of the breakdown location (at least by 30% of the chordlength) which we suspect is also the case in Ref. 9. As explained below, this difference with the present experiments is more likely to be the source of the discrepancy. Below, we attempt to explain

the above observations.

In Ref. 7, 9 the variation of f with X was insightfully explained by combining the following two arguments: (a) the radius of the helical instability grows proportionally to the local vortex size, or the local semi-span, i.e., r_{inst}/X proportional to s/X = const., where r_{inst} is the local helix radius and s is the local semi-span, and (b) downstream of breakdown, the azimuthal velocity, which is responsible for the rotation of the helical instability, obeys a nearly conical pattern, as shown in figure 8 (taken from Ref. 7), where r is the radial distance from the vortex axis and x the chordwise distance from the apex. From the above arguments and simple algebra it follows that fX/U=const. Although the first argument might be true for locations away from breakdown by more than 30% of the chord, it does not seem to be the case for the first 0.15C of the helix immediately downstream of breakdown. In this region, the helical structure expands in size with downstream distance with rates higher than s/X. This is illustrated in figure 9. In this figure, the thick solid line and the dashed line indicate the locations of the leading-edge and the wing symmetry axis, respectively. The thin solid line geometrically represents the rate of growth of the helix radius. This rate is clearly larger than s/X (helix growth line forms an angle with wing axis larger than the angle the leading-edge forms with the wing axis). This observation might explain the fact that the frequency f is constant for the first two wavelengths: r_{inst}/X increases with X and therefore, from figure 8, the azimuthal velocity of the instability increases. At the same time, the azimuthal path of the instability increases downstream since r_{inst} increases so that the ratio of the azimuthal velocity over the azimuthal path, which is the frequency, stays almost constant.

DPIV Measurements

As it was previously seen in the flow visualization section, at chordwise locations downstream of breakdown and away from it by more than two wavelengths of the helix, turbulent mixing prevents the unobscured visualization of the helical structure. Thus, no unequivocal conclusions can be drawn from visual inspection. The clear, periodic rotation of the helix observed immediately downstream of breakdown is obscured here. Instead, the phenomenon becomes rather quasi-periodic and hard to track, spatially and temporally. However, evidence of the helical structure and its motion is provided through Digital Particle Image Velocimetry (DPIV). The technique provided instantaneous velocity distributions along two planes. The first plane was oriented normal to the wing planform and was located at X/C=0.75. The angle of attack was 40° and the free-stream velocity was 4.6 cm/sec. To increase the spatial resolution of the measurements, the camera was focused only on one of the leading-edge vortices. Two images were captured at times t_1 and $t_1+\Delta t_{fr}$, where Δt_{fr}=1/30 sec is the time between consecutive images (frames). Cross correlation of the two images yielded the velocity field presented in figure 10. The circle drawn in the figure indicates the location of the main vortical structure in the cross-flow plane. This vortex is identified as the intersection of the helical structure with the plane. Two images captured at a later time t_2 yielded the velocity field of figure 11. The vortical structure has now displaced itself with respect to its position in figure 10. Although, due to the quasi-periodicity of the phenomenon, it is hard to capture a frame sequence that would clearly illustrate an entire period of the structure's rotational motion, the two previous figures reveal movement of the vortical structure, although not its path. This movement is bound to register in point velocity measurements and possibly in their power spectra.

More insight in the shape and movement of the helix was obtained through DPIV measurements along a plane oriented so that it goes through the axes of the leading-edge vortices, as determined through flow visualization (fig. 12(a) and (b)). The camera was again focused onto one of the vortices. Sixteen consecutive images were captured. The first two and the last two (fifteenth and sixteenth) images were correlated to generate the velocity distribution at times t_3 and t_3+0.5 sec, respectively. For each distribution, its spatial mean streamwise velocity was calculated and subtracted from each velocity vector. This yielded the velocity distributions in a reference frame moving with the structure. These two flowfields are presented in figures 13 and 14. In-plane velocity vectors are superimposed on azimuthal vorticity contours. The circles identify the vortical structures which are the result of the multiple intersections of the helix with this plane (figure 12). A vortical pattern that resembles a Karman vortex street is evident. The downstream convection of the structure between figures 13 and 14 is also evident. In Figure 14, vortex 3 convected out of the measurement domain while a new vortex 0 is about to enter the field. Vortices 1 and 2 are present in both fields, although at different locations. The measurement field extends from approximately X/C=0.5 to X/C=0.8. It should be noted here that the velocity vectors have not been quantified in terms of the free-stream velocity, although their relative magnitude is correct. The convection observed above is consistent with the assumption of a helical vortical structure, with a helical sense opposite to the rotation of

the leading-edge vortex, and rotating in the same sense as the leading-edge vortex. In figure 12, the marked locations on the helix correspond to the vortical structures of figure 13. These structures are the imprint of the helix as it crosses the measurement plane. At the location of vortex 1 the helix is directed into the page while at vortex 2 it is coming out of the page. This is in fact the direction of the vorticity lines downstream of breakdown. Longer time records of the velocity distribution on such chordwise planes can provide information on propagation speeds, and measurements at different chordwise locations can yield chordwise wavelength variation. However, such information should be extracted through statistical means, since the motions are quasi-periodic and thus not perfectly repeatable. Such means were employed in the hot-wire measurements described in the following section.

Hot-Wire Measurements

The phenomenon of vortex breakdown is very sensitive to interfering objects. The present group has experimented with laser-Doppler velocimetry and flow visualization to estimate the magnitude of interference due to the proximity of a hot wire or a seven-hole probe to the vortex. It was indicated that the vortex is most sensitive if a probe is inserted in the core of the vortex. In the present study, the signal from the fixed wire A was checked for frequency variation for each measurement location of the traversing wire B. We typically observed small variations of the frequency detected by both wires. These usually small frequency changes are attributed to probe interference. Frequencies obtained by the fixed wire A which was positioned far from the core of the vortex usually changed by at most 5% due to the traversing of the wire B. However for a few measuring locations of wire B the interference was significant (20% frequency change). This is why the data in some of the graphs were discarded, as non-reliable.

Figure 15 shows a typical velocity power spectrum obtained by the fixed wire A. The frequency, corresponding to the dominant peak of the spectrum, was around 48 Hz. This yields a non-dimensional frequency of fX/U=1.25, which is agreement with Gursul[9]. Figure 16 and 17(a) and (b) present typical coherence and cross-spectrum plots ((a) magnitude, (b) phase) between the two wires A and B, respectively.

The spiral shape of the dye streak stretches and expands downstream but at the same time it rotates. Although we were able to visually estimate the frequency of rotation of the spiral for a short distance downstream of breakdown, such an approach is hindered further downstream since the visual identity of the spiral is destroyed. There, flow visualization means can not be used to link the spiral structure rotation to the frequencies picked up by pressure or velocity sensors. The following questions then arises: At chordwise locations well downstream of breakdown, where the flow is dominated by turbulence, is there a coherent non-axisymmetric structure preserved? And if so, could the unsteadiness measured be attributed to a rotation of such a structure?

To confirm that the rotation of some type of asymmetric structure creates the periodic disturbance measured by pressure or velocity sensors, the relative phases of the signals were mapped out along each measuring plane. Rotation would be indicated by a continuous change of the phase in the circumferential direction. The experimental evidence obtained here supports this argument. Plotted in fig 18(a) and (b) are phase contours between the fixed probe A and the traversing probe B, along planes 1 and 4, respectively. It should be noted here that the location of the vortex axis as estimated from time-averaged velocity measurements is around (0.7, 0.6). A first glance quickly indicates that phase variations are confined to a nearly circular region which coincides with the vortex. All disturbances outside this region develop in phase with each other. We observe a strong tendency for the phase contours to have azimuthal variations, or equivalently, it appears that within the experimental error, phases do not vary radially. This implies that disturbances travel in the azimuthal direction and therefore flow structures are spinning about the axis of the vortex.

The coherence between probes A and B is also plotted in the form of contour elevations in fig. 19. In this figure we observe that in the region around the plane of symmetry (lower right boundary) as well as immediately above the wing (lower left boundary; the cross-flow plane along which the data is plotted is viewed from upstream) the coherence is close to unity. This simply signifies that all points in this space respond simultaneously to whatever disturbance is driving them from outside their domain. The circular cross-section of the vortex is also evident in this graph. We observe that a ring of low coherence defines the outer edge of the vortex. This is followed by a ring of higher coherence. The core also stands out. In the upper part of the graph the data was discarded due to interference with the development of vortex breakdown.

Coherence and phase data smoothing

The coherence and phase data was smoothed before plotting using a fuzzy logic predictor to fill in

intermediate points in the position grid. The predictor is based on an optimized fuzzy logic system[20] for identifying non-linear systems in control applications. The program which was used to smooth the data has been under development with the goal of eventually controlling systems whose aerodynamic effects are too complex to model for classical control purposes. The program has been used successfully to fit complex curves based on partial data sets in its early stages of development. Thus it is reasonable to assume that it can fill intermediate points in a full set of data with sufficient accuracy.

The program accepts as input the following data: A cluster radius for determining the complexity of the fuzzy rule base, a gaussian membership function shape variable which determines the effect of a fuzzy rule on its surroundings, and the training input-output pairs. The cluster radius determines the minimum amount that one point in the training data must differ from all other points in order to be part of a new fuzzy rule. The advantage of this clustering method is that for any given system and cluster radius there is a limit to the number of fuzzy rules which can be created. Thus the cluster radius directly determines the complexity of the fuzzy rule base for any given system. In this instance, the cluster radius was chosen so that each input-output pair created a new rule, thereby ensuring that the program would return accurate values at the original data points. The gaussian membership function shape variable has by far the most significant effect on the smoothing effect of the predictor program and therefore the most care must be taken in its specification. If the shape variable is too small, then all predicted values will take on the magnitude of the nearest fuzzy rule, resulting in large regions of like points. If on the other hand, the shape variable is chosen too large, then a fuzzy rule will effect a large area of surrounding values possibly including other rule supports or center values. This will result in very smooth but inaccurate data contours. It is, therefore, imperative that a reasonable compromise be determined between these conditions. For the purposes of producing these graphs, this compromise was found through trial and error although it seems likely that with a thorough knowledge of the input-output ranges and the cluster radius, a more rigorous method of determining this value should be possible.

In this case, the training data for each plane of data was the entire set of data taken for that plane. This ensures that the system returns exact values at the data points and only interpolates in the intermediate area. It is important to note that although the prediction routine requires a fully populated matrix as input, certain points were missing from the data due to positioning restrictions of the acquisition system. It was therefore necessary to fill these blank points with data which would not result in erroneous interpretations of the data. For most graphs, these points were filled with data which was slightly out of the range of the rest of the data. This range was then assigned the color white on the contour plots, resulting in the abrupt fade to white which is evident on several of the plots. The reader should keep in mind when viewing these plots that any area of pure white at the edge of a graph is evident of a lack of data in that area and thus no physical significance should be assumed. The one exception to this method was the phase plot for plane 3 where no appropriate filling data could be found. The empty points for this plot were filled with the value of their nearest neighbor so that they would not influence the smoothing in that area and were then removed from the data set after the smoothing process was completed.

Conclusions

Flow visualization, digital particle image velocimetry and hot-wire anemometry were employed to study the origin and behavior of a certain class of quasi-periodic phenomena observed in the flow over a delta wing. This quasi-periodicity is associated with the breakdown of the leading-edge vortices and is distinct from periodic phenomena developing due to the Kelvin-Helmholtz instabilities of the leading-edge shear layer. It is also possibly distinct from vortex shedding occurring at higher angles of attack, although a smooth transition of the non-dimensional frequencies of the two phenomena is observed as the angle of attack increases (Rediniotis et. al.[13]). Moreover, the phenomenon, at present, seems disassociated from previously observed oscillations of the breakdown position[5]. The non-dimensional frequencies of the two phenomena differ by an order of magnitude. However, given the well-documented breakdown sensitivity to downstream disturbances, it is not unlikely that the downstream behavior of the helical structure contributes to the mechanisms driving the breakdown position oscillations.

The present work provides evidence that the quasi-periodic oscillations that dominate velocity and pressure spectra downstream of breakdown should be attributed to the rotations of the helical structure that originates at breakdown, has a helical sense opposite to the rotation of the leading edge vortex and rotates with the vortex. At locations significantly downstream of breakdown where visual studies as a diagnostics tool of the global structure are hard to impossible, DPIV global techniques captured a brief temporal evolution of the helical structure. Similar studies and findings were reported by Towfigli and Rockwell[21]. The rotation of the

helical structure causes the observed downstream propagation of staggered vortical structures on a measurement plane almost parallel to the wing and passing through the vortex axis. These vortical structures are the intersection of the helix with the measurement plane.

Immediately downstream of breakdown, the non-dimensional rotational frequencies of the helical structure were higher than those measured further downstream. The difference is attributed to different growth rates of the helix radius.

Hot-wire anemometry offered evidence that the phase difference between oscillations obtained along points on a plane normal to the vortex axis vary circumferentially. This provides further support to the hypothesis that the quasi-periodic phenomenon we detect is due to the rotation of a pattern about the axis of the vortex.

Lastly, it should be noted that although the Reynolds number for the experiments reported herein varies between 9,100 and 210,000, the findings are consistent and support the same physical processes.

Acknowledgements

This work was supported by the Air Force Office of Scientific Research, Project No. AFOSR-91-0310. One of the authors (S.M.K.) is carrying a NASA student researcher's stipend (NASA Grant No. NGT-50978). The authors would like to thank the Carderock Division of the Naval Surface Warfare Center for their help with the DPIV data reduction. The authors' appreciation is also expressed to Ms. Deborah Furey for insightful conversations.

References

1. Gad-el Hak, M. and Blackwelder, R. F., "The Discrete Vortices from a Delta Wing," AIAA Journal, Vol. 23, No.6, June 1985, pp. 961-962.

2. Lowson, M. V., "The Three-Dimensional Vortex Sheet Structure on Delta Wings," Fluid Dynamics of Three-Dimensional Turbulent Shear Flows and Transition, AGARD-CP-438, Cesme, Turkey, Oct. 1988.

3. Gordnier, R. E. and Visbal, M. R., "Unsteady Vortex Structure over a Delta Wing," Journal of Aircraft, Vol. 31, No. 1, Jan-Feb 1994, pp. 243-248.

4. Monkewitz, P. A., and Huerre, P., "Influence of the Velocity Ratio on the Spatial Instability of Mixing Layers," Physics of Fluids, Vol. 25, No. 7, 1982, pp. 1137-1143.

5. Gursul, I. and Yang, H., "On Fluctuations of Vortex Breakdown Location," Physics of Fluids, Vol. 7, No. 1, Jan. 1995.

6. Payne, F. M., Ng, T. T., Nelson, R. C. and Schiff, L. B., "Visualization and Wake Surveys of the Vortical Flow over a Delta Wing," AIAA J., Vol. 26, No. 2, pp. 137-143, Febr. 1988.

7. Roos, F. W. and Kegelman, J. T., "Recent Explorations of Leading-Edge-Vortex Flowfields," High-Angle-of-Attack Technology, NASA CP 3149, Part 1, 1992.

8. Rediniotis, O. K., "The Transient Development of Vortices Over Delta Wings," Doctoral Dissertation, Va Tach, October 1992.

9. Gursul, I., "Unsteady Flow Phenomena over Delta Wings at High Angle of Attack," AIAA Journal, Vol. 32, No. 2, pp. 225-231, Feb. 1994.

10. Rediniotis, O. K. and Schaeffler, N. W., "Breakdown of Conical Vortices - An Experimental Investigation Via 3-D LDV Measurements," FED-Vol. 191, pp. 29-34, Laser Anemometry 1994: Advances and Applications, ASME 1994.

11. Hubner, J. P. and Komerath, N. M. "Visualization of Quasi-Periodic Structures in a Vortex Flow," to appear, Journal of Aircraft.

12. Visbal, M. R., "Computational and Physical Aspects of Vortex Breakdown on Delta Wings," AIAA Paper No. 95-0585, 33rd Aerospace Sciences Meeting, Jan. 1995, Reno, Nevada.

13. Rediniotis, O. K., Stapountzis, H., and Telionis, D. P., "Periodic Vortex Shedding over Delta Wings," AIAA Journal, Vol. 31, No. 9, 1993, pp. 1555-1562.

14. Willert, C. E., and Gharib, M., "Digital Particle Image Velocimetry," Experiments in Fluids, Vol. 10, pp. 181-193, 1993.

15. Hubner, J. P. and Komerath, N. M., "Spectral Mapping of Quasi-Periodic Structures in a Vortex Flow," AIAA Paper No. 93-2914, 24th AIAA Fluid Dynamics Conference, Orlando, Florida, !993.

16. Gursul, I., Lusseyran, D., and Rockwell, D., "On Interpretation of Flow Visualization of Unsteady Shear Flows," Experiments in Fluids, Vol. 9, No.5, 1990, pp. 257-266.

17. Visser, K. D. and Nelson, R. C., "Measurements of Circulation and Vorticity in the Leading-Edge Vortex of a Delta Wing," AIAA J., Vol. 31, No. 1, 1993, pp.104-111.

18. Mathioulakis, D. S., Kim, M. J., Telionis, D. P. and Mook, D. T., "On the Wake of a Pitching Airfoil," AIAA Paper No. 85-1621, Reno, Nevada, 1985.

19. Visbal, M. R., "Numerical Simulation of Spiral Vortex Breakdown Above a Delta Wing," to be presented, AIAA 26th Fluid Dynamics Conference, June 1995.

20. Wang, L. X., Adaptive Fuzzy Systems and Control: Design and Stability Analysis. Englewood Cliffs, NJ: Prentice-Hall, Inc., 1994.

21. Towfighi, J. And Rockwell, D., "Instantaneous Structure of Vortex Breakdown on a Delta Wing via Particle Image Velocitmetry," AIAA J., Vol. 31, No. 6, June 1993, pp. 1160-1162.

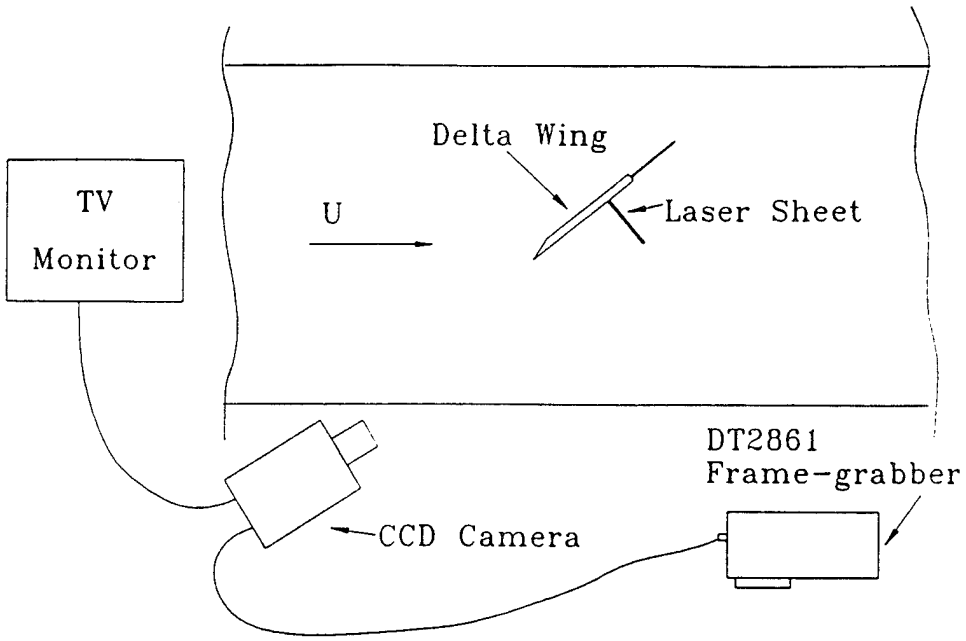

Figure 1. Water tunnel experimental layout.

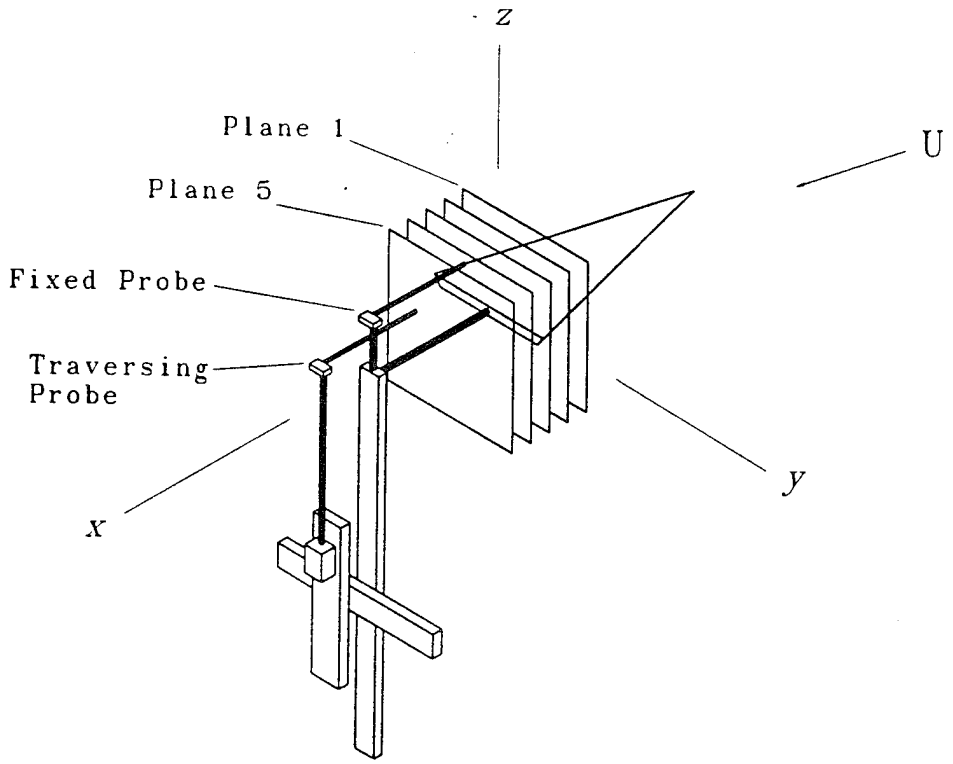

Figure 2. Wind tunnel experimental layout.

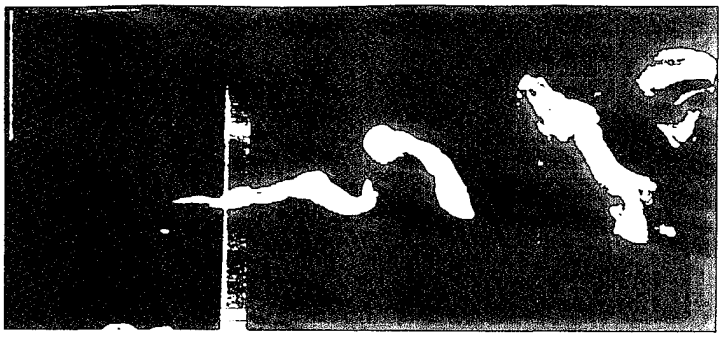

Figure 3. Typical vortex core visualization image.

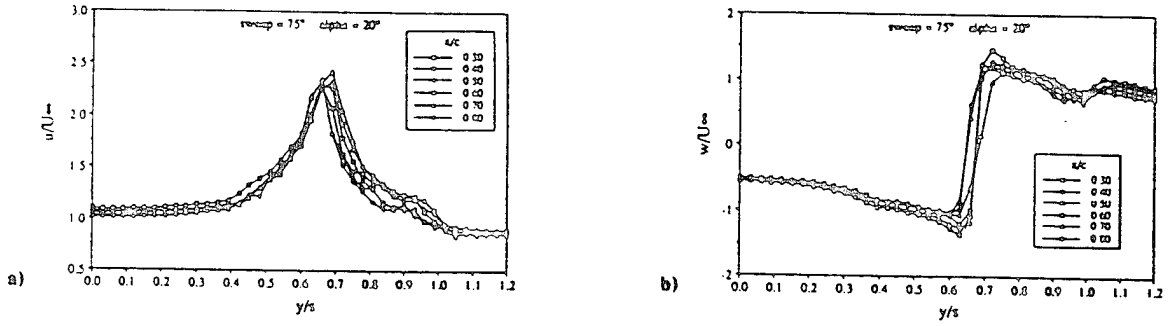

Figure 4. Velocity distribution in vortex core: (a) axial velocity, (b) tangential velocity (from reference 17).

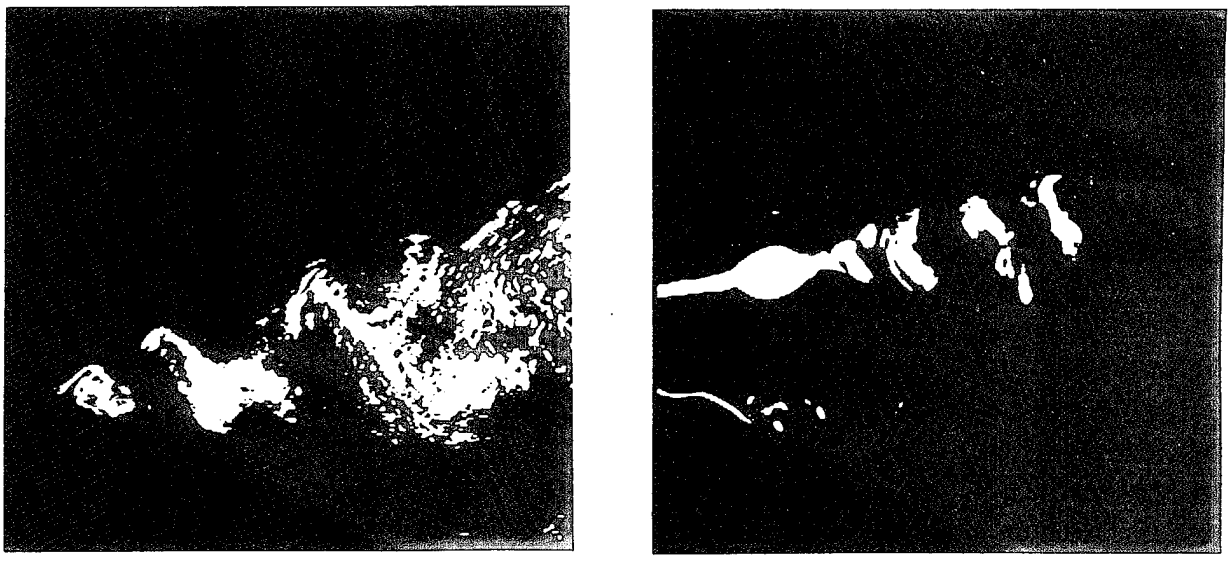

(a) (b)

Figure 5. Vortex breakdown visualization: (a) spiral type, (b) bubble type.

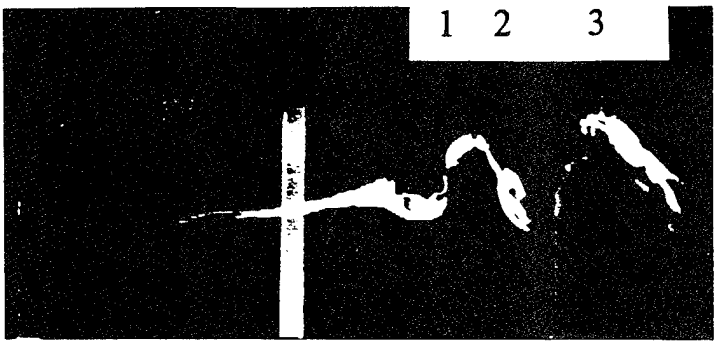

Figure 6. Location of visual estimation of rotation frequency.

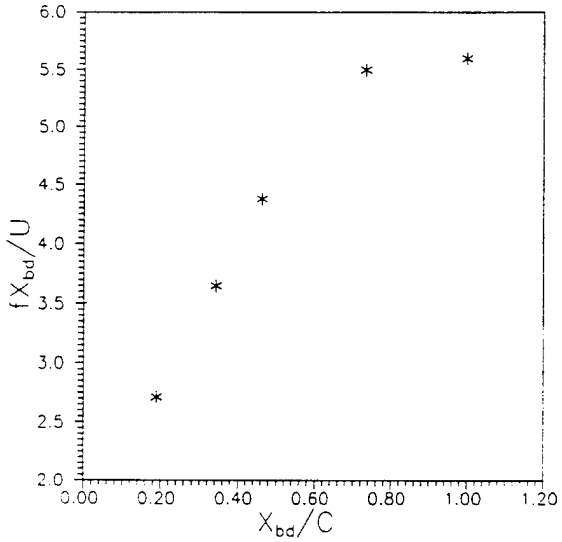

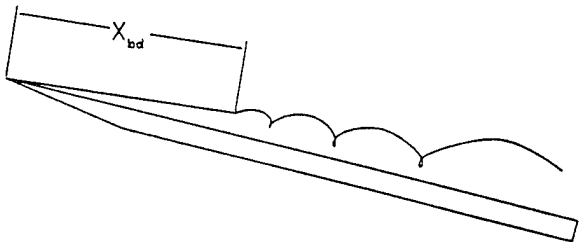

Figure 7. Non-dimensional frequency at breakdown versus chordwise breakdown location.

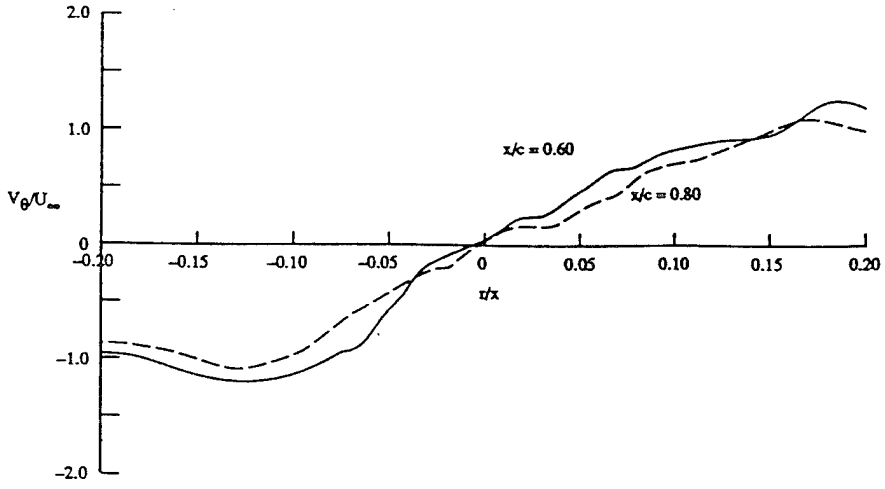

Figure 8. Azimuthal velocity distribution downstream of breakdown.

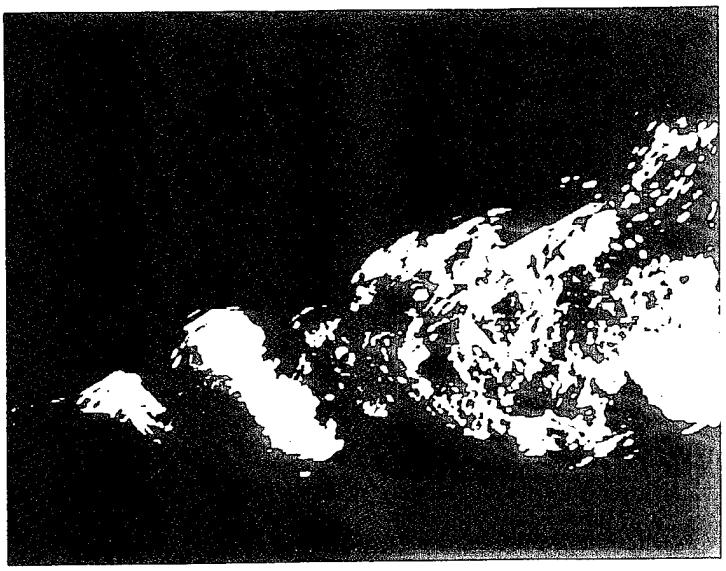

Figure 9. Visualization of spiral radius growth rate.

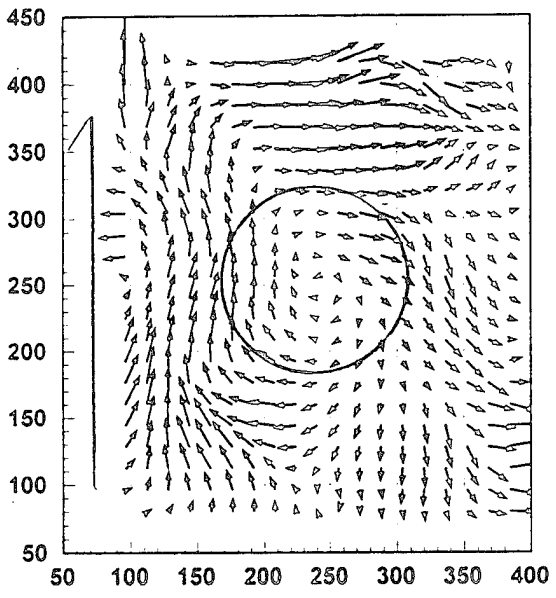

Figure 10. Instantaneous crossflow at x/c=0.75, at time t_1.

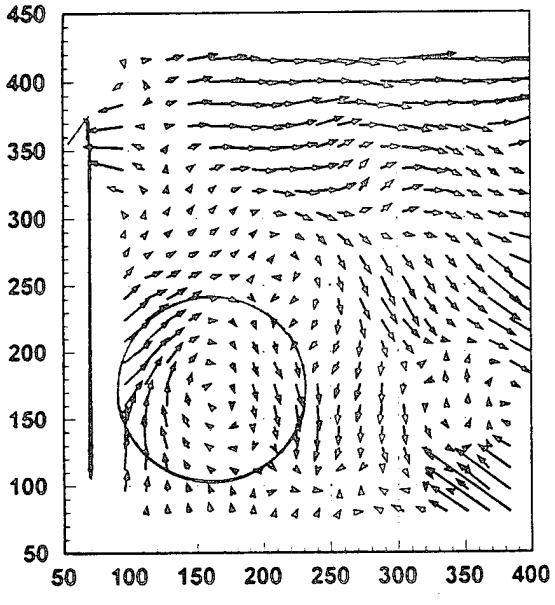

Figure 11. Instantaneous crossflow at x/c=0.75, at time t_2.

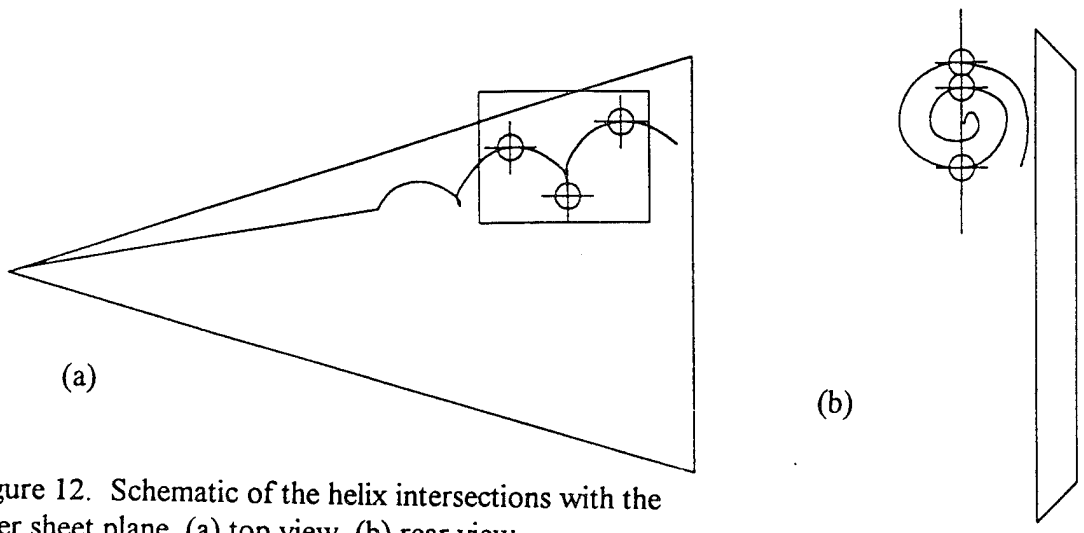

Figure 12. Schematic of the helix intersections with the laser sheet plane. (a) top view, (b) rear view.

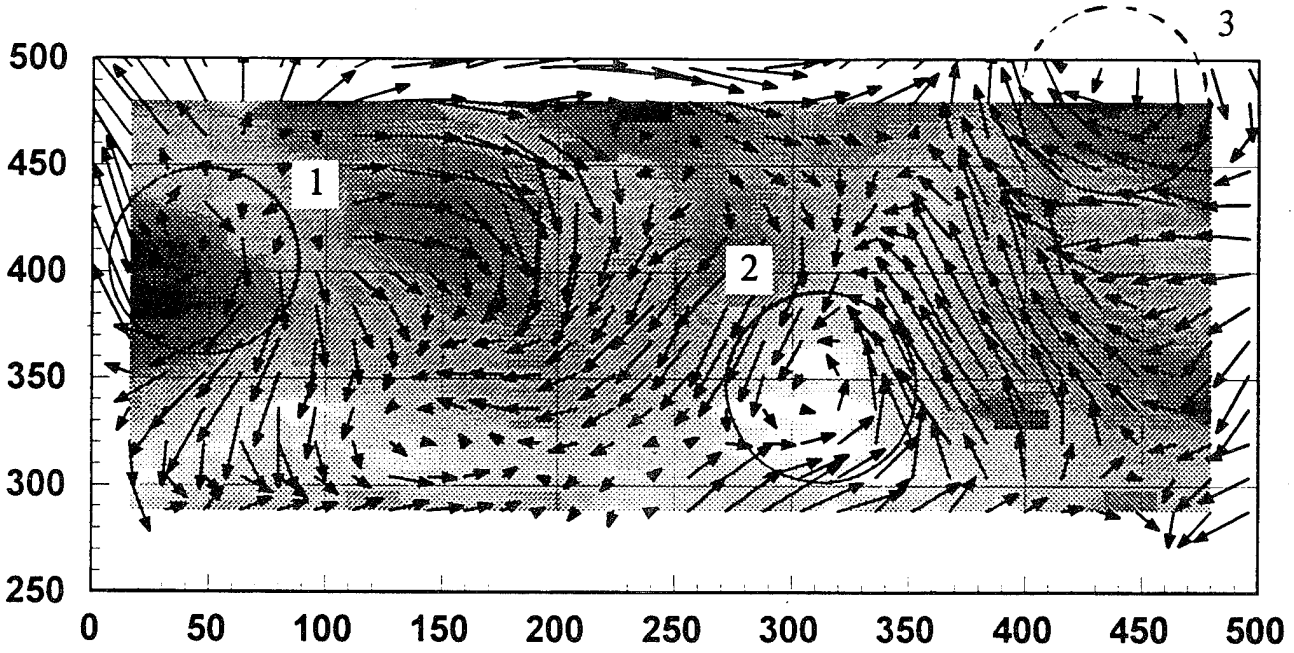

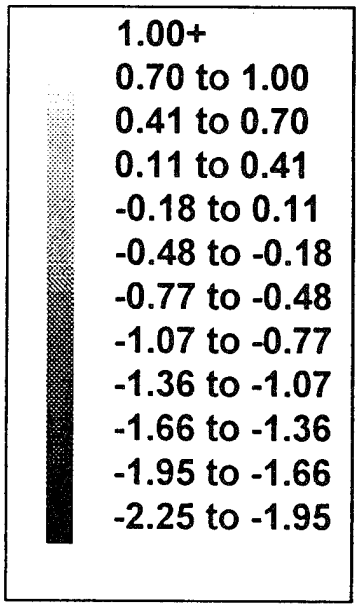

Figure 13. Instantaneous flowfield along the plane of Figure 12, at t_3.

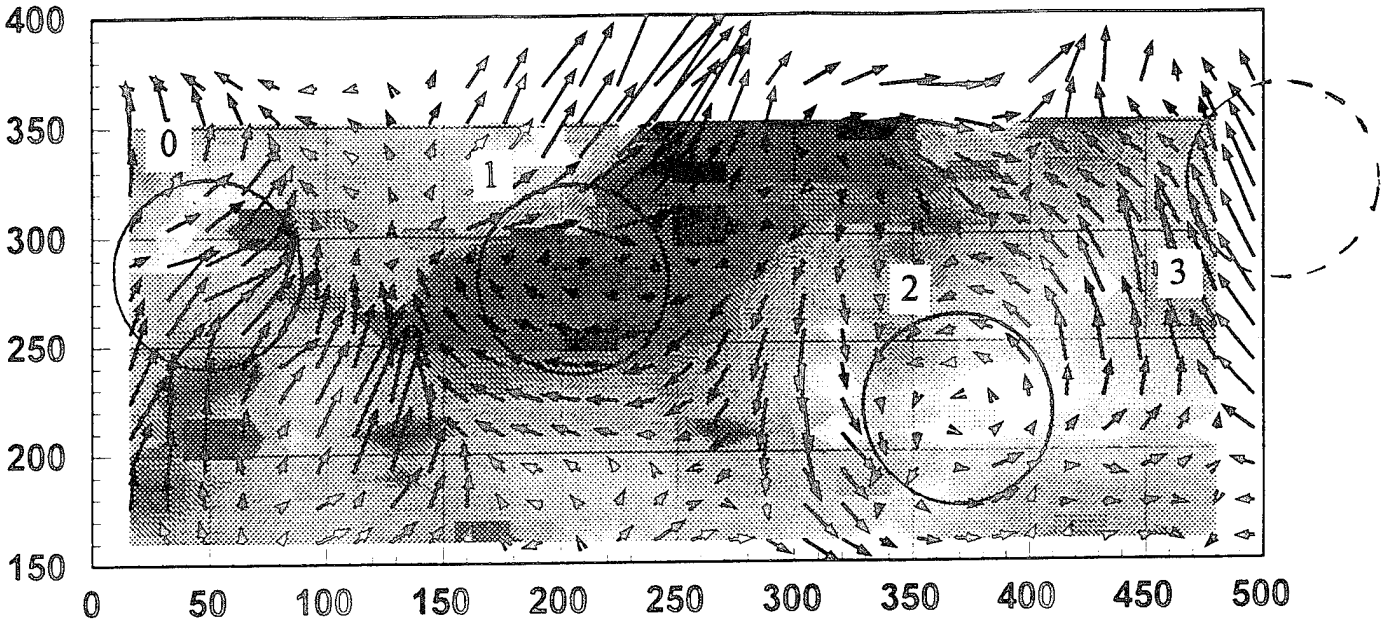

Figure 14. Instantaneous flowfield along the plane of Figure 12, at t_3+.5 sec.

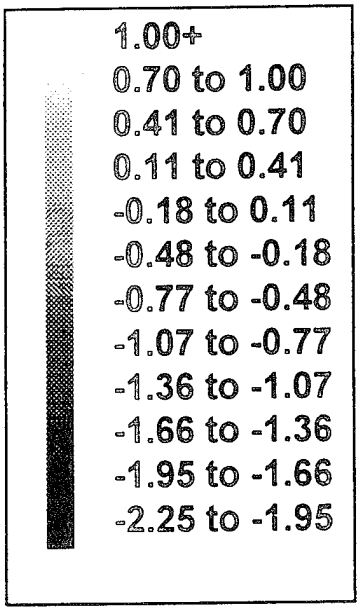

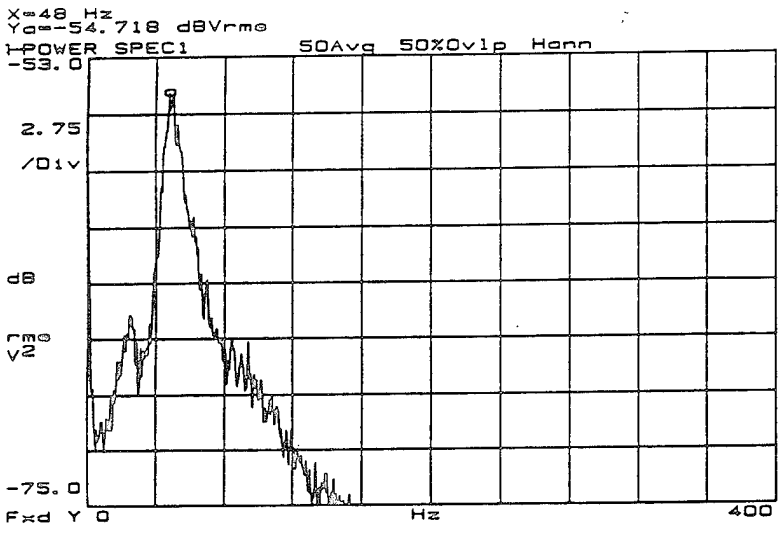

Figure 15. Typical velocity power spectrum measured by the fixed wire A.

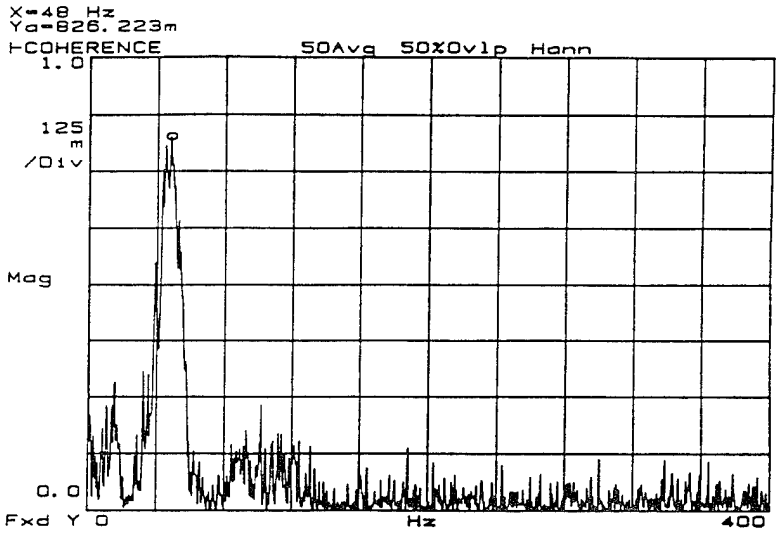

Figure 16. Typical coherence plot between wires A and B.

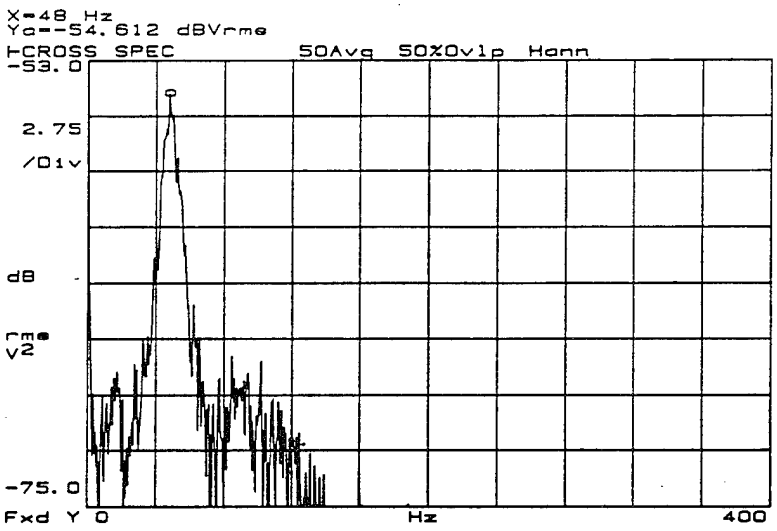

Figure 17. Typical cross spectrum plots between wires A and B: (a) magnitude, (b) phase.

(a)

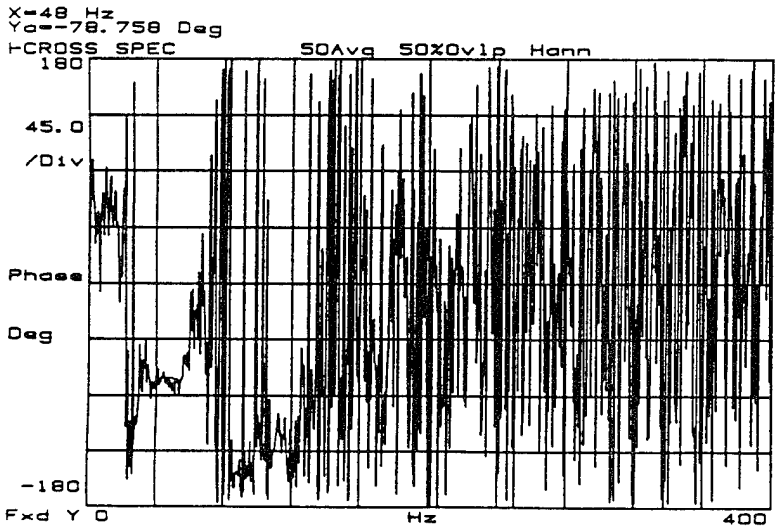

(b)

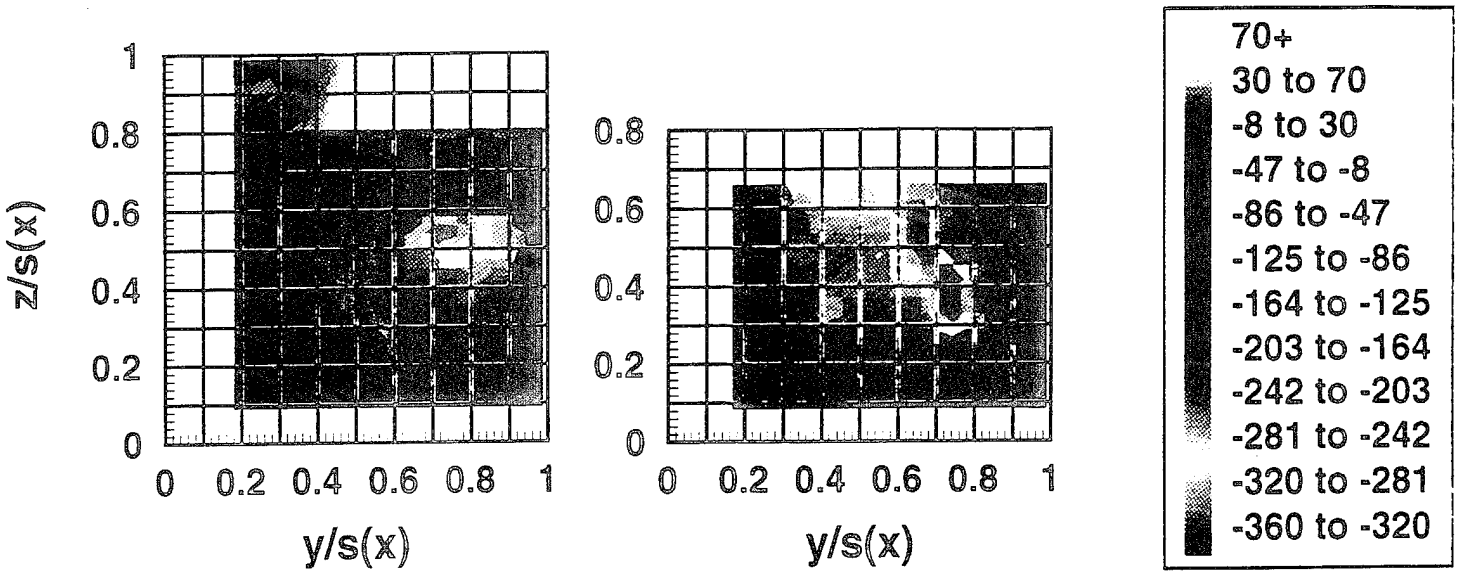

(a) (b)

Figure 18. Phase plots (degrees) along (a) plane 1, (b) plane 4.

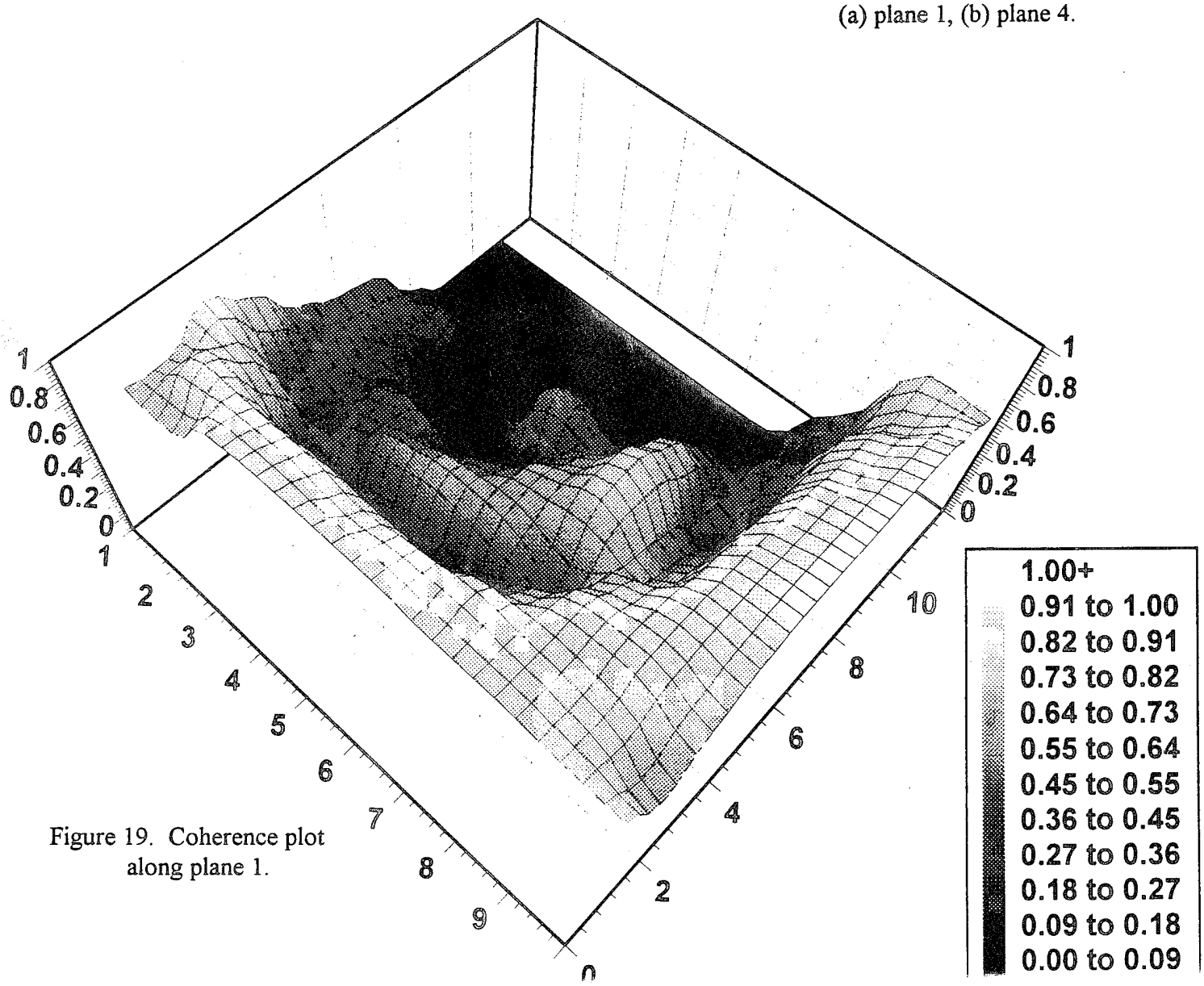

Figure 19. Coherence plot along plane 1.